

AD 763798

# SONIC FATIGUE TEST METHODS AT ELEVATED TEMPERATURES

*M. H. HIEKEN*

*W. E. NOONAN*

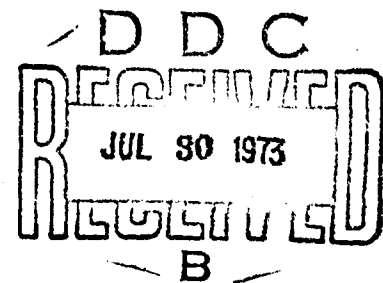
*E. F. SHROYER*

*MCDONNELL DOUGLAS CORPORATION*

TECHNICAL REPORT AFFDL-TR-73-8

Reproduced by  
NATIONAL TECHNICAL  
INFORMATION SERVICE  
U.S. Department of Commerce  
Springfield VA 22151

JUNE 1973



Approved for public release; distribution unlimited.

AIR FORCE FLIGHT DYNAMICS LABORATORY  
AIR FORCE SYSTEMS COMMAND  
WRIGHT-PATTERSON AIR FORCE BASE, OHIO

AD-763 798

SONIC FATIGUE TEST METHODS AT ELEVATED TEMPERATURES

MCDONNELL AIRCRAFT CO.

PREPARED FOR  
AIR FORCE FLIGHT DYNAMICS LABORATORY

JUNE 1973

Distributed By:

**NTIS**

National Technical Information Service  
U. S. DEPARTMENT OF COMMERCE

# NOTICE

When Government drawings, specifications, or other data are used for any purpose other than in connection with a definitely related Government procurement operation, the United States Government thereby incurs no responsibility nor any obligation whatsoever; and the fact that the government may have formulated, furnished, or in any way supplied the said drawings, specifications, or other data, is not to be regarded by implication or otherwise as in any manner licensing the holder or any other person or corporation, or conveying any rights or permission to manufacture, use, or sell any patented invention that may in any way be related thereto.

ACCESSION for	
NTIS	White Section <input checked="" type="checkbox"/>
DDC	Self Section <input type="checkbox"/>
UNANNOUNCED	<input type="checkbox"/>
JUSTIFICATION	
BY	
DATE	
DIST. NO. / ACT. NO.	
A	

Copies of this report should not be returned unless return is required by security considerations, contractual obligations, or notice on a specific document.

Unclassified

Security Classification

DOCUMENT CONTROL DATA - R & D		
(Security classification of title, body of abstract and indexing annotation must be entered when the overall report is classified)		
1. ORIGINATING ACTIVITY (Corporate author) McDonnell Douglas Corporation McDonnell Aircraft Company Division St. Louis, MO 63166		2a. REPORT SECURITY CLASSIFICATION Unclassified
3. REPORT TITLE  SONIC FATIGUE TEST METHODS AT ELEVATED TEMPERATURES		2b. GROUP
4. DESCRIPTIVE NOTES (Type of report and inclusive dates) FINAL - March 1971 to December 1972		
5. AUTHOR(S) (First name, middle initial, last name) M. H. Hieken W. E. Noonan E. F. Shroyer		
6. REPORT DATE June 1973	7a. TOTAL NO. OF PAGES -143 145	7b. NO. OF REFS 33
8a. CONTRACT OR GRANT NO. F33615-71-C-1217	9a. ORIGINATOR'S REPORT NUMBER(S)  MI-C A1622	
b. PROJECT NO. 4437	9b. OTHER REPORT NO (this report) other numbers that may be assigned AFFDL-TR-73-8	
c. Task Nr. 443703		
d.		
10. DISTRIBUTION STATEMENT  Approved for public release; distribution unlimited.		
11. SUPPLEMENTARY NOTES		12. SPONSORING MILITARY ACTIVITY Air Force Flight Dynamics Laboratory Wright-Patterson AFB, OH 45433
13. ABSTRACT <p>Sonic fatigue testing at elevated temperatures has become increasingly important as aerospace vehicle structures are designed for the combined environments. Work is described in four areas related to thermal/acoustic testing: acoustic simulation, thermal simulation, specimen mounting effects, and instrumentation and measurements.</p> <p>Acoustic field studies considered the directional properties of various fields, as well as coupling of the acoustic fields with structural specimens. Thermal environment studies dealt with predicting temperatures in a heated structural specimen. The design of heating systems was also discussed. In specimen mounting effects, equations were presented to show how thermal loads enter into the general dynamic equations. Panels with free edges and panels with fixed edges were treated in detail. Measurement methods related to sonic fatigue testing at elevated temperatures were surveyed for availability of devices which operate in the combined environment.</p> <p>Results presented here indicate that good estimates of specimen response can be made for basic specimen geometries, mounting conditions and orientations in the excitation field. Methods are suggested for extending the results to more complex cases.</p>		

DD FORM 1473  
1 NOV 65

Unclassified

Security Classification



UNCLASSIFIED

**Security Classification**

12.	KEY WORDS	LINK A		LINK B		LINK C	
		ROLE	WT	ROLE	WT	ROLE	WT
	SONIC FATIGUE						
	ACOUSTIC ENVIRONMENT SIMULATION						
	THERMAL/ACOUSTIC ENVIRONMENTS						
	ACOUSTIC TESTING MEASUREMENTS						
	DYNAMIC RESPONSE						

UNCLASSIFIED

**Security Classification**

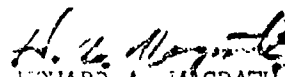
ia

## FOREWORD

This report was prepared by the McDonnell Douglas Corp. for the Aero-Acoustics Branch, Vehicle Dynamics Division, Air Force Flight Dynamics Laboratory, Wright-Patterson Air Force Base, Ohio, under Contract F33615-71-C-1217. This research program was conducted under Project 4437 "High Intensity Sound Environment Simulation for Air Force Systems Testing", Task 443703 "Development of Acoustic Testing Techniques for Aircraft Components and Equipment". The Air Force Project Engineer was Mr. N. D. Wolf. This study was performed during the period March 1971 to December 1972.

Manuscript was released by the authors in December 1972 for publication as an AFFDL Technical Report, and assigned the McDonnell Douglas number MDC A1622.

This Technical Report has been reviewed and is approved.

  
EDWARD A. MCGRATH

Director  
Vehicle Dynamics Division

## ABSTRACT

Sonic fatigue testing at elevated temperatures has become increasingly important as aerospace vehicle structures are designed for the combined environments. Work is described in four areas related to thermal/acoustic testing: acoustic simulation, thermal simulation, specimen mounting effects, and instrumentation and measurements.

Acoustic field studies considered the directional properties of various fields, as well as coupling of the acoustic fields with structural specimens. Thermal environment studies dealt with predicting temperatures in a heated structural specimen. The design of heating systems was also discussed. In specimen mounting effects, equations were presented to show how thermal loads enter into the general dynamic equations. Panels with free edges and panels with fixed edges were treated in detail. Measurement methods related to sonic fatigue testing at elevated temperatures were surveyed for availability of devices which operate in the combined environment.

Results presented here indicate that good estimates of specimen response can be made for basic specimen geometries, mounting conditions, and orientations in the excitation field. Methods are suggested for extending the results to more complex cases.

## TABLE OF CONTENTS

Section	Page
1.0 INTRODUCTION .....	1
2.0 ACOUSTIC ENVIRONMENT SIMULATION .....	2
2.1 Acoustic Fields .....	2
2.1.1 Progressive Wave Fields .....	2
2.1.2 Reverberant Fields .....	4
2.2 Acoustic Coupling .....	8
2.3 Temperature Effects on Acoustic Fields .....	16
2.4 Test Techniques - Acoustic Environment Simulation .....	23
3.0 THERMAL ENVIRONMENT SIMULATION .....	29
3.1 Thermal Field Studies .....	29
3.2 Design of Heat Sources .....	32
3.2.1 Reflector Design Considerations .....	33
3.2.2 Quartz Lamp Installations .....	34
4.0 SPECIMEN MOUNTING EFFECTS .....	40
4.1 Governing Equations .....	40
4.2 Thermal Effects .....	42
4.3 Dynamic Effects .....	68
4.4 Thermal/Acoustic Mounting .....	70
5.0 SONIC FATIGUE INSTRUMENTATION AND MEASUREMENTS .....	83
5.1 Sonic Fatigue Measurements .....	83
5.1.1 Acoustic Field Measurements .....	83
5.1.2 Sonic Fatigue Strain Measurements .....	86
5.1.3 Displacement Measurements .....	87
5.1.4 Temperature Measurements .....	89
5.2 Sonic Fatigue Crack Detection .....	90
6.0 SUMMARY AND RECOMMENDATION .....	95
APPENDIX A - STRUCTURAL COUPLING AND ACOUSTIC FIELDS .....	97
APPENDIX B - TEMPERATURE PREDICTION COMPUTER PROGRAM .....	105
APPENDIX C - DERIVATION OF GOVERNING EQUATIONS .....	108
APPENDIX D - COMPUTER PROGRAMS FOR THERMAL STRESS CALCULATION .....	114
REFERENCES .....	133

## LIST OF ILLUSTRATIONS

Figure	Title	Page
1	Progressive Wave Test Section .....	3
2	Structural Resonances .....	7
3	Participation Factor Variation - One Dimensional - Progressive Wave .....	13
4	Participation Factor Variation - Two Dimensional - Progressive Wave .....	14
5	First Mode Wavelength Ratio, Beams .....	17
6	First Mode Wavelength, Ratio, Plates .....	18
7	Normalized Wavelength Ratio - Free Boundary .....	19
8	Normalized Wavelength Ratio - Fixed Boundary .....	20
9	Normalized Wavelength Ratio - Simply Supported Boundary .....	21
10	Power Requirements .....	22
11	Transfer Functions - Ambient Temperature .....	24
12	Transfer Functions - 475° .....	25
13	Analytical Model for Temperature Prediction .....	30
14	Strain Response of Quartz Lamp - Acoustic Excitation .....	36
15	LT-100 Lamp Holder .....	37
16	RI 8325-1 Lamp Holder .....	39
17	Thermal Stress Response .....	49
18	Thermal Stress Distribution - Fixed Boundary, 1st Order .....	50
19	Thermal Stress Distribution - Fixed Boundary, 2nd Order .....	51
20	Thermal Stress Distribution - Fixed Boundary, 3rd Order .....	52
21	Thermal Stress Distribution - Fixed Boundary, 4th Order .....	53
22	Thermal Stress Distribution - Free-Free Boundary, 1st Order .....	54
23	Thermal Stress Distribution - Free-Free Boundary, 2nd Order .....	55
24	Thermal Stress Distribution - Free-Free Boundary, 3rd Order .....	56
25	Thermal Stress Distribution - Free-Free Boundary, 4th Order .....	57
26	Test Setup for Free Panel .....	58
27	Test Setup for Fixed Panel .....	59
28	Thermal Stress Response .....	63

# LIST OF ILLUSTRATIONS (Continued)

Figure	Title	Page
29	Rectangular Plate Model - Closed Form - Finite Difference Comparison .....	64
30	4-Level Latin Square .....	67
31	Panel Models for Analytical Studies .....	71
32	Panel Modal Characteristics .....	72
33	Acceleration Response - Free Panel - Ambient .....	73
34	Acceleration Response - Free Panel - 450°F .....	74
35	Acceleration Response - Fixed Panel - Ambient .....	75
36	Acceleration Response - Fixed Panel - 480°F .....	76
37	Static Boundary Design .....	79
38	Thermal/Acoustic Specimen Mounting .....	81
39	Coupling Acoustic Field to a Microphone Through a Tube .....	85
40	Crack Detection Panel Design .....	92
41	Oscilloscope Trace at Failure .....	93
42	Thermal Stress Programs .....	115
43	Finite Difference Model of Panel .....	116

# LIST OF TABLES

Number	Title	Page
1	Wavelength Ratio . . . . .	26
2	Participation Factors . . . . .	28
3	Thermal Stress Data for Free Panel . . . . .	47
4	Thermal Stress Data for Fixed Panel . . . . .	48
5	Experimental Evaluation of $\bar{T}_c$ . . . . .	61
6	Experimental Thermal Stress Data Analysis . . . . .	62
7	Comparison of Finite Difference - Closed Form Solutions for a Rectangular Plate . . . . .	66
8	Change in Natural Frequency of Panel Due to Thermal Effects . . . . .	77

# LIST OF SYMBOLS

A	area; intermediate temperature distribution; coefficients of temperature distribution	R	cross correlation function; real (subscript); structural response (subscript)
B	boundary (subscript)	S	power spectral density
C	damping constant; equation constants; center (subscript)	T	temperature; translation (subscript)
$C_{pipj}$	normalized cross power spectrum of pressure between the $i^{th}$ and the $j^{th}$ locations	V	room volume
D	plate stiffness	W	power; normalized peak displacement in z direction
E	Young's modulus	a	width of panel
F	absorbed radiant heat flux; body force	$a_i$	beam constant
$F_d$	view factor	b	length of panel
$F_e$	emissivity factor	c	speed of sound; thickness of panel
G	shear modulus	$c_p$	specific heat at constant pressure
H	complex frequency response function	e	natural logarithmic base, 2.718 energy
I	imaginary (subscript)	f	cyclic frequency; arbitrary functions
J	mechanical equivalent of heat	g	acceleration due to gravity
K	stiffness; arbitrary constants	h	impulse response function; thickness
M	mass; index	i	index (subscript)
N	number of modes; index; in-plane force	j	imaginary operator; index (subscript)
P	pressure; load per unit length	k	wave number; coefficient of thermal conductivity



# LIST OF SYMBOLS (Continued)

$l$	length	$\Phi$	normalized modal deflection
$m$	mode number in y direction (section 2.2); index (subscript)	$\alpha$	coefficient of thermal expansion
$n$	constant; mode number in x direction (Section 2.2); mode number (Section 2.1.2); index (subscript)	$\beta$	particle displacement
$p$	pressure	$\gamma$	shear strain
$q$	heat flux	$\delta$	normalized coordinates; unit impulse function
$\dot{q}$	heat generated per unit volume per unit time	$\epsilon$	emissivity; normal strain
$r$	spatial coordinate	$\xi$	damping ratio
$t$	time; with respect to time (subscript)	$\eta$	normal coordinate
$u$	displacement in x direction	$\lambda$	wavelength
$v$	displacement in y direction	$\lambda_p$	wavelength of acoustic pressure
$v_i$	component of velocity	$\lambda_r$	wavelength of structural response
$w$	displacement in z direction	$\nu$	Poisson's ratio
$x$	spatial coordinate; with respect to x coordinate (subscript)	$\pi$	3.14159 . . . .
$y$	spatial coordinate; with respect to y coordinate (subscript)	$\rho$	density
$z$	spatial coordinate; with respect to z coordinate (subscript)	$\sigma$	Stephen-Boltzmann constant; stress
$\Gamma$	participation factor	$\tau$	time
$\Delta$	incremental quantity; Fourier transform of normal coordinates	$\phi$	stress function
		$\psi$	strain function
		$\omega$	angular frequency

# LIST OF OPERATORS

$\nabla$	partial derivative operator	$\underline{\quad}$	row matrix
$*$	complex conjugate	$\begin{bmatrix} & \\ & \end{bmatrix}$	diagonal matrix
$\underline{\quad}$	nondimensional quantity	$\{I\}$	identity matrix
$\begin{bmatrix} \end{bmatrix}$	square matrix	$\Sigma$	summation
$\begin{bmatrix} \end{bmatrix}^T$	transpose of matrix	$\wedge$	normal coordinates
$\begin{Bmatrix} \end{Bmatrix}$	column matrix		

## SECTION I

### INTRODUCTION

Sonic fatigue testing at elevated temperatures has become a matter of considerable importance in recent years. The application of new materials and advanced fabrication methods to high performance aircraft has brought a need for evaluation of the structural elements in the combined high intensity noise/high temperature environment.

The study effort reported here considered all aspects of high temperature sonic fatigue testing. Characteristics of the acoustic environment are discussed, along with coupling of the acoustic excitation with the test specimen. Thermally and dynamically induced stresses are considered in detail, including the effect of the specimen mounting on the resultant specimen response. Information is reported on methods and devices for measuring all the parameters that enter into combined thermal/acoustic testing.

Following a brief summary of the above findings, recommendations are made for applications to combined environment tests, and areas for further study are indicated.

## SECTION 2

### ACOUSTIC ENVIRONMENT SIMULATION

Sonic fatigue tests are usually conducted in facilities that produce either progressive wave or reverberant (diffuse) acoustic fields. One phase of this program was to investigate the use of such facilities for sonic fatigue tests at elevated temperatures. Since the purpose of a sonic fatigue test is to determine the ability of a structural specimen to withstand acoustically induced stresses, a study of acoustic environment simulation should also consider the coupling between the acoustic field and the specimen. Accordingly, this section first considers mathematical representations for progressive wave and reverberant fields. Then, utilizing the dynamic properties of a structural specimen, a method is developed for estimating the response of a structure to an acoustic field. The effects of temperature on the acoustic field in a representative test application are then discussed.

#### 2.1 ACOUSTIC FIELDS

The analysis of the progressive wave and reverberant fields follows the usual assumptions of elementary acoustics. The sound pressure and particle velocities are assumed to be small compared to the static pressure and sound velocity, respectively. Attenuation in the medium will be neglected.

##### 2.1.1 Progressive Wave Fields

A commonly used sonic fatigue test enclosure is the progressive wave tube, consisting of a constant cross-section duct with an acoustic source at one end, and some provision for mounting a structural specimen in the wall of the duct. The acoustic pressures in such an enclosure are considered to be uniform across any cross-section so that the progressive wave field is a one-dimensional acoustic field.<sup>1</sup> Therefore, the one-dimensional wave equation

$$\frac{\partial^2 p(x, t)}{\partial x^2} = \frac{1}{c^2} \frac{\partial^2 p(x, t)}{\partial t^2} \quad (2.1)$$

can be used to describe the progressive wave field. The solution of equation (2.1) depends on the boundary conditions at the end of the enclosure. For the arrangement shown in Figure 1 for example, the solution for a perfectly anechoic termination (i.e., no pressure wave reflected from the end) is of the form

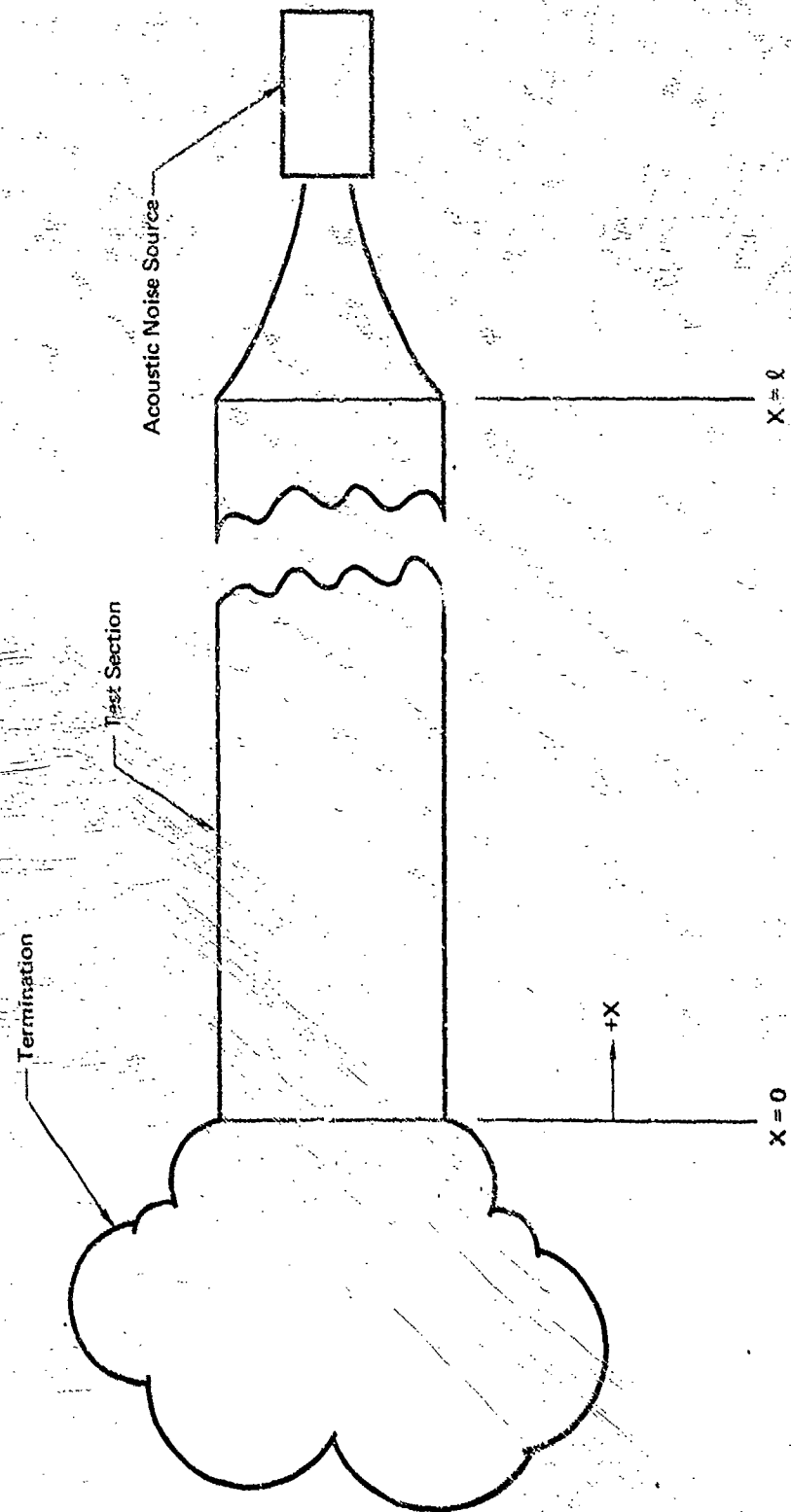
$$p(x, t) = P_0 e^{j(\omega t + \frac{2\pi x}{\lambda})} \quad (2.2)$$

This solution is for a simple harmonic excitation at an angular frequency  $\omega$  and represents a pressure wave traveling in the  $-x$  direction. The pressure amplitude envelope is equal to  $P_0$  and is constant along the length of the tube, while the phase of the pressure between two points varies linearly with the distance between these points.

Other types of terminations will yield different pressure functions for the progressive wave enclosure. If the anechoic termination were replaced by an infinitely rigid closure at the  $x=0$  plane, then a pressure wave is reflected back toward the source, and the pressure in the enclosure is given by<sup>2</sup>

$$p(x, t) = \frac{P_0}{\sin k\ell} \cos \frac{2\pi x}{\lambda} e^{j\omega t} \quad (2.3)$$

FIGURE 1  
PROGRESSIVE WAVE TEST SECTION



Neglecting the time-varying component of the pressure, we note that the envelope of the magnitude of the standing pressure wave is a cosine function. The maximum value of the pressure envelope is a function of the length of the enclosure,  $\ell$ , and the frequency at which the test section is excited. The frequency dependence is contained in the wave number  $k$ , defined as

$$k = \frac{2\pi}{\lambda} \quad (2.4)$$

Equation (2.3) does not consider any losses; and therefore suggests that the pressure becomes infinite at frequencies and enclosure lengths such that

$$k\ell = n\pi, \quad n = 1, 2, 3, \dots \quad (2.5)$$

In practice, some damping is always present to limit the pressure to a finite value, although the standing wave ratio is a maximum when the conditions of equation (2.5) are met.

A third form of the pressure function results if the enclosure is allowed to open directly into free space at the  $x=0$  plane. In this case, there will be a pressure antinode at the interface, with the pressure distribution in the duct being

$$p(x, t) = \frac{p_0}{\cos k\ell} \sin \frac{2\pi x}{\lambda} e^{j\omega t} \quad (2.6)$$

Comments relative to the peak value of pressure for the rigid termination case are also applicable to the enclosure with an open end, except that pressure maxima occur at

$$k\ell = \frac{n\pi}{2}, \quad n = 1, 3, 5, \dots \quad (2.7)$$

The simple trigonometric functions in equations (2.2), (2.3), and (2.6) are convenient to describe the pressure distributions in progressive wave test sections, since the test specimens are mounted in the wall of the test section. The frequency range encompassed by sonic fatigue tests, combined with the cross-sectional areas likely to be used for progressive wave sections, may yield conditions such that the acoustic waves do not travel along the enclosure with plane fronts. This factor is not important for the present discussion, since the pressure distribution along the surface of the enclosure is still described by the trigonometric functions. Still another effect may be encountered at various combinations of test frequency and enclosure size. An acoustic field may be established somewhere between that which would be expected for an anechoic termination and an abrupt termination. In such cases, a combination of trigonometric functions may be needed to represent the acoustic field. Later in this section, we will utilize trigonometric representations of acoustic fields for estimating structural response to the fields.

### 2.1.2 Reverberant Fields

Another common type of acoustic test enclosure is a large room that is characterized by low acoustic absorption at the internal surfaces of the room. In such a room, a large percentage of the acoustic energy incident upon a given surface is reflected from that surface. The resulting reverberant (diffuse) acoustic field has uniform energy density throughout the volume of the enclosure, and all directions of propagation are equally probable.

An analysis of the acoustic field in a reverberant room begins with the general wave equation, although the equation must now account for propagation in three directions. In its general form, the wave equation can be written as:

$$\nabla^2 p = \frac{1}{c^2} \frac{\partial^2 p}{\partial t^2} \quad (2.8)$$

where the  $\nabla^2$  operator indicates the second partial derivatives with respect to the x, y, and z directions. Solutions which satisfy equation (2.8) can be of the form:

$$p(x, y, z, t) = P_0 (\cos k_x x) (\cos k_y y) (\cos k_z z) e^{j\omega t} \quad (2.9)$$

provided the constants  $k_x$ ,  $k_y$ , and  $k_z$  satisfy

$$k = \frac{\omega}{c} = \sqrt{k_x^2 + k_y^2 + k_z^2} \quad (2.10)$$

These constants are also related to "component" wavelengths, the wavelengths associated with the three coordinate axes, by

$$k_x = \frac{2\pi}{\lambda_x} = \frac{n_x \pi}{\ell_x} \quad (2.11a)$$

$$k_y = \frac{2\pi}{\lambda_y} = \frac{n_y \pi}{\ell_y} \quad (2.11b)$$

$$k_z = \frac{2\pi}{\lambda_z} = \frac{n_z \pi}{\ell_z} \quad (2.11c)$$

The characteristic frequencies in the room are restricted to values such that<sup>3</sup>

$$f = \frac{\omega}{2\pi} = \frac{c}{2} \sqrt{\left(\frac{n_x}{\ell_x}\right)^2 + \left(\frac{n_y}{\ell_y}\right)^2 + \left(\frac{n_z}{\ell_z}\right)^2} \quad (2.12)$$

This analysis may appear to contradict the previously stated reverberant field conditions of uniform energy density and absence of a preferred direction of propagation. Equation (2.9) does, in fact, show that the pressure waves in a reverberant enclosure, at a normal mode frequency of the enclosure, are highly directional. The acoustic energy density, which is proportional to the pressure squared, will also vary widely in a room excited at a single normal mode frequency. Therefore, in order to obtain a diffuse field, the room must be excited by a number of normal mode frequencies. Stated differently, a diffuse field can be established in a reverberant room only if the room is excited by a signal that has energy distributed in a band of frequencies; e.g., by a random signal.

The exact number of modes that are excited in a given band of frequencies can be determined from equation (2.12). As an example, consider a room with dimensions  $\ell_x=30$ ,  $\ell_y=40$ , and  $\ell_z=50$  feet. The (1,1,1) mode ( $n_x=n_y=n_z=1$ ) is seen to be 25.2 Hz, the (1,1,2)

mode is 31.5 Hz, and so on. Each of these normal mode frequencies can be considered to be a vector in a frequency space with orthogonal axes  $f_x$ ,  $f_y$ , and  $f_z$ . The total number of modes below a given frequency,  $f$  is then approximated by

$$N = \frac{4\pi}{3c^3} V f^3 \quad (2.13)$$

where  $V$  is the volume of the room. Differentiation of equation (2.13) yields an expression for the number of modes,  $\Delta N$ , within a band of frequencies of  $\Delta f$  centered at a frequency  $f$ :

$$\Delta N = \frac{4\pi V}{c^3} f^2 \Delta f \quad (2.14)$$

A minimum of 10 modes should be excited within a given band in order to achieve uniform energy density throughout the volume of the room, and thereby establish a reasonably diffuse field in the room.<sup>4</sup>

The present study is concerned with sonic fatigue, so we need some means to relate the above properties of the test room to the response of the structure undergoing sonic fatigue testing. The test enclosure/structural response dependence begins with the principle that most of the energy acceptance of a structure occurs near the normal mode frequencies of the structure. Just how near the excitation frequency must be to the normal mode frequency is determined by the damping of the structure. Panel structures of the type commonly used in aerospace structures have low damping, typically  $\zeta < 0.02$ . The bandwidth of a normal mode frequency,  $\Delta f$ , for a panel with damping ratio  $\zeta$ , is approximated from

$$\Delta f = 2\zeta f \quad (2.15)$$

This expression combined with equation (2.14), yielding

$$N = \frac{8\pi V \zeta f^3}{c^3} \quad (2.16)$$

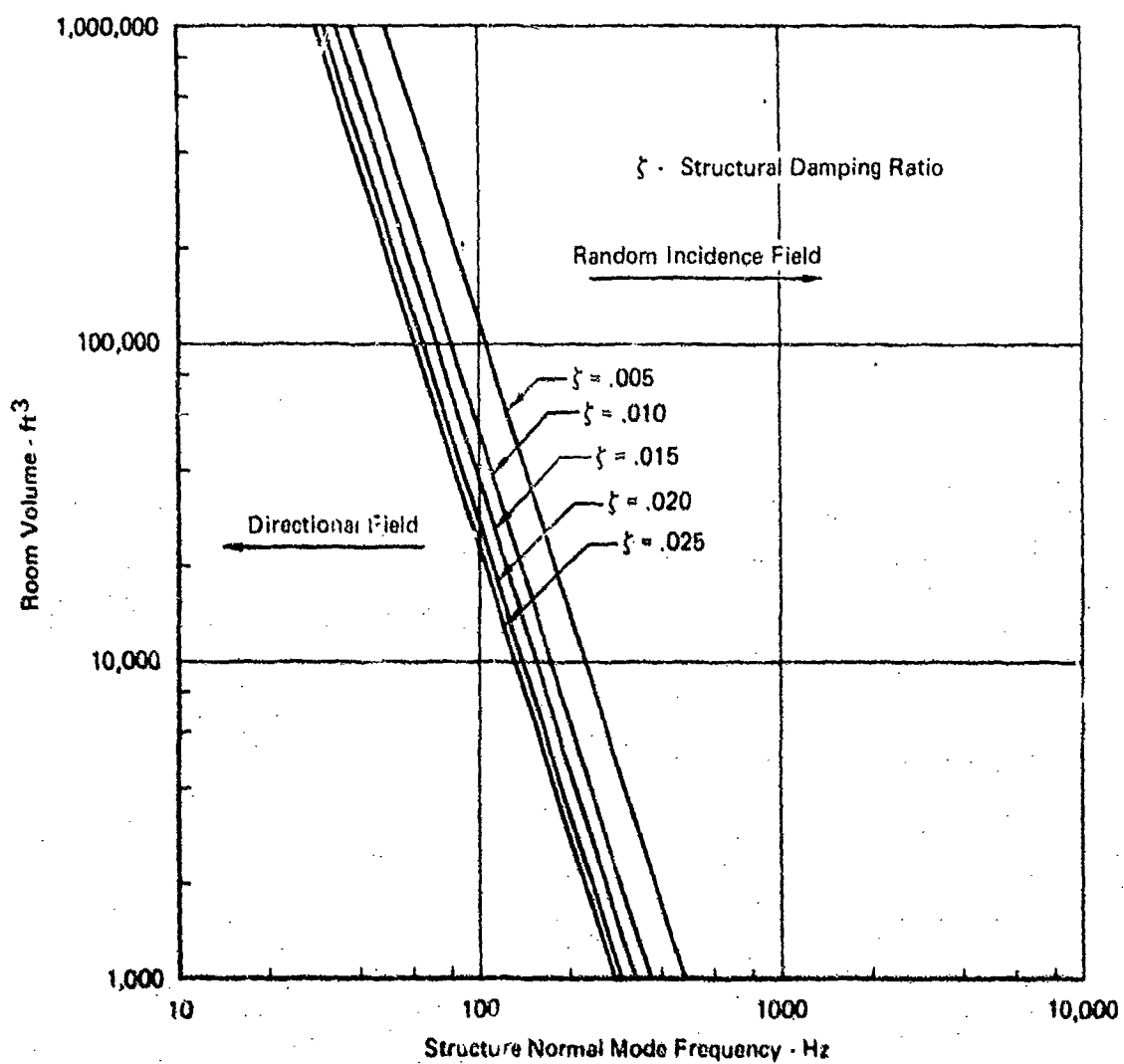
Equation (2.16) thus shows the number of room modes that will be excited within a structural resonant bandwidth, for a resonance with a center frequency  $f$  and damping ratio  $\zeta$ . If the previously stated criterion of 10 modes is applied, equation (2.16) may be solved for  $V$ , the room volume. Figure 2 presents a family of curves, for various values of  $\zeta$ , for the lowest frequency at which 10 modes are excited in a given room volume. At frequencies below this minimum frequency, the acoustic field will become more directional and will have properties similar to the progressive wave fields. Above the minimum frequency, the acoustic field is diffuse, with a corresponding absence of directional properties.

Pressure distributions in a large room excited by a random source cannot be described with exact expressions, as was the case for simple harmonic sources. The pressures must instead be discussed in terms of their power spectra or correlation functions. For example, the normalized cross-power spectrum for a bandwidth-limited random acoustic field is given by<sup>5</sup>

$$C_{p_i, p_j}(r_i, r_j, \lambda) = \frac{\sin \frac{2\pi(r_i - r_j)}{\lambda}}{\frac{2\pi(r_i - r_j)}{\lambda}} \quad (2.17)$$



FIGURE 2  
STRUCTURAL RESONANCES  
10 Enclosure Normal Modes



where  $\lambda$  is the wavelength associated with the upper frequency of the band, and the indices  $i$  and  $j$  represent locations in the field. This expression is valid for a diffuse field in which a large number of room modes are excited within the bandwidth of the structure. The value of the function depends on the separation between two points in the field rather than the exact location at which the function is measured. If the size of the enclosure is such that only a very few normal modes of the enclosure are excited, then the random acoustic field becomes directional. For this case, the normalized cross-power spectral density can be approximated by

$$C_{p_i p_j}(x, y, z, f) = (\cos k_x x_i)(\cos k_y y_i)(\cos k_z z_i)(\cos k_x x_j)(\cos k_y y_j)(\cos k_z z_j) \quad (2.18)$$

where  $k_x$ ,  $k_y$ , and  $k_z$  represent the wave numbers of the characteristic frequencies of the enclosure in the  $x$ ,  $y$ , and  $z$  directions, as defined in equation (2.11).

Studies described in the remainder of this section will consider acoustic fields which can be described by the simple trigonometric functions.

## 2.2 ACOUSTIC COUPLING

A description of the acoustic field in a sonic fatigue test is one of two elements needed to estimate the response of a structural specimen in an acoustic environment. The other factor involves the dynamic properties of the structure itself. In this section, the important dynamic characteristics of test specimens will be discussed, and methods will be shown for coupling the acoustic fields with the structures to provide an estimate of the structural response.

The structural system considered here is assumed to be a linear system, such that the free vibrations of the system can be described by a set of homogeneous second-order linear differential equations,<sup>6</sup>

$$[M] \{\ddot{w}\} + [C] \{\dot{w}\} + [K] \{w\} = 0 \quad (2.19)$$

If the damping term is momentarily neglected, the set of equations can be solved to give the undamped natural frequencies of the structural system, and the corresponding mode shapes. Letting  $[\Phi]$  represent the mode shapes, we can introduce the transformation matrix

$$\{w\} = [\Phi] \{\eta\} \quad (2.20)$$

where  $\eta$  is the normal coordinate. Substitution of equation (2.20) into equation (2.19) and pre-multiplication by the transpose of the modal matrix permits the equations of motion to be re-written in normal coordinates as

$$\{\ddot{\eta}\} + [2\xi\omega_n] \{\dot{\eta}\} + [\omega_n^2] \{\eta\} = 0 \quad (2.21)$$

Equation (2.21) includes the effect of proportional damping, and displays the natural frequencies of the structure,  $\omega_n$ . Note that the matrices containing  $\xi$  and  $\omega_n$  are diagonal. This property has the effect of uncoupling each equation from the others. Later in this Section, a normalized forcing function known as the participation factor will be introduced that permits the response at each mode to be estimated by using the uncoupled equations of motion in normal coordinates.

Returning to equation (2.21), we consider a system whose normal mode frequencies and damping properties are known. This equation describes  $n$  single-degree-of-freedom systems whose responses combine linearly to describe the behavior of the total system.

The response of the system at each normal mode frequency can be discussed in terms of the angular frequency and the damping. The angular frequency of the  $n^{\text{th}}$  normal mode is denoted by  $\omega_n$ . At that frequency, the effect of damping in the system is described by  $\xi_n$ , where  $\xi$  is the non-dimensional damping ratio. If a single-degree-of-freedom system characterized by  $\omega_n$  and  $\xi_n$  is excited by a unit impulse function  $\delta(t)$ , the response of the system is commonly designated by  $h(t)$ , the unit impulse response function.

From  $h(t)$ , another widely used property of dynamic systems, the complex frequency response  $H(\omega)$ , can be defined as

$$H(\omega) = \int_{-\infty}^{\infty} h(t)e^{-j\omega t} dt \quad (2.22)$$

The form of the integral in equation (2.22) indicates the frequency response function is the Fourier transform of the impulse response function,  $h(t)$ . The complex frequency response function for a single degree of freedom system in non-dimensional form is

$$H(\omega) = \frac{1}{1 - \left(\frac{\omega}{\omega_n}\right)^2 + j2\xi_n \frac{\omega}{\omega_n}} \quad (2.23)$$

For typical aerospace structures, equation (2.23) describes the system at each of the  $n$  normal mode frequencies of the distributed structure.

Another property of the vibrating structural specimen is the dynamic mode shape assumed by the structure at a normal mode frequency. For the present, panel mode shapes will be represented by characteristic beam functions. This simplification will clarify the acoustic field/structural response coupling that is of primary interest here. For example, consider a panel with simply supported edges, and length  $\ell$ . The normalized mode shape along the  $x$ -dimension of the panel, as  $x$  varies from 0 to  $\ell$ , may then be represented by

$$\Phi_x = \sin \frac{2\pi x}{\lambda_r} \quad (2.24)$$

where

$$\lambda_r = \frac{2\ell}{n} \quad (n = 1, 2, 3, \dots) \quad (2.25)$$

The term  $\lambda_r$  represents the wavelength of the structural response mode. Note that for  $n=1$ , the mode shape function is a simple half-sine wave, with maximum deflection at the center of the panel. For  $n=2$ , a full sine-wave mode shape results.

The expressions for pressure distribution developed in Section 2.1 can now be combined with the mode shape functions to yield a parameter known as the participation factor,  $\Gamma$ , defined for one dimensional continuous system by

$$\Gamma_x = \frac{1}{\ell} \int_0^{\ell} p(x) \Phi_x(x) dx \quad (2.26)$$

The two-dimensional case, which includes panels, is a logical extension of equation (2.26). Since both the pressure distribution and the mode shape are separable functions of  $x$  and  $y$ , the participation factor for panels can likewise be represented by a product of the participation factors in the  $x$  and  $y$  directions.

$$\Gamma_{x,y} = \Gamma_x \Gamma_y \quad (2.27)$$

The participation factor is a measure of the extent to which each mode shape  $\Phi$  participates in the response of the structure to a given pressure distribution,  $p(x)$ . It is the mean value of the product of the structural mode shape and the pressure distribution along the structure. When the structural mode shape and the pressure distribution have the same phase relationship, strong coupling exists between the acoustic field and the structure, and significant structural response will result. To illustrate the value of the participation factor in estimating the structural response, equation (2.21) can be rewritten with the excitation expressed in terms of the participation factor for the  $r$ th mode as

$$\ddot{\eta}_r + 2\zeta_r \omega_r \dot{\eta}_r + \omega_r^2 \eta_r = \frac{P_0}{M_r} \Gamma_r p(t) \quad (2.28)$$

The solution to equation (2.28) can be stated in terms of the previously-developed complex frequency response function  $H(\omega)$ . For a simple harmonic excitation at a frequency  $\omega_0$ , the normalized response in the  $r$ th mode is given by

$$\eta(\omega_0) = \frac{P_0 \Gamma_r}{\omega_r^2 M_r} H(\omega) F(\omega_0) \quad (2.29)$$

This result, which is derived in Appendix A, is readily extended to any periodic function that can be separated into its harmonic components through a Fourier series analysis. At each of the  $m$  harmonics of the fundamental frequency, the solution becomes

$$\eta(m\omega_0) = \frac{P_0 \Gamma_r}{\omega_r^2 M_r} H(m\omega_0) F(m\omega_0) \quad (2.30)$$

The response of the structure is found by making the transformation from normal coordinates back to the original coordinate system,

$$\{w(\omega_0)\} = \{\Phi\} \{\eta(\omega_0)\} \quad (2.31)$$

For random forcing functions, the excitation and response of the system will be expressed in terms of power spectral density functions. The excitation can be represented by  $\{S_p\}$ , a matrix containing the auto- and cross-power spectral densities of the excitation in normal coordinates. Then, with the complex response frequency  $H(\omega)$  as defined earlier, the response is

$$\{S_\eta\} = \left[ H^*(\omega) \right] \{S_p\} \left[ H(\omega) \right] \quad (2.32)$$

where  $\{S_\eta\}$  is the matrix of power spectral density functions for the normalized responses

In terms of the participation factors, equation (2.32) is rewritten as

$$\{S_\eta\} = \left[ H^*(\omega) \right] \left[ \Gamma_i \Gamma_j \right] \left[ H(\omega) \right] S_{p_i p_j} \quad (2.33)$$

where the  $\Gamma$  terms are the participation factors for the  $i^{\text{th}}$  and  $j^{\text{th}}$  modes.  $S_{p_i p_i}$  is the auto-power spectral density of the excitation pressure at some arbitrary point in the acoustic field.

For structural panels, the dissipation is usually low, and the equations relating the response to the excitation can be simplified, as discussed in Appendix A. In equation (2.33), the off-diagonal terms may be neglected, yielding

$$S_{\eta} = \left[ |\Gamma|^2 |H(\omega)|^2 \right] S_{p_i p_i} \quad (2.34)$$

This result shows that the response in normal coordinates is reduced to a function of the participation factors and the frequency response functions. The response may be stated in terms of the original coordinate system by making the transformation from normal coordinates,

$$[S_w] = [\Phi] [S_{\eta}] [\Phi]^T \quad (2.35)$$

Continuing with the participation factor concept, we can now show how the pressure distributions and mode shapes are related to produce significant excitation on a test specimen. As an example, the pressure distribution in a progressive wave section with perfectly anechoic termination was given in equation (2.2). Neglecting the time-varying component and rewriting equation (2.2), we can express the spatial distribution of the pressure by

$$p(x) = \left[ \cos \frac{2\pi x}{\lambda_p} + j \sin \frac{2\pi x}{\lambda_p} \right] \quad (2.36)$$

Equation (2.36) is for a system with geometry as shown in Figure 1. The addition of a constant to the distance variable  $x$  in this equation would cause the pressure distribution to be correspondingly shifted along the  $x$  axis. Equation (2.36) is derived in Appendix A.

From equation (2.24), we can now select a mode shape which we wish to examine for its coupling with the above pressure distribution. If we let  $n=1$ , the participation factor for this combination of pressure distribution and mode shape is evaluated as

$$\Gamma_R = \left| \frac{1}{L} \int_0^L \cos \frac{2\pi x}{\lambda_p} \sin \frac{2\pi x}{\lambda_1} dx \right| \quad (2.37a)$$

and

$$\Gamma_I = \left| \frac{1}{L} \int_0^L \sin \frac{2\pi x}{\lambda_p} \sin \frac{2\pi x}{\lambda_1} dx \right| \quad (2.37b)$$

The subscript R and I are used to denote real and imaginary components, to account for the imaginary operator in the  $p(x)$  expression. The components are combined to give the absolute value of the magnitude of the participation factor for the progressive wave section with perfectly anechoic termination.

$$\Gamma = (\Gamma_R^2 + \Gamma_I^2)^{1/2} \quad (2.38)$$

Participation factors for other terminations, where the pressure distribution is represented by a single real trigonometric function, are found in a similar manner. Only a real value for  $\Gamma$  will result, as in equation (2.37a). For a progressive wave section with a rigid termination, the pressure distribution takes the form

$$p(x) = P_0 \cos \frac{2\pi x}{\lambda_p} \quad (2.39)$$

where the exact location of the distribution within an enclosure can be shifted by adding a constant to the  $x$  variable. The participation factor for  $n=1$  mode now becomes

$$\Gamma = 1/l \int_0^l \cos \frac{2\pi x}{\lambda_p} \sin \frac{2\pi x}{\lambda_r} dx \quad (2.40)$$

It is interesting to compare the progressive wave test section with a normal incidence test section. In normal incidence testing, the acoustic waves travel in a direction perpendicular to the test specimen surface, and the excitation pressure is essentially uniform across the specimen. At low values of wavelength ratio, where the structural response wavelength is much less than the acoustic excitation wavelength, the pressures are also uniform along the specimen. Under the condition of low wavelength ratio, a consideration of the specimen response would show no difference between the progressive wave test section and the normal incidence arrangement.

The participation factor provides some insight into the coupling between the potentially large number of combinations of structural modes and excitation frequencies. In the above expressions for  $\Gamma$ , the term  $\lambda_r$  represents the wavelength of the structural response, as related to the geometry of the structure according to equation (2.25).  $\lambda_p$ , on the other hand, is the wavelength associated with the excitation pressure frequency, as determined from the usual relationship between wavelength, velocity of propagation, and frequency,

$$\lambda_p = c/f \quad (2.41)$$

We can now define a new parameter, wavelength ratio,  $\lambda_r/\lambda_p$ , such that

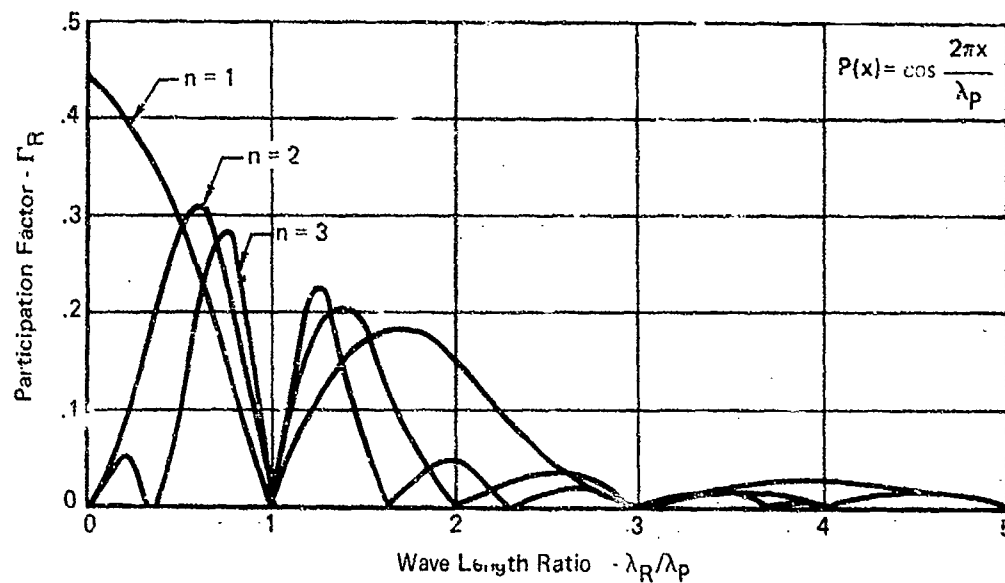
$$\text{wavelength ratio} = \frac{\lambda_r}{\lambda_p} = \frac{2\pi n}{c/l_p} = \frac{2\pi n l_p}{nc} \quad (2.42)$$

Using wavelength ratio as an independent variable, participation factors can be evaluated for various structure modes; that is, for a given value of  $n$ , the participation factor  $\Gamma$  can be evaluated as the wavelength ratio is allowed to vary. Figure 3 is a family of curves for the participation factor, as given in equations (2.37), for a progressive wave section with perfectly anechoic termination. The participation factors are presented as RMS quantities to facilitate addition of components. The in-phase component of participation factor has a maximum value for the first structural mode ( $n=1$ ) at a wavelength ratio of zero. This represents the case where the wavelength of the excitation pressure is much larger than the structural response wavelength, so that the structure appears to be excited by a pressure distribution that is uniform across the structure. The higher order modes have a maximum value of participation factor near a wavelength ratio of one. The quadrature component of participation factor always has a maximum value at a wavelength ratio of one, and a value of zero at a wavelength ratio of zero. It is significant that the participation factor becomes very small for wavelength ratios greater than five. At larger wavelength ratios, acoustic energy becomes very inefficient as a mechanism for producing stress in a structural specimen. In Figure 4, the total participation factor has been plotted, according to equation (2.38).

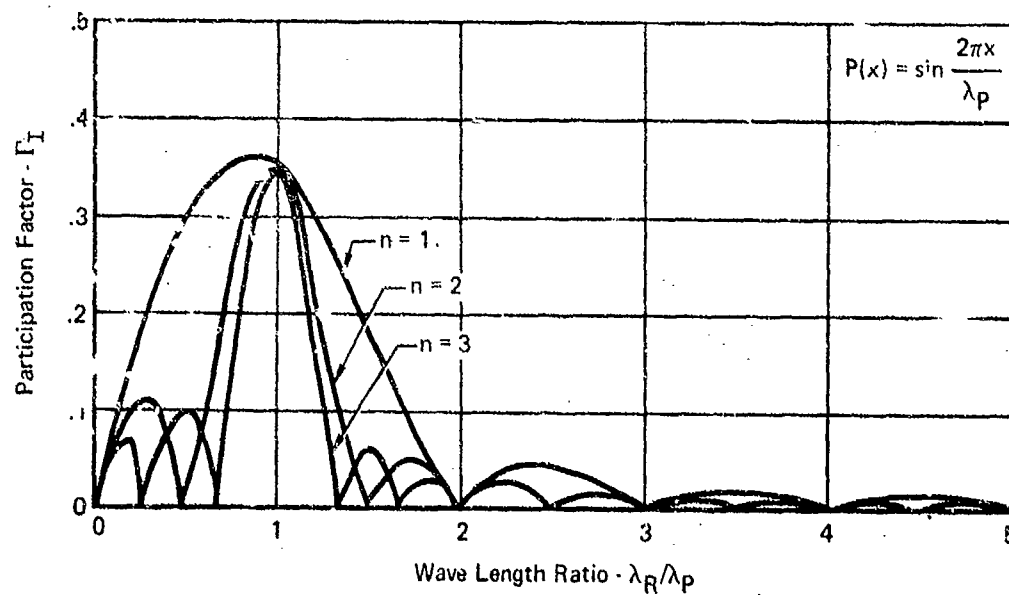
FIGURE 3  
PARTICIPATION FACTOR VARIATION

One Dimensional - Progressive Wave  
Anechoic Termination

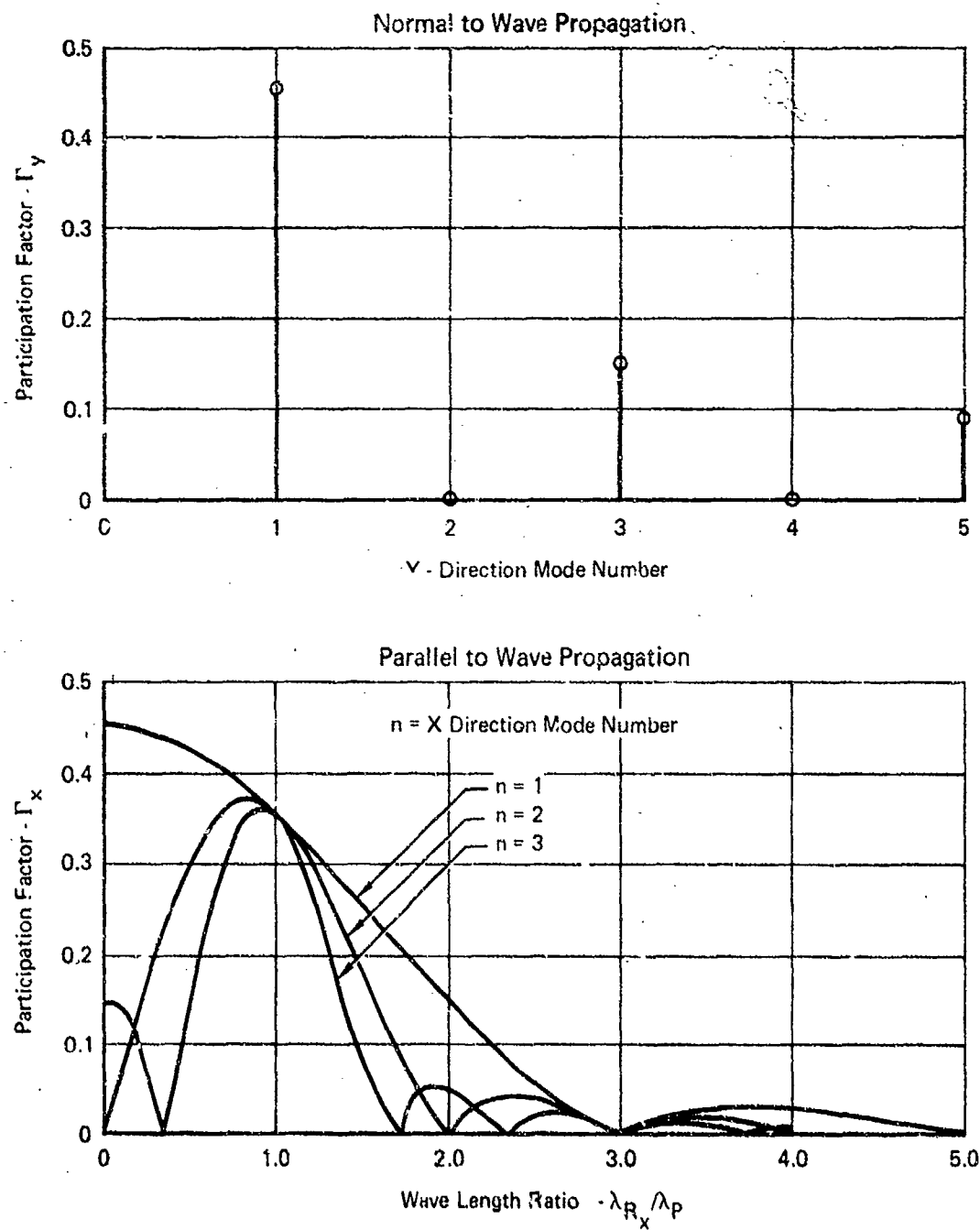
Real Component



Imaginary Component



**FIGURE 4**  
**PARTICIPATION FACTOR VARIATION**  
 Two Dimensional - Progressive Wave  
 Anechoic Termination





The above discussions have considered only those structural modes in the x direction, the direction of the pressure distribution. In a progressive wave test section, the pressure is essentially uniform in the y direction (perpendicular to the wave propagation). Therefore, if we consider the structural modes in the y direction, the participation factor will be zero for all the odd-number modes. This result is plotted in Figure 4, where the participation factor has been calculated from an expression similar to equation (2.26) except that the variable has been replaced by y. With uniform pressure distribution in the y direction,  $p(y)$  becomes a constant, and the points shown in Figure 4 result from integrating the simple trigonometric mode shapes. As in the case for participation factors in the x direction, it is apparent that the acoustic-structural coupling is very poor at all wavelength ratios except ratios near unity.

As examples of how the wavelength ratio and participation factor concepts can be used to estimate structural response, two types of structural configurations - beams and plates - will be considered here. This discussion will assume that the excitation frequency coincides with the structural resonance frequency, again recognizing that the acceptance of energy by structural members occurs principally at resonances. For rectangular cross-section beams, the bending frequencies are determined from

$$f_r = a_i \frac{h}{\ell^2} \sqrt{\frac{E}{\rho}} \quad (2.43)$$

where  $h$  and  $\ell$  are the thickness and length of the beam, respectively, and  $a_i$  is a constant determined by the end conditions of the beam and the order of the mode being considered. For many commonly used engineering materials, the  $E/\rho$  ratio does not change widely, and a value of  $1.02 \times 10^8$  (inches) was used here. The expression for the resonant frequency of the structure may then be written as

$$f_r = a_i \frac{h}{\ell^2} \quad (2.44)$$

to show the desired dependence on thickness and length only. If we now constrain the frequency of the excitation pressure,  $f_p$ , to be equal to the structural resonance, and solve for the wavelength of the pressure from equation (2.41), we obtain

$$\lambda_p = c/f_p = \frac{c}{a_i h/\ell^2} = \frac{c\ell^2}{a_i h} \quad (2.45)$$

Finally, using the expression for structural response wavelength as given in equation (2.25) for the first resonant mode of the beam ( $n=1$ ), the wavelength ratio is determined as

$$\lambda_r/\lambda_p = \frac{2\ell}{c\ell^2/a_i h} = \frac{a_i}{c} h/\ell \quad (2.46)$$

where the new constant,  $a_i''$ , includes the effect of boundary conditions, mode number, speed of sound and physical properties of the beam material. The values of wavelength ratio for three end conditions for beams, as a function of  $h/l$ , are plotted in Figure 5. These curves, then, become the first step in estimating the response of a beam to an acoustic excitation. From the  $h/l$  ratio and end conditions of the beam, the wavelength ratio is determined directly from the curve. The wavelength ratio is used to enter a curve of participation factor for the type of acoustic field being considered, as for example, Figure 3. The relative magnitude of the participation factor gives an indication of the effectiveness of a given test method for inducing response in a structure.

Square panel structures have been treated in a manner similar to the beam analysis, and the results are plotted in Figure 6. Three edge conditions are considered for panels: fixed, simply supported, and free. As in the case of the beams, results are shown only for the first mode resonances. For panels, however, it is important to show how the wavelength ratio changes with higher order modes. The curves in Figures 7, 8, and 9 are plots of normalized wavelength ratios for square plates. Values of mode-number in the x-direction are used as the abscissa, while mode-numbers in the y direction are shown as constant lines on the plot. The structural response wavelength in the x direction (direction of acoustic propagation) has been used in the numerator of the wavelength ratio expression. Each wavelength ratio is normalized relative to the wavelength ratio for the first mode,

$$\frac{\lambda_{rx}}{\lambda_p} = \frac{\lambda_{rx}/\lambda_p}{(\lambda_{rx}/\lambda_p)_{m=1, n=1}} \quad (2.47)$$

Examination of Figures 7, 8, and 9, along with a plot of the participation factor for the type of acoustic enclosure used on a particular test, provides some insight into the coupling that might be expected between a specimen and an acoustic field.

### 2.3 TEMPERATURE EFFECTS ON ACOUSTIC FIELDS

Experiments were conducted to determine the effect of thermal energy on the acoustic field. The experimental apparatus (described in more detail in Section 4, Figure 26) consisted of a rectangular cross-section test enclosure with a bank of 16 quartz lamps, each rated at 1600 watts, heating a 15-inch-square panel. Tests were conducted at panel temperatures ranging from 150°F to 475°F. Measurements were made to determine the power required to hold the panel center temperature at various levels, both in still air and with an air flow over the heated panel. The results are plotted in Figure 10, where the air mass flow is shown per unit cross-section area of the enclosure. The increase in electrical power generates heat that is lost through several mechanisms - the test panel, the surrounding support structure, the lamp-bank reflector, and the air in the test section. If it is assumed that all of the increase in electrical power is converted into an increase in the gas stagnation temperature, then the increase in gas temperature can be computed from the power increase, mass flow, and specific heat from<sup>7</sup>

$$\Delta T = \frac{W}{\dot{M} C_p} \quad (2.48)$$

FIGURE 5  
FIRST MODE WAVE LENGTH RATIO.

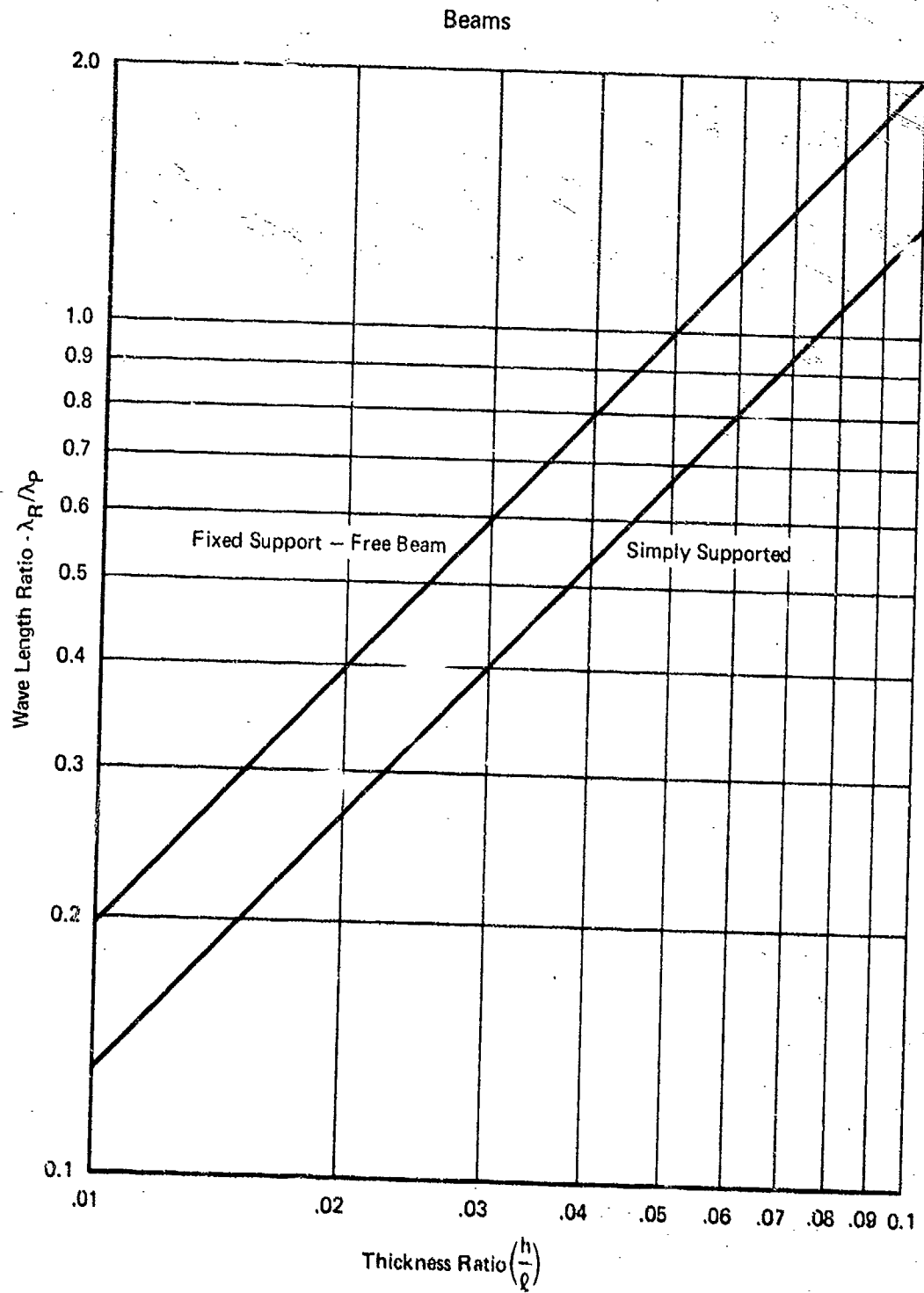


FIGURE 6  
FIRST MODE WAVE LENGTH RATIO

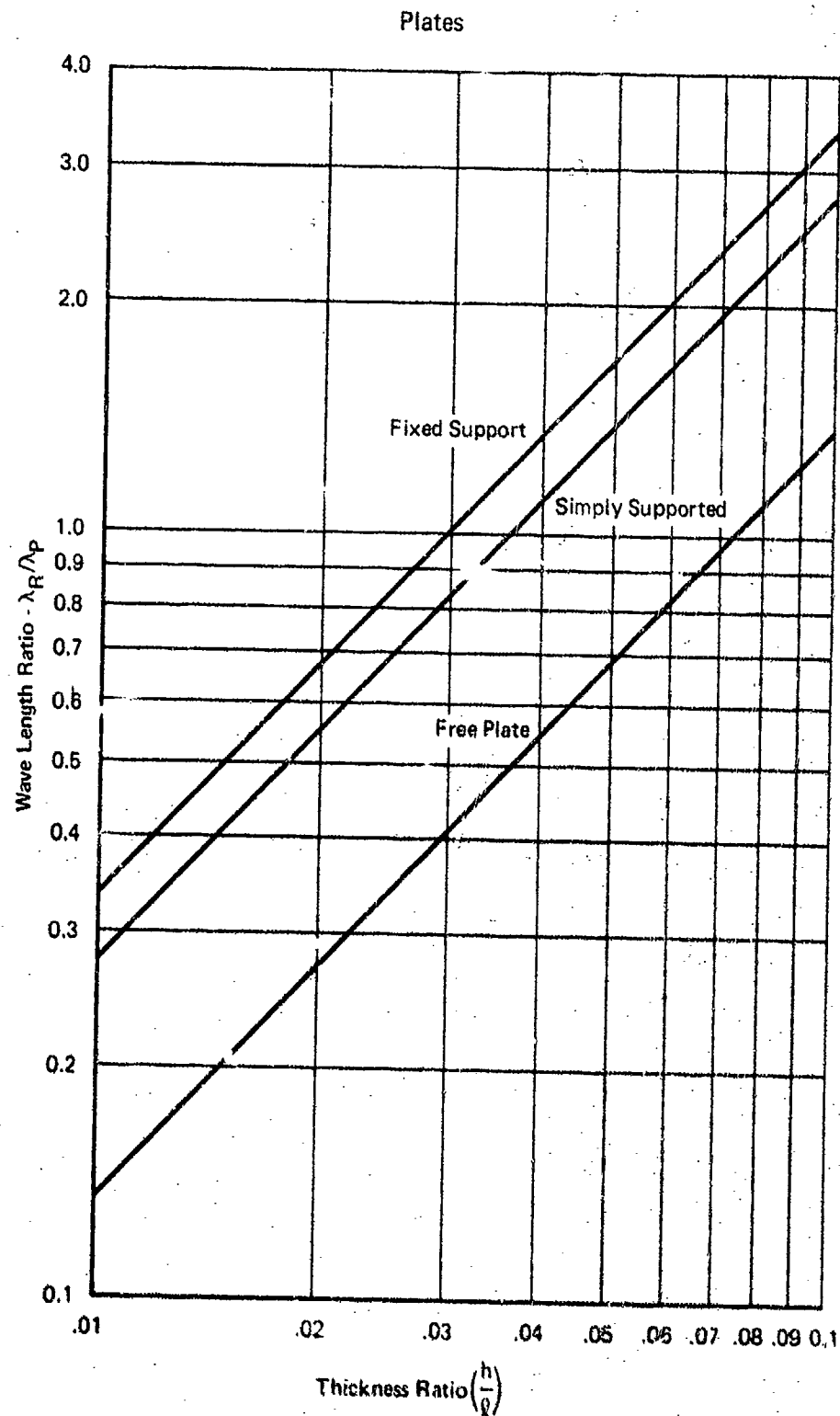


FIGURE 7  
NORMALIZED WAVE LENGTH RATIO

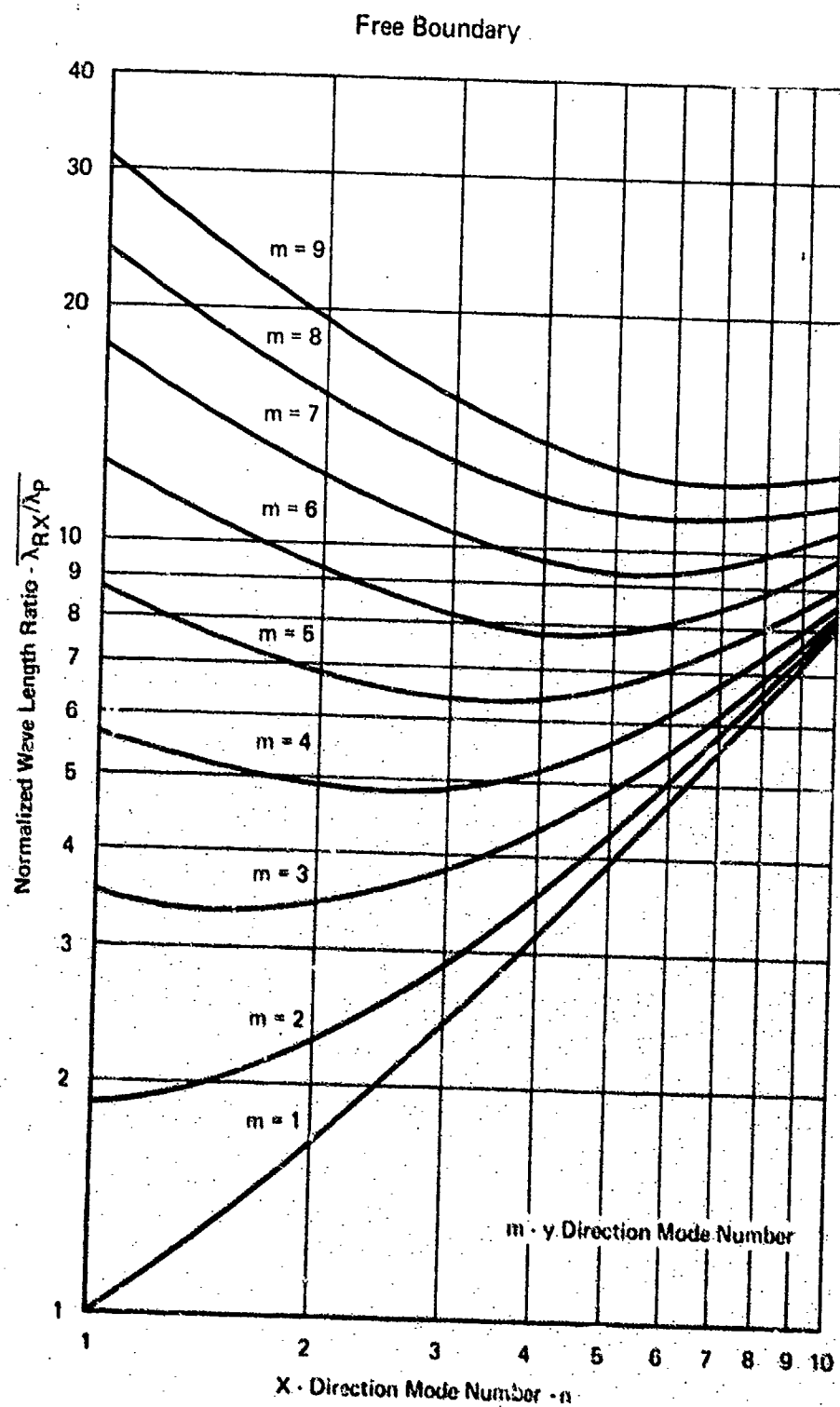


FIGURE 8  
NORMALIZED WAVE LENGTH RATIO

Fixed Boundary

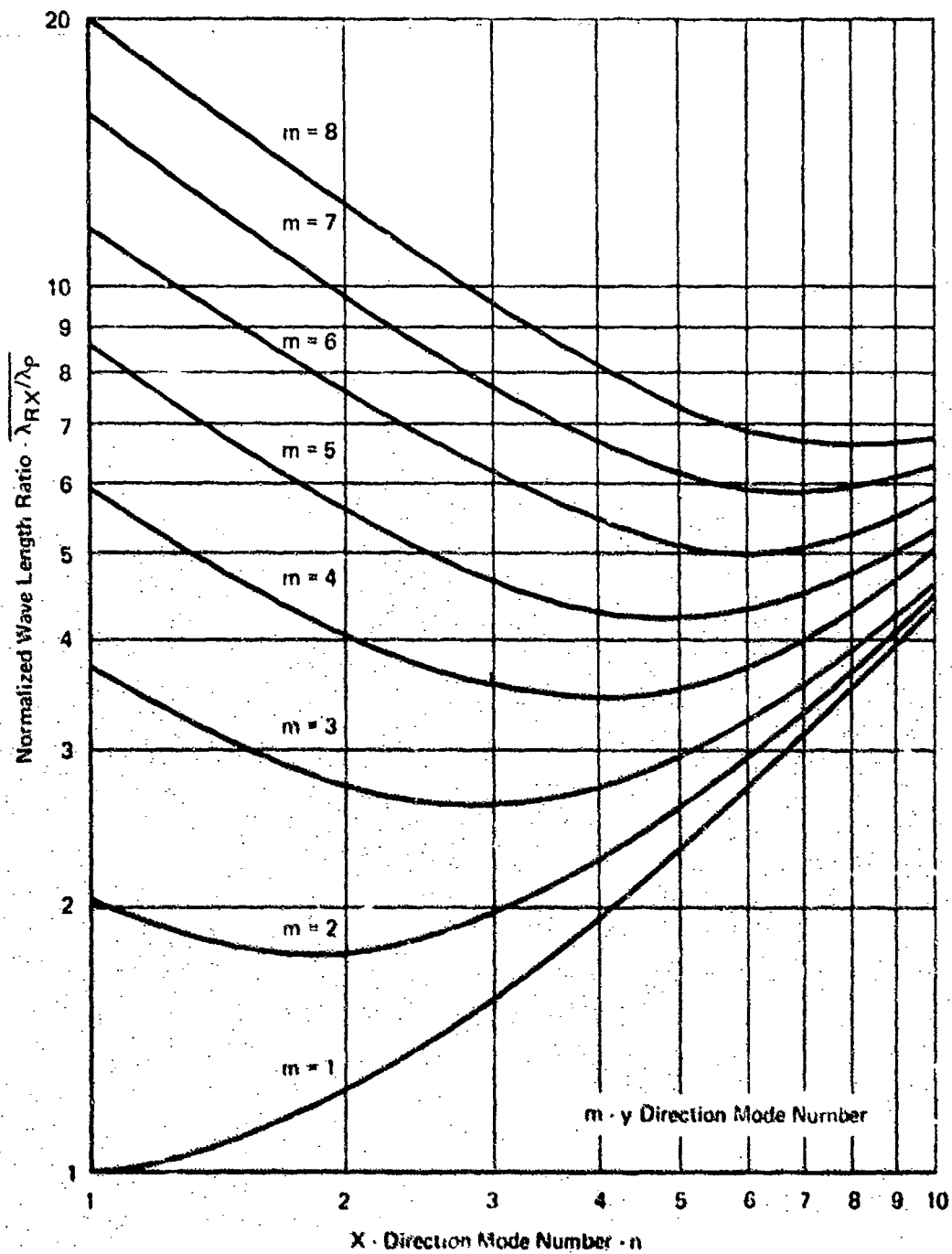


FIGURE 9  
NORMALIZED WAVE LENGTH RATIO

Simply Supported Boundary

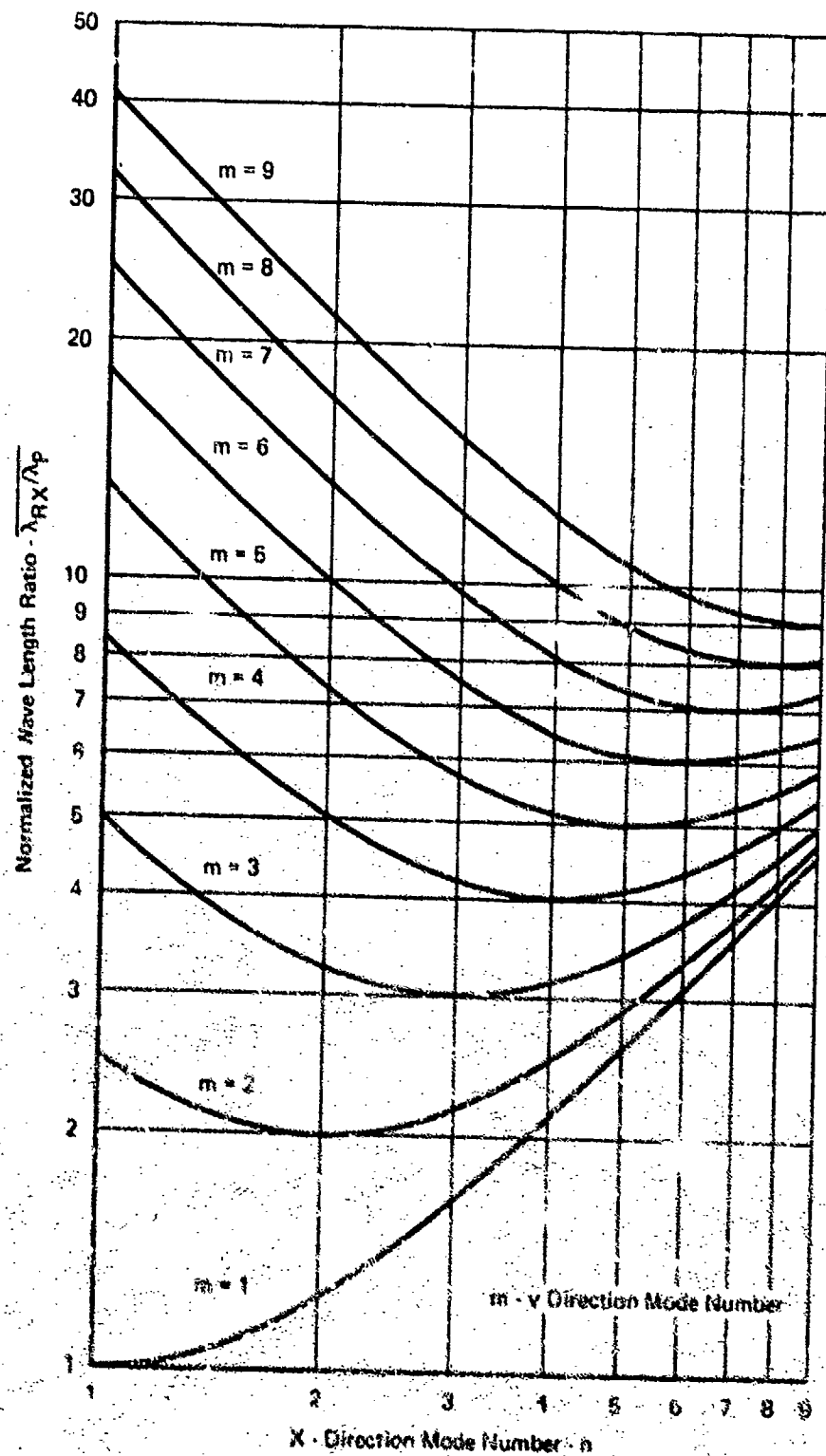
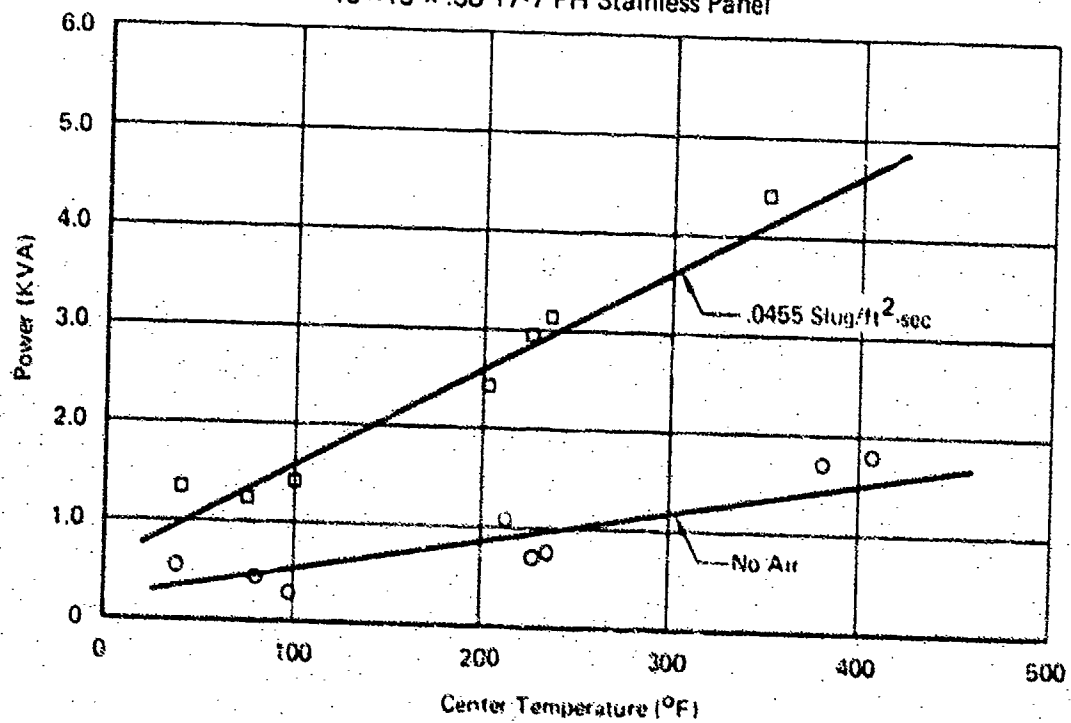


FIGURE 10  
POWER REQUIREMENTS

16-1600 W. Lamp Setup  
15 x 15 x .38 17-7 PH Stainless Panel





The increase in power at a panel temperature of 475° was approximately 2600 watts. This power increase, combined with a mass flow for the gas of 2.5 pounds per second, corresponds to an increase of 4°F in the gas temperature. This small change in gas temperature was verified by the experimental work, where no increase in gas temperature was observed. Since the increase in gas temperature can be considered negligible, corresponding changes in gas properties (speed of sound and density) can also be neglected. This conclusion is further verified by comparing the transfer functions for the pressure data in Figures 11 and 12. These curves represent transfer functions between two microphones at two temperature conditions. One microphone was located in the thermal field near the center of the panel, and its output is normalized with respect to a reference microphone located at the input to the test section, but outside of the thermal field.

The effect of a significant increase in gas temperature on the acoustic fields would be to increase  $c$ , the velocity of sound, and decrease  $\rho_0$ , the equilibrium density of the gas. These changes would invalidate the basic wave equations, which are derived on the basis of the equilibrium density and velocity of propagation being uniform throughout the medium. Introduction of spatial variations in  $c$  and  $\rho_0$  would require the derivation of a new set of wave equations. As a practical matter, however, the air flows that are normally associated with conventional acoustic noise sources, such as air-stream modulators, are sufficient to keep the air at a near-ambient temperature. Consequently, the effect of air temperature changes on the acoustic fields can be neglected in elevated temperature sonic fatigue tests.

## 2.4 TEST TECHNIQUES - ACOUSTIC ENVIRONMENT SIMULATION

Numerous test techniques are available for conducting sonic fatigue tests on panel structures. In Sections 2.1 through 2.3, the acoustic fields for sonic fatigue tests were described, and the coupling of the acoustic fields with structural specimens was discussed. In this section, earlier results will be used in a numerical example to illustrate application of those results to an experimental situation.

Before proceeding with the example, it should be noted that the ultimate objective of a sonic fatigue test is to induce a certain dynamic stress in the test specimen. In meeting this objective, it might not be necessary to simulate, in great detail, the actual in-service acoustic environment. A study of the dynamic properties of the structure should reveal the most likely service failure mode of the specimen, and the acoustic field should be tailored to achieve this failure mode in the laboratory.

The test panel selected for the present example is a square aluminum panel, with dimensions of 12 x 12 x 0.032 inches. The panel is considered to be mounted in a manner that provides simply supported edges. The first panel characteristic of interest is the thickness-to-length ratio,  $h/L$ , which is 0.0026. Extrapolation of the curve in Figure 6 gives a value of 0.073 for the first mode wavelength ratio,  $\lambda_1/\lambda_p$ . Next, we refer to Figure 9, which shows the normalized wavelength ratio for the higher order modes. The values of wavelength ratio in Figure 9 are normalized with respect to the wavelength ratio at the first mode, so the values taken from Figure 9 must be multiplied by 0.073 to give the actual wavelength ratios for this specimen. Table I presents both the normalized wavelength ratio,  $\lambda_r/\lambda_p$ , and the actual value, for mode number variations from 1 to 3 for both  $n$  ( $x$  direction) and  $m$  ( $y$  direction).

FIGURE 11  
TRANSFER FUNCTION  
PANEL CENTER PRESSURE TO REFERENCE PRESSURE  
TEMPERATURE: AMBIENT

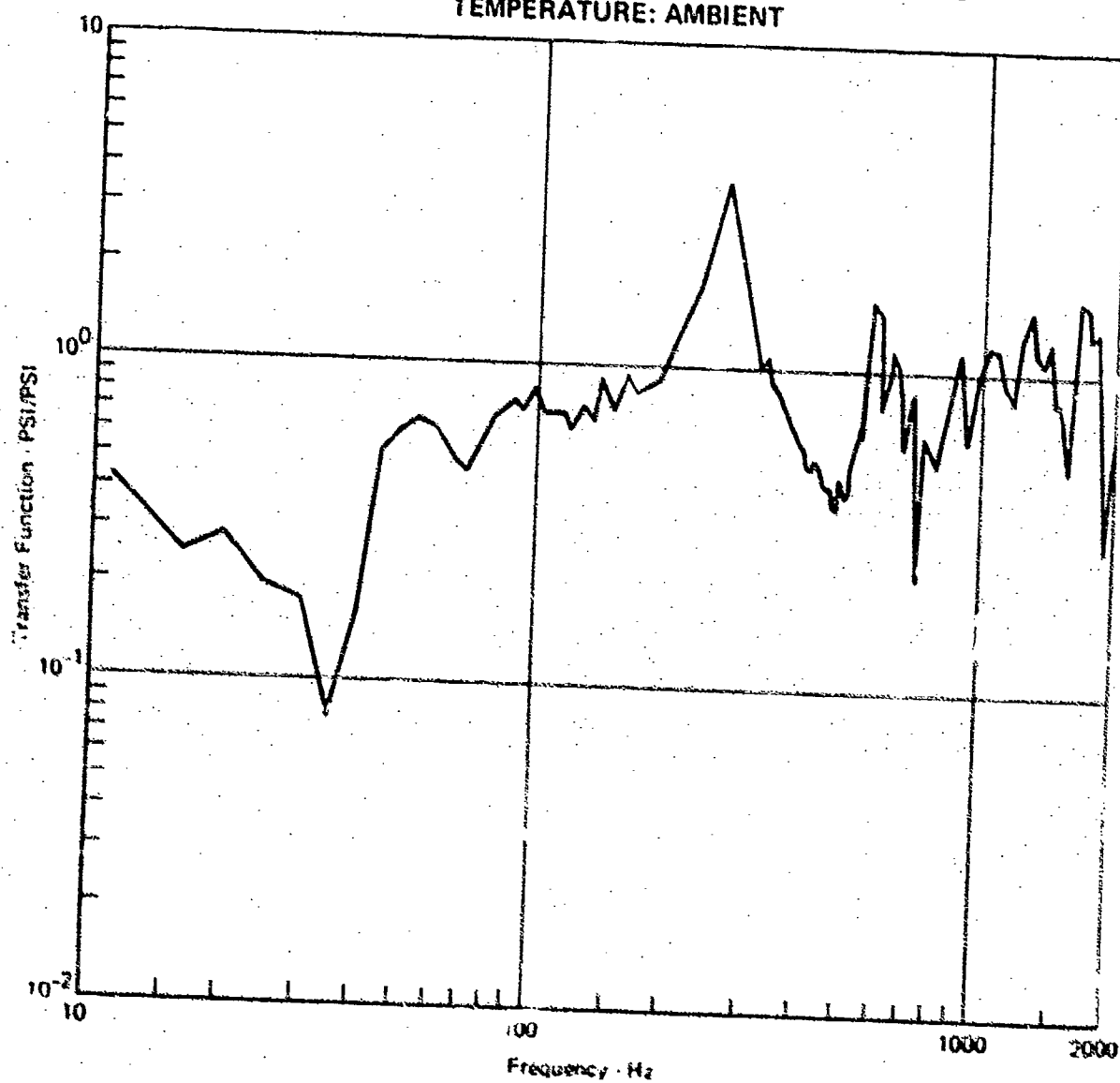


FIGURE 12  
TRANSFER FUNCTION  
PANEL CENTER PRESSURE TO REFERENCE PRESSURE  
TEMPERATURE: 475°F

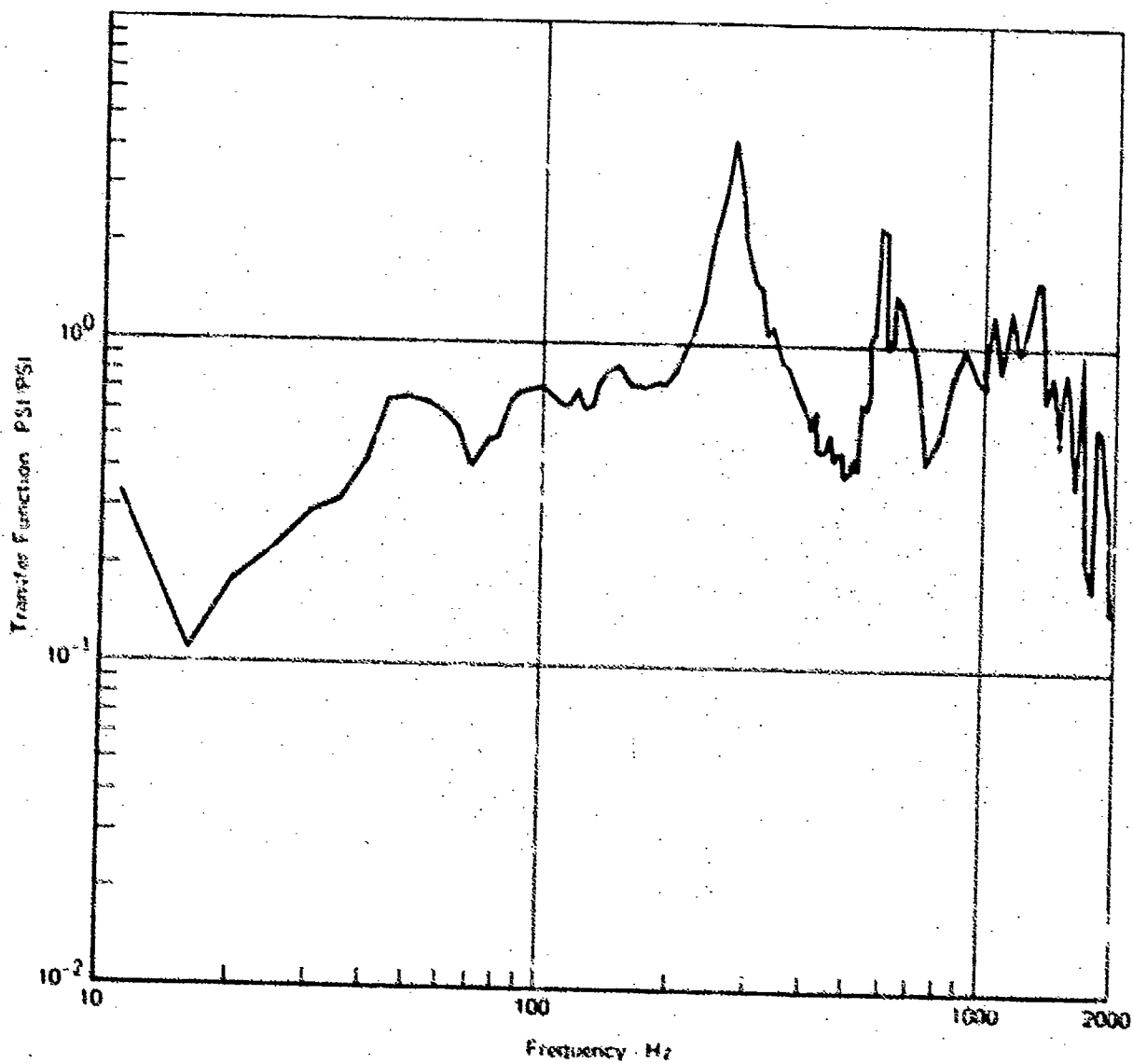


TABLE 1  
WAVELENGTH RATIO

n - Mode Number in x Direction	m - Mode Number in y Direction					
	1		2		3	
	$\lambda/\lambda_p$	$\lambda/\lambda_p$	$\lambda/\lambda_p$	$\lambda/\lambda_p$	$\lambda/\lambda_p$	$\lambda/\lambda_p$
1	1.0	0.073	2.5	0.1825	5.0	0.365
2	1.3	0.095	2.0	0.146	3.2	0.233
3	1.7	0.124	2.2	0.1606	3.0	0.219

It will now be assumed that the panel will be installed in the wall of a progressive wave test section with perfectly anechoic termination. The total participation factor will be the product of the participation factors in the x and y directions,  $\Gamma_x \Gamma_y$ , according to equation (2.27). The x and y participation factors can be taken from the curves in Figure 4. The values of participation factor are tabulated in Table 2 for the same variation in mode numbers.

An inspection of the values of  $\Gamma_x \Gamma_y$  in Table 2 shows that the first mode ( $n=m=1$ ) is the most strongly excited mode. The excitation of the next strongest mode ( $n=1, m=3$ ) is only 30% of the first mode, and the other modes are even less responsive.

Use of the wavelength ratio parameter also permits us to compare the progressive wave test section with a normal incidence test arrangement. We recall that the first mode ratio was 0.073 for the progressive wave setup, giving a participation factor 0.20. For normal incidence testing, the pressure across the specimen would be uniform, corresponding to a  $\lambda_p$  that approaches infinity, and a corresponding wavelength ratio of zero. The zero wavelength ratio for normal incidence testing gives essentially the same participation factor as that for the progressive wave section.

A similar argument can be made for testing this panel in a large reverberation chamber. In this case, we must first determine if the acoustic field appears to be directional or diffuse in the frequency range of the 1,1 mode of the panel specimen. The first mode frequency can be computed from the first mode wavelength ratio and the panel length

$$f_{1,1} = \frac{c (\lambda_x / \lambda_p)}{2\ell} \quad (2.49)$$

Equation (2.49) yields a first mode frequency of 40.5 Hz for the panel. If we now assume that the panel is lightly damped, and let  $\zeta = 0.01$  for this mode, we can enter Figure 2 and see that a room volume of approximately 600,000 ft<sup>3</sup> would be required in order to obtain a truly diffuse acoustic field at the first mode resonance. From equation (2.16), we see that a room volume of 80,000 ft<sup>3</sup> would be required to have even a single mode excited within the bandwidth of the structural resonance. The acoustic field for such a room would be considered purely directional at the first mode resonance, and the same participation factor computed for the progressive wave section would apply.

This example indicates that the choice of grazing or normal incidence field may not have much significance from a consideration of the response induced in the test specimen. Enclosures with perfectly anechoic terminations will result in both sine and cosine terms in the pressure distribution, and will consequently have a higher probability of exciting structural modes.

**TABLE 2**  
**PARTICIPATION FACTORS**

m - Mode number in y direction

n - Mode Number in x Direction	1			2			3		
	$\Gamma_x$	$\Gamma_y$	$\Gamma_x\Gamma_y$	$\Gamma_x$	$\Gamma_y$	$\Gamma_x\Gamma_y$	$\Gamma_x$	$\Gamma_y$	$\Gamma_x\Gamma_y$
1	0.44	0.44	0.20	0.44	0	0	0.44	0.15	0.06
2	0.03	0.44	0.01	0.03	0	0	0.13	0.15	0.02
3	0.13	0.44	0.05	0.13	0	0	0.08	0.15	0.01

## SECTION 3

### THERMAL ENVIRONMENT SIMULATION

Laboratory simulation of the thermal environment is an important aspect of sonic fatigue testing at elevated temperatures. The usual problems of temperature simulation are compounded by the requirement that the thermal source apparatus be capable of surviving in the high intensity acoustic sound field. This section describes a procedure for calculating the temperature distribution in a heated panel. A discussion of methods for implementing heat sources for sonic fatigue testing is then presented.

#### 3.1 THERMAL FIELD STUDIES

Prediction of the temperature distribution in a heated sonic fatigue specimen is based primarily on the intensity of the heat source and the thermodynamic properties of the test specimen. A secondary consideration is the effect of air flow associated with the acoustic noise sources in a given experimental arrangement. The latter effect will be neglected while the procedure for predicting temperatures from a radiant heat source is discussed. The analysis is described for a simple panel, but can be modified to account for such conditions as nonuniform heat flux, variable edge temperatures, and configurations that represent more complex aerospace panels.

The analytical model used is shown in Figure 13. The panel was considered to be symmetrical about a center-line parallel to the direction of air flow, with the  $i$  and  $j$  directions as shown. Square elements, with sides equal to  $\Delta x$ , were chosen for simplicity in calculation. The intersections of the grid lines were the points at which the temperature was to be computed.

At any intersection  $(i, j)$  a heat balance may be written. The algebraic sum of the conduction from each of the four neighboring intersections, plus the heat generated (absorbed) must be equal to zero in the steady state. The heat generated from absorbed radiation is expressed as

$$q_{\text{gen}} = F (\Delta x)^2 \quad (3.1)$$

where  $F$  is the absorbed radiant heat flux in BTU per second per unit area. Actual values of  $F$  that may be used in a given experimental situation will be discussed in Section 3.2.

The conduction from a neighboring intersection may be written

$$q_{\text{cond.}} = k \Delta x \Delta z \frac{(T_{i-1,j} - T_{i,j})}{\Delta x} \quad (3.2)$$

$$q_{\text{cond.}} = k \Delta z (T_{i-1,j} - T_{i,j}) \quad (3.3)$$

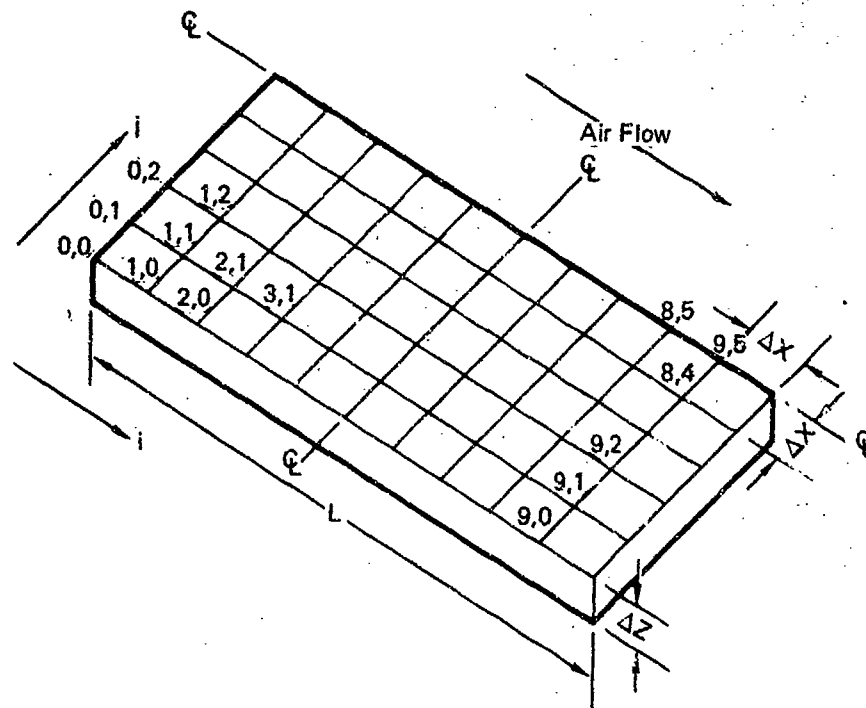
where  $q_{\text{cond}}$  is the heat conducted from the  $(i-1, j)$  intersection to the  $(i, j)$  intersection. Similar expressions are written for the three remaining intersections, and these are combined with equation (3.1) to yield the heat balance equation

$$k \Delta z [T_{i-1,j} + T_{i,j+1} + T_{i+1,j} + T_{i,j-1} - 4 T_{i,j}] + F(\Delta x)^2 = 0 \quad (3.4)$$

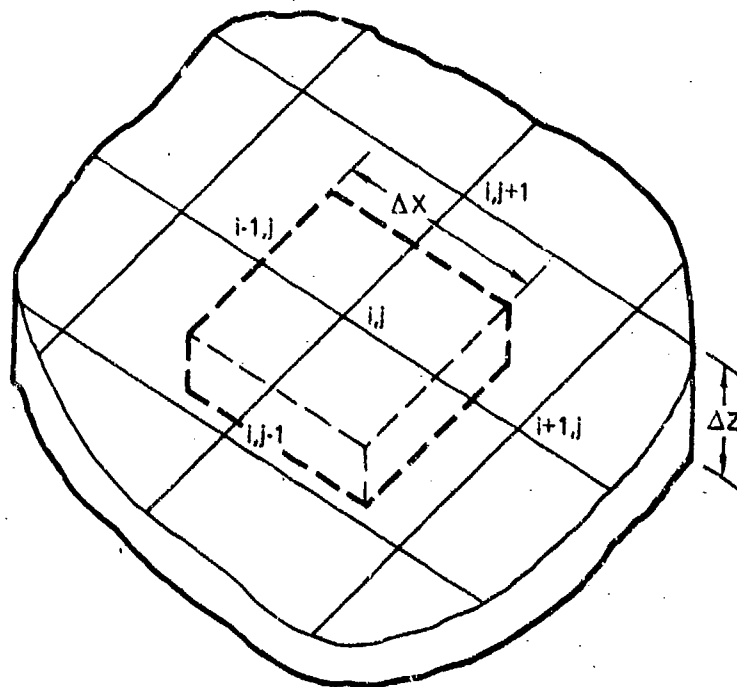
Solving for  $T_{i,j}$  yields

$$T_{i,j} = \frac{1}{4} \left[ T_{i-1,j} + T_{i,j+1} + T_{i+1,j} + T_{i,j-1} + \frac{F(\Delta x)^2}{k \Delta z} \right] \quad (3.5)$$

FIGURE 13  
ANALYTICAL MODEL FOR TEMPERATURE PREDICTION



ELEMENT OF THERMAL MODEL





Equation (3.5) must be evaluated for each intersection point on the grid. An iterative technique is used, in which an initial temperature distribution is assumed. A "new" temperature is calculated for each point using the "old" temperature for the neighboring points in the calculation. Each "new" temperature then becomes the "old" temperature for the next series of calculations, and this procedure is repeated as the difference between the "new" and "old" temperature becomes vanishingly small. When this difference is less than some specified value, the calculation is considered complete.

The analysis must also account for the radiation into and away from the test specimen. A given test setup will include an array of quartz lamp radiant heaters backed up by reflectors on as many sides as possible, consistent with the air flow requirements of the acoustic noise sources. To enhance the radiant heat transfer efficiency of the setup, the lamp array and reflectors would be placed close to the test panel.

The thermal model for the radiative heat transfer problem considers the lamp reflectors to be cooled, high reflectivity, diffuse reflecting surfaces. The specimen panel "sees" above itself a diffuse reflection of itself; i.e., another panel with approximately the same emissivity and surface temperature. The equation expressing the net radiant power transferred out of the (i, j) intersection in such a configuration is written

$$q_{out(i,j)} = \sigma F_e F_a (\Delta x)^2 (T_{i,j}^4 - T_r^4) \quad (3.6)$$

The emissivity factor,  $F_e$ , for the case of a small area  $A_1$  of emissivity  $\epsilon_1$ , surrounded by a larger area  $A_2$  of emissivity  $\epsilon_2$  can be expressed as

$$F_e = \frac{1}{1/\epsilon_1 + \frac{A_1}{A_2} \left( \frac{1}{\epsilon_2} - 1 \right)} \quad (3.7)$$

When  $A_2$  is much greater than  $A_1$ , which is the case for the assumed model, it is noted that

$$F_e \rightarrow \epsilon_1 \text{ as } \frac{A_1}{A_2} \rightarrow 0 \quad (3.8)$$

Similarly, for this geometry, the view factor  $F_a$  (ratio of the solid angle subtended by  $A_2$  from  $A_1$  to the solid angle of hemispherical space) approaches 1.0 as  $A_1/A_2$  approaches zero.  $T_r$  is the effective reradiative temperature produced by the diffuse reflector reflecting the specimen panel radiation. The reradiative temperature is considered to be spatially uniform, and equal to a fourth power average of the specimen plate temperature, as follows,

$$T_r^4 = \frac{1}{M \times N} \sum_{i=0}^M \sum_{j=0}^N (T_{i,j})^4 \quad (3.9)$$

where  $M$  and  $N$  are the number of interior grid lines on the panel in the  $i$  and  $j$  directions, respectively.

Equating the heat balance equation (equation (3.4)) to the radiant exchange (equation (3.6)) yields

$$k \Delta z [T_{i-1,j} + T_{i,j+1} + T_{i,j-1} + T_{i+1,j} - 4 T_{i,j}] + F(\Delta x)^2 - \sigma \epsilon_1 (\Delta x)^2 (T_{i,j}^4 - T_r^4) = 0 \quad (3.10)$$

Rearranging the terms yields

$$T_{i-1,j} + T_{i,j+1} + T_{i+1,j} + T_{i,j-1} - 4T_{i,j} + \frac{F(\Delta x)^2}{k\Delta z} - \frac{\sigma\epsilon_1(\Delta x)^2}{k\Delta z} (T_{i,j}^4 - T_r^4) = 0 \quad (3.11)$$

which is the basic equation to be solved for  $T_{i,j}$ . The presence of the fourth power terms complicates the solution, and so a linearization scheme has been applied to the equation. At the same time, an algorithm is used which prevents the iterative solution from diverging. In linearizing the fourth order term, the "old" temperatures are assigned the value  $A_{i-1,j}, A_{i,j+1}, \dots$  etc., while the "new" temperature remains  $T_{i,j}$ . Using this nomenclature,  $[T_{i,j}]^4$  is written as

$$T_{i,j}^4 = 4A_{i,j}^3 T_{i,j} - 3A_{i,j}^4 \quad (3.12)$$

Then, using this result in equation (3.11), the basic equation becomes

$$A_{i-1,j} + A_{i,j+1} + A_{i+1,j} + A_{i,j-1} - 4T_{i,j} + \frac{F(\Delta x)^2}{k\Delta z} - \frac{\sigma\epsilon_1(\Delta x)^2}{k\Delta z} [4A_{i,j}^3 T_{i,j} - 3A_{i,j}^4] + \frac{\sigma\epsilon_1(\Delta x)^2}{k\Delta z} T_r^4 = 0 \quad (3.13)$$

As a further simplification, two new constants are defined,

$$K = \frac{F(\Delta x)^2}{k\Delta z} \quad (3.14)$$

and

$$K_1 = \frac{\sigma\epsilon_1(\Delta x)^2}{k\Delta z} \quad (3.15)$$

Finally, solving for  $T_{i,j}$  yields

$$T_{i,j} = \frac{1}{4} \left\{ \frac{A_{i-1,j} + A_{i,j+1} + A_{i+1,j} + A_{i,j-1} + K + 3K_1 A_{i,j}^4 + K_1 T_r^4}{1 + K_1 A_{i,j}^3} \right\} \quad (3.16)$$

This equation, then, is solved in exactly the same manner as equation (3.5) for the conduction case only. A computer program for the temperature distribution, as defined in equation (3.16), is presented in Appendix B.

### 3.2 DESIGN OF HEAT SOURCES

Quartz lamp banks and their associated reflectors were used as heat sources in this study effort. While quartz lamps have been widely used in standard laboratory conditions for a number of years, the introduction of these lamp banks into a high intensity acoustic environment has brought new problems. In the following paragraphs, the overall considerations for a lamp bank design will first be considered. Then, some details of the lamp installation will be discussed.

### 3.2.1 Reflector Design Considerations

The purpose of a quartz lamp bank/reflector assembly is to convert electrical energy into thermal energy that is absorbed on a test specimen. The efficiency with which this objective is reached is a measure of the success of a given design. A number of high quality quartz lamp banks are available commercially. The specified performance of these lamp banks can be used in equation (3.14) as part of the heater design for sonic fatigue testing. The basic parameter for this purpose is the radiated heat flux from the lamp bank. For a representative lamp bank, 75 watts per inch<sup>2</sup> (approximately 10 BTU per ft<sup>2</sup>-second) can be conservatively obtained at the face of the lamp bank. This output is for each lamp in the bank, based on a lamp spacing of 1 inch between centers, and electrical power of 100 watts per inch applied to the lamps. This example represents an electrical-to-thermal power conversion efficiency of 75%. Higher flux densities may be obtained by a combination of closer lamp spacing and higher power applied to the lamps, with a corresponding decrease in the useful life and reliability of the lamp bank.

The actual value of heat flux absorbed by the specimen depends on a number of factors, such as the distance of the lamp bank from the specimen, the absorptivity of the specimen, and losses from the specimen. Therefore, the value for  $F$  used in equation (3.14) should be lower than the nominal heat flux that a lamp bank can generate. A bright, highly polished specimen, for example, generally absorbs less radiant heat energy than a dull, darkened specimen. Likewise, a panel with insulation on the side away from the radiant heater could be raised to a specified temperature with less applied heat than a similar uninsulated panel. These factors can be controlled to a large extent in sonic fatigue tests.

As stated previously, the acoustic environment introduces new problems in the use of quartz lamp banks. Existing commercial equipment is designed to be used in ambient conditions. Therefore, a special quartz lamp reflector was designed for use in the present study. The reflector is conventional in several respects. First, a sheet of 0.10-inch thick copper is used as the basic reflector. The reflector was drilled to permit installation of sixteen T3/CL quartz heat lamps at a lamp spacing of 1.0 inch. These are standard 16-inch long, 1600-watt quartz lamps.

A unique feature of the reflector assembly is the reflective surface itself. Most reflectors are designed with a specular finish. The reflector for this study, however, was designed to provide a diffuse surface, while retaining a high degree of reflectivity. Therefore, the side of the reflector facing the quartz lamps was surfaced with a sheet of fine emery paper, onto which a very thin layer of gold had been vacuum deposited. The resulting surface had the desired diffusion properties, combined with a reflectivity of approximately 95%.

Another departure from conventional reflector design was the introduction of damping into the reflector to reduce its response to the acoustic field. A rigid plate (1.0-inch thick aluminum) was bolted to the back of the copper reflector plate, with a constrained layer of RTV 655 Silicone Rubber between the reflector and the back-up plate. Although RTV 655 breaks down at temperatures above 500°F, the material was not permitted to reach that temperature in this installation. The relatively low temperatures maintained in the RTV 655 resulted from a combination of the low thermal transmission of the special reflective surface and the cooling effect of the water circulated through the copper coils on the back of the reflector. The damping effect provided by the RTV 655 reduced the response of the main reflector to an acceptable level throughout the high temperature acoustic tests.

The thermodynamic performance of the lamp bank/reflector assembly was evaluated in a sonic fatigue test installation. The total electrical power required to heat the test panel to a given center temperature was recorded with no air flow, and then with an air flow representative of a sonic fatigue test. Since commonly used acoustic noise sources modulate a stream of compressed air, some air flow can be anticipated in elevated temperature sonic fatigue tests. Figure 10 shows the electrical power required to maintain a given center temperature on the test panel as the air flow is increased to a typical value for the Wyle WAS-3000 noise source. The curve is given in units of air mass per second per unit cross sectional area of the test enclosure. This data indicates that the additional power required to maintain specimen temperature in the presence of air flow does not exceed the capacity of a representative lamp bank.

In addition to structural dynamic and thermodynamic influences on reflector design, the effect of the reflector on the acoustic field must be considered. Three types of acoustic test arrangements will be discussed: progressive wave, normal incidence, and large reverberant enclosures. The last two - normal incidence and reverberant - can be considered at the same time, since in both arrangements a lamp bank reflector will effectively mask the test specimen from the acoustic excitation field. If the lamp bank is moved away from the specimen to permit the acoustic field to reach the specimen, a corresponding reduction in heat flux density is experienced. This method might prove satisfactory in cases where a relatively low percent of the available energy from a lamp bank is needed to bring the specimen to test temperature. Alternatively, it might be possible to heat the test specimen from the side away from the acoustic field. In the case of plain panels with no stiffeners, this technique should cause no problem. For a panel with structural members on its back face, heating from the back would result in hot spots on the structural members, while the specimen panel itself would not receive uniform heating. The structural members could be insulated from the heating system to reduce the hot spots, but this would not alleviate the non-uniform heating of the specimen panel.

For the progressive wave test sections, the lamp bank has far less effect on the acoustic field. The lamp bank can be oriented so that only the edge of the reflector presents itself to the acoustic field. The thickness of the panel is small compared to the cross-section dimension of the enclosure, resulting in virtually no distortion of the acoustic field. While it is possible to set up standing waves between the reflector and the test specimen, the frequencies at which standing waves would appear depend on the spacing between the reflector and the test specimen. A typical spacing would be in the range of three to six inches, which would support standing waves at 2000 Hz and 1000 Hz, respectively. These frequencies are above the range in which fundamental structural resonances normally occur. Under these conditions, the effect of the lamp banks on the acoustic field in a progressive wave test section can be neglected.

### 3.2.2 Quartz Lamp Installations

Normal installations of quartz lamps in reflectors do not consider the dynamic motion of the reflector. The high intensity acoustic noise environment, however, causes some motion of the reflector, even in the highly-damped reflector described above. A series of experiments was conducted to determine the ability of quartz lamps to withstand dynamic environments.

In one test, an unpowered quartz lamp was instrumented with strain gages to detect bending strain in the quartz envelope of the lamp. The lamp was then freely suspended in front of an acoustic noise source, and subjected to increasing sound pressure levels up to 161 dB. The strain in the quartz envelope was recorded at several sound pressure levels, as plotted in Figure 14. Extrapolation of this data indicates that the quartz lamps will sustain acoustically-induced loads at sound pressure levels in excess of 170 dB.

This conclusion was substantiated by conducting vibration tests on a quartz lamp. For the vibration testing, the ends of the lamp were rigidly bonded to a vibration fixture, permitting excitation to be applied through the ends of the lamp. The lamp was excited at input levels up to 30 g's at the first bending mode frequency of the lamp, with no failure of the envelope. Failure of a filament occurred at 21 g's, at which level the stress in the quartz envelope was approximately 3600 psi, which is half of the nominal ultimate strength of the quartz material. The vibration testing was considered to be a far more severe test of the lamp than the acoustic testing, since no filament failures were experienced during acoustic testing. In addition to the filament failure, the quartz lamp showed signs of "etching" inside the lamp as a result of motion of the filament support discs during both vibration and acoustic testing.

Quartz lamps were also subjected to testing at elevated temperatures. One lamp, which had experienced etching as a result of earlier acoustic tests, was taken to full rated power without failure, indicating that the etching had no effect on lamp performance. Another quartz lamp was operated at half rated power and subjected to sinusoidal vibration tests. The vibration input was applied at the first bending frequency of the lamp, at levels up to 42 g's. No failures occurred during this test.

The tests described above indicate that direct excitation of the quartz lamps by the acoustic field can be neglected. This observation is reasonable from a consideration of the size of the lamps (3/8-inch diameter) relative to the acoustic wavelengths (greater than 1 foot) at the lamp resonances. At these wavelengths, the pressure gradient across the lamp is negligible, so that no significant pressure differential appears across the lamp to excite it. On the other hand, vibrational excitation can be transmitted to the lamp by the reflector.

The reflector design described in Section 3.2.1 reduced the vibration in the reflector. Some vibration is still present in the reflector, however, and is transmitted to the lamps through the lampholders. Therefore, the lampholder installation itself was investigated as an area for potential improvement.

The original quartz lamp installations used in the experimental part of this study were made with standard ceramic LT-100 lampholders, as shown in Figure 15. An excessive number of lamp failures was experienced with this installation when the high intensity acoustic noise environment exceeded 160 dB. One predominant type of failure was a fracture of the quartz envelope at the end seal, an area where the envelope makes a transition from a circular cross section to a flat tab. It is through this tab that the lead wire is brought out. Another typical failure mode was fatiguing of the stranded lead wire just outside the envelope. Both of these types of failures result from motion of the lamp ends within the ceramic holder, since the lamps fit freely in the holders in a normal installation.

FIGURE 14  
STRAIN RESPONSE OF QUARTZ LAMP (ACOUSTIC EXCITATION)

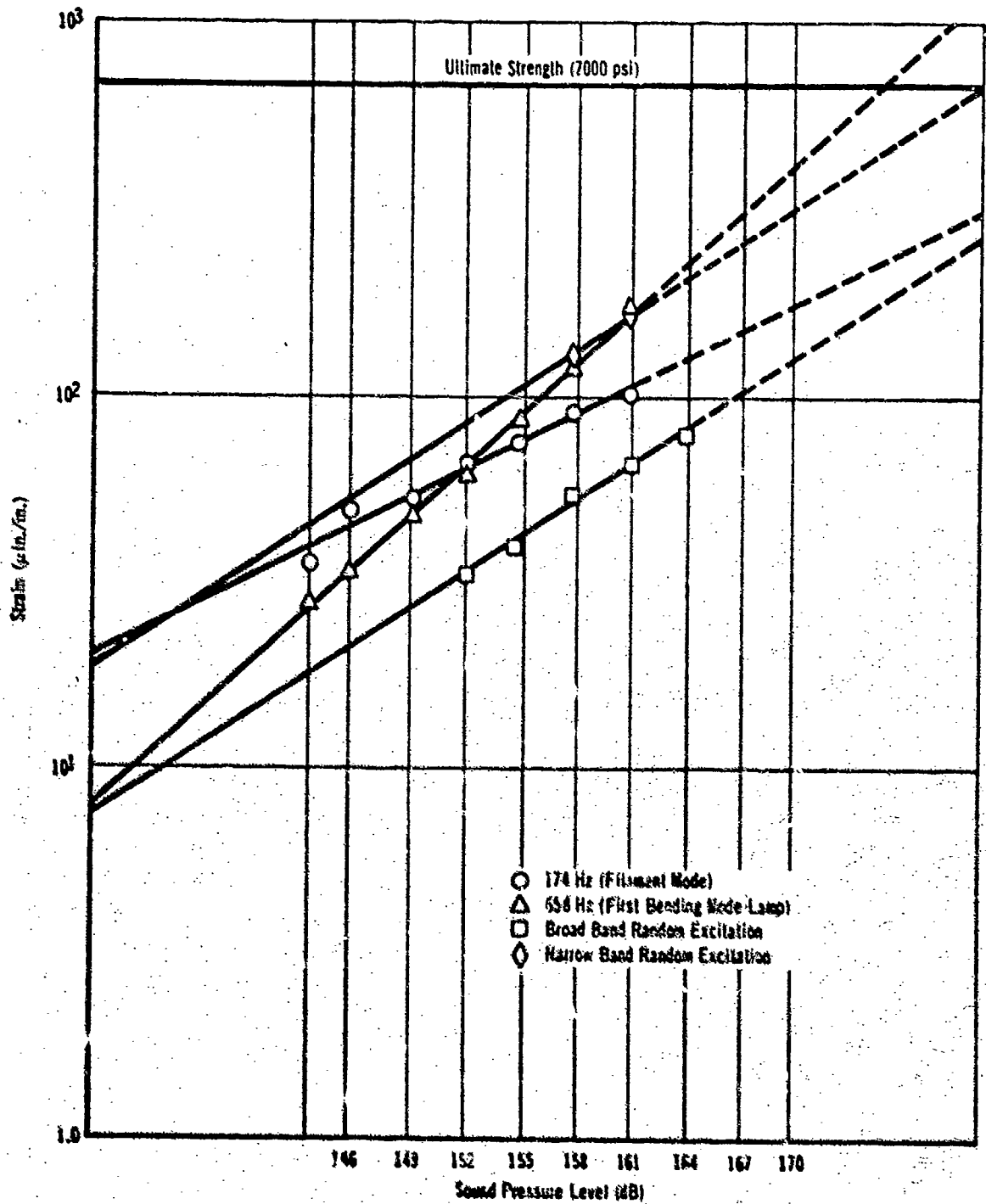
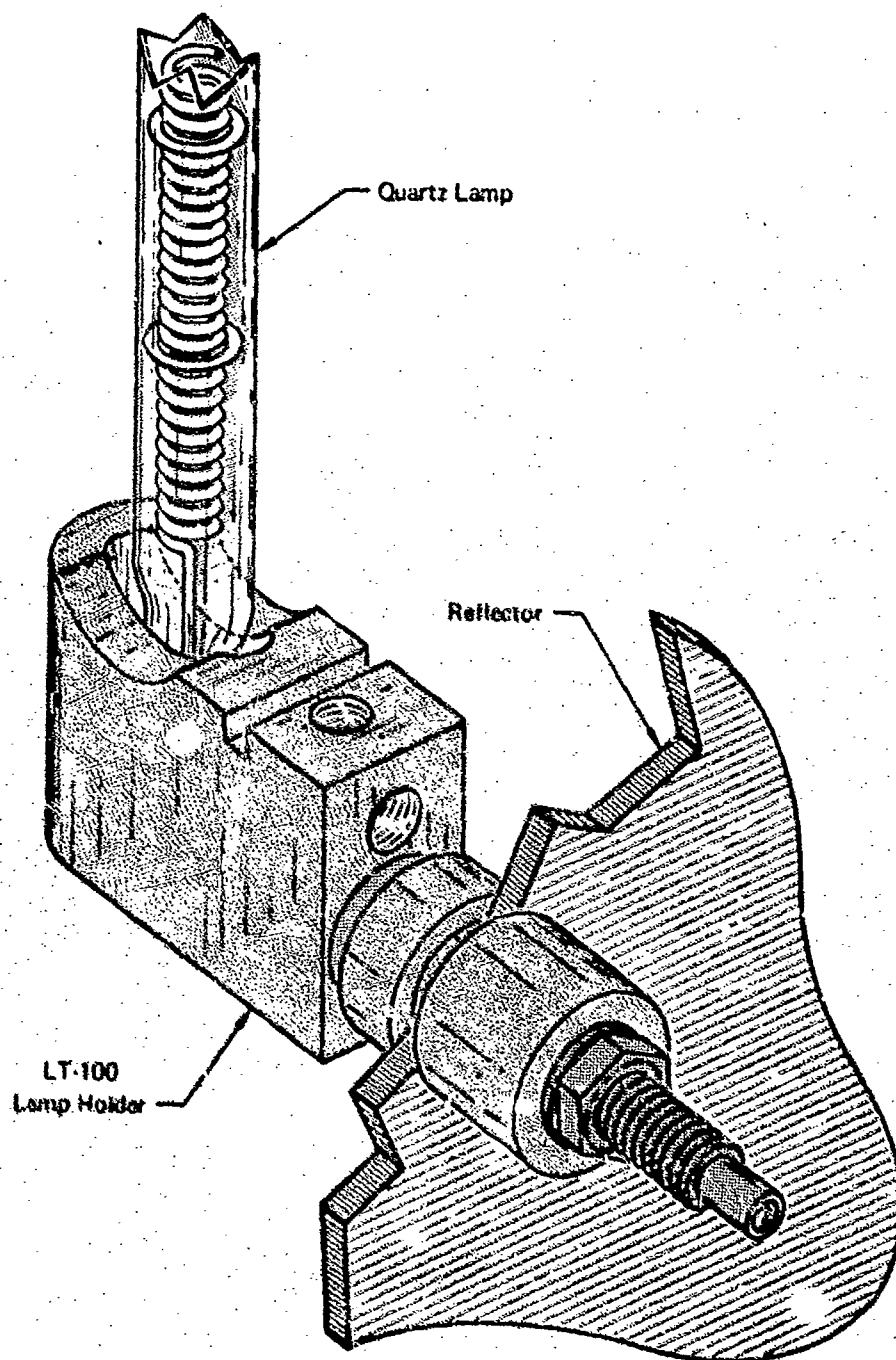


FIGURE 15  
LT-100 LAMP HOLDER



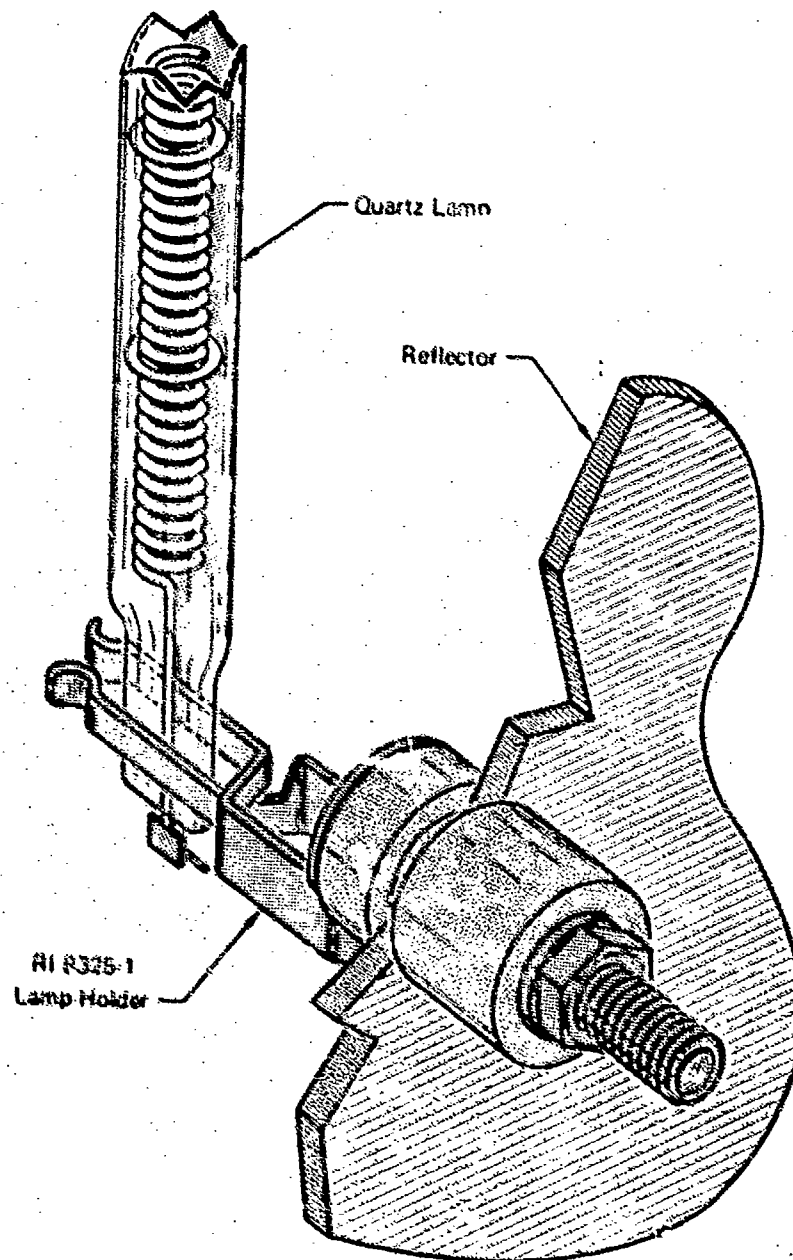
Modifications to the normal lamp installation in the LT-100 holders were tried on several test runs. One modification was to use self-locking nuts on the lampholder, to prevent the holder from becoming loose on the reflector. Another change was to pack asbestos cloth or fiberglass cloth around the lamp end seals to reduce motion of the lamps within the holders. These modifications were successful in reducing the frequency of lamp failures. The cloth materials, however, could not be reliably retained in the holders during high intensity acoustic testing. These modifications also tended to change the predominant mode of lamp failure to a failure within the quartz envelope.

A different type of lampholder was evaluated on some lamps. This holder, manufactured by Research Incorporated, is identified as the RI 8325-1 holder. It consists of a metal slip that securely clamps the flat end of the quartz lamp, as shown in Figure 16. The 8325-1 holder was evaluated in its "as-supplied" condition, as well as with asbestos or fiberglass cloth wrapped around the endseals. Some failures were still experienced with the 8325-1 holder. The addition of the asbestos or fiberglass cloth on the endseals did not improve the failure rate with the 8325-1 holder. In general, it is concluded that the 8325-1 holder, retained by the self-locking nuts, and without any cloth wrapping on the endseals, provided the lowest lamp failure rate. This lamp mounting method, combined with a highly damped reflector, is considered to be the best of the heater arrangements evaluated in this study.

Further experimentation in techniques for holding the lamps is still needed. One approach that might be pursued would be to mechanically uncouple the lampholders from the reflector. This could be achieved with vibration isolators that would isolate the lamps in the frequency range where filament and envelope resonances exist.



FIGURE 16  
RI 8325-1 AMP HOLDER



## SECTION 4

### SPECIMEN MOUNTING EFFECTS

Specimen mounting is one of the most important considerations in combined thermal/acoustic environment testing. Even when the acoustic and thermal environments are accurately controlled, improper boundary simulation can lead to incorrect loads in the test specimen. The specimen mounting restrains one or more of the degrees of freedom at the points of attachment, and thereby significantly affects the specimen response.

In the following section, particular attention will be paid to panel structures. This is done for ease of analysis and experiment; however, the methods developed here may be extended to the analysis of more complicated structures. It will also be shown that in many cases specimen response to a combined thermal/acoustic forcing function may be determined from the superposition of responses to the individual forcing functions. Where superposition is valid, the boundary conditions in the combined environment may also be treated separately.

Requirements for a combined thermal/acoustic test generally fall in one of two categories. First one may be required to test a specimen to a prescribed response level. Second, an environment (service or modeled) may be specified. In either case, prediction of the magnitude and distribution of specimen stress is essential to proper boundary design and instrumentation location.

It is the purpose of this work to examine the effects of specimen mounting on panel state of stress in a combined environment. Both analytical and experimental techniques are discussed and information on free and fixed panels is presented. Following the statement of the governing equations, response to thermal and dynamic environments will be discussed separately. Consideration of specimen mounting in the combined environment will then be discussed along with recommendations for extending the methods developed here.

#### 4.1 GOVERNING EQUATIONS

The analysis of the general thermal/dynamic stress problem can be accomplished by obtaining the solution to the eleven governing equations. These equations are the continuity equation, the equations of motion, and the energy equation, and the constitutive equations, which are presented in Appendix C as Equations (C1), (C2), (C3), and (C5), respectively.

For purposes of later analysis and generalization it will be convenient to write the governing equations in dimensionless form. The following substitutions will be made

$$\begin{aligned} \bar{x} &= \frac{x}{a}, \quad \bar{y} = \frac{y}{b}, \quad \bar{w} = \frac{w}{c}, \quad \bar{T} = \frac{T - T_B}{T_C} \\ q &= \frac{q \cdot ab}{k T_C}, \quad \bar{\psi} = \frac{\psi}{ab}, \quad \bar{\phi} = \frac{\phi}{\left( \frac{E \cdot ab}{1+\nu} \right)} \end{aligned} \quad (4.1)$$

As explained in Appendix C, the assumption of negligible thermal rates due to mechanical motion and negligible strain rates due to temperature changes leads to the quasi-static thermoelastic theory. Under the above assumptions we find that the temperature distribution in a body can be calculated from the Poisson equation for a steady state system. Letting  $\dot{q}$  represent the heat generated per unit volume per unit time internally in the body, the total heat flow to a specimen including net absorbed radiation and convective losses may be treated as the amount of heat flow required ( $\dot{q}$ ) to produce a given temperature distribution. The temperature is then computed subject to the given boundary conditions. For the case of the thin panels considered here, the  $\partial_z$  term is assumed to be zero. Thus the Poisson equation can be written as

$$\partial_{\bar{x}\bar{x}} \bar{T} + \left(\frac{a}{b}\right)^2 \partial_{\bar{y}\bar{y}} \bar{T} = \frac{a}{b} \bar{q} \quad (4.2)$$

The analysis of the state of stress for a panel subjected to a temperature distribution calculated from equation 4.2 requires the solution of the equilibrium and compatibility equations. With the usual assumptions of small deflections of a linear, elastic material, two methods may be employed to reduce the required number of partial differential equations to one. The two functions which may be employed are the Airy's stress function (biharmonic) and the strain (or displacement) potential function (harmonic).<sup>8</sup> For the case of plane stress the state of stress in terms of the stress function is specified by

$$\partial_{xxxx} \phi + 2 \partial_{xxyy} \phi + \partial_{yyyy} \phi = \alpha E (\partial_{xx} T + \partial_{yy} T) \quad (4.3a)$$

$$\sigma_{xx} = \partial_{yy} \phi, \quad \sigma_{yy} = \partial_{xx} \phi, \quad \sigma_{xy} = -\partial_{xy} \phi \quad (4.3b)$$

The state of stress in terms of the strain potential for plane stress is given in dimensionless form by

$$\partial_{\bar{x}\bar{x}} \bar{\psi} + \left(\frac{a}{b}\right)^2 \partial_{\bar{y}\bar{y}} \bar{\psi} = \left(\frac{a}{b}\right) (1 + \nu) \alpha (T_C \bar{T} + T_B) + C \quad (4.4a)$$

It is assumed, in equation (4.4a) that  $\nabla^2 \bar{\psi}$  and  $T$  are differentiable functions of  $x$  and  $y$ . The strain potential and stress relations are then given by

$$\epsilon_{\bar{x}\bar{x}} = \frac{b}{a} \partial_{\bar{x}\bar{x}} \bar{\psi}, \quad \epsilon_{\bar{y}\bar{y}} = \frac{a}{b} \partial_{\bar{y}\bar{y}} \bar{\psi}, \quad \epsilon_{\bar{x}\bar{y}} = 2 \partial_{\bar{x}\bar{y}} \bar{\psi} \quad (4.4b)$$

and

$$\sigma_{\bar{x}\bar{x}} = \frac{E}{(1-\nu^2)} \left[ \frac{b}{a} \partial_{\bar{x}\bar{x}} \bar{\psi} + \nu \frac{a}{b} \partial_{\bar{y}\bar{y}} \bar{\psi} - (1+\nu) \alpha T \right] \quad (4.5a)$$

$$\sigma_{\bar{y}\bar{y}} = \frac{E}{(1-\nu^2)} \left[ \frac{a}{b} \partial_{\bar{y}\bar{y}} \bar{\psi} + \nu \frac{b}{a} \partial_{\bar{x}\bar{x}} \bar{\psi} - (1+\nu) \alpha T \right] \quad (4.5b)$$

$$\sigma_{\bar{x}\bar{y}} = \frac{E}{(1+\nu)} \partial_{\bar{x}\bar{y}} \bar{\psi} \quad (4.5c)$$

It can be shown, by applying the substitutions indicated in equation (4.1) to (4.3a), that equation (4.3a) is the Laplacian of equation (4.4a). For ease of numerical solution in the present discussion solutions will be obtained using the strain potential.

The in-plane forces on a panel may now be determined by substitution of equations (4.5) into the relations

$$N_{xx} = \int_{-\frac{c}{2}}^{\frac{c}{2}} \sigma_{xx} dz, \quad N_{yy} = \int_{-\frac{c}{2}}^{\frac{c}{2}} \sigma_{yy} dz, \quad N_{xy} = \int_{-\frac{c}{2}}^{\frac{c}{2}} \sigma_{xy} dz \quad (4.6)$$

The dynamic plate equation (equation C2i) may be written in dimensionless form as

$$\begin{aligned} & \partial_{\bar{x}\bar{x}\bar{x}\bar{x}} \bar{W} + 2\left(\frac{a}{b}\right)^2 \partial_{\bar{x}\bar{x}\bar{y}\bar{y}} \bar{W} + \left(\frac{a}{b}\right)^4 \partial_{\bar{y}\bar{y}\bar{y}\bar{y}} \bar{W} - \\ & 12 \left\{ \left[ \frac{b}{a} \partial_{\bar{x}\bar{x}} \bar{\psi} + \nu \frac{a}{b} \partial_{\bar{y}\bar{y}} \bar{\psi} - (1+\nu)\alpha T \right] \left(\frac{a}{c}\right)^2 \partial_{\bar{x}\bar{x}} \bar{W} + \right. \\ & \left. \left[ \frac{a}{b} \partial_{\bar{y}\bar{y}} \bar{\psi} + \nu \frac{b}{a} \partial_{\bar{x}\bar{x}} \bar{\psi} - (1+\nu)\alpha T \right] \left(\frac{a}{b}\right)^2 \left(\frac{a}{c}\right)^2 \partial_{\bar{y}\bar{y}} \bar{W} + \right. \\ & \left. \frac{(1+\nu)}{2} \left(\frac{a}{b}\right)\left(\frac{a}{c}\right)^2 \partial_{\bar{x}\bar{y}} \bar{\psi} \partial_{\bar{x}\bar{y}} \bar{W} \right\} - \frac{12(1-\nu^2)\rho a^4}{gE c^2} \omega_n^2 \bar{W} = 0 \end{aligned} \quad (4.7)$$

where the  $\bar{\psi}$  values are known from equation (4.4a).

On the basis of the preceding equations, (4.1) through (4.7), the solutions to the thermal and dynamic stress problems may be determined for a given dynamic forcing function and damping value. Due to the complexity of the problem numerical solutions to the thermal stress problem were obtained principally for free and fixed boundary conditions on a square, steel plate. Experimental solutions were obtained for a boundary condition between free and fixed. A determination of the effect of in-plane forces on the resonant frequencies of a panel was obtained experimentally. Methods for extending this information to other boundary conditions, shapes, and materials are presented in sections 4.2 through 4.4.

## 4.2 THERMAL EFFECTS

The governing equation used in the study of thermal stress in panels is equation (4.4). Since this equation is derived by the integration of two equilibrium equations an arbitrary constant is included. If the potential and its derivatives are taken to be zero at infinity the constant is zero. There are, however, classes of practical problems which can be solved conveniently by choosing a reference for the potential function at a point in space other than infinity. In these cases it will be necessary to retain and evaluate the constant of integration, C, in equation (4.4).

Evaluation of the constant, C, requires the evaluation of the expression

$$\partial_{\bar{x}\bar{x}} \bar{\psi} + \left(\frac{a}{b}\right)^2 \partial_{\bar{y}\bar{y}} \bar{\psi} - \left(\frac{a}{b}\right) (1+\nu) \alpha T = C \quad (4.8)$$

at some point  $x_0, y_0$ . To do this equations (4.4b) are substituted into equation (4.4a) and evaluated at  $x_0, y_0$

$$\epsilon_{xx} \bigg|_{\substack{\bar{x}=x_0 \\ \bar{y}=y_0}} + \epsilon_{yy} \bigg|_{\substack{\bar{x}=x_0 \\ \bar{y}=y_0}} - (1+\nu) \alpha T \bigg|_{\substack{\bar{x}=x_0 \\ \bar{y}=y_0}} = C \quad (4.9)$$

The following discussion will be limited to square free and fixed panels with a constant boundary temperature. It will be shown later that equation (4.8) may be applied to more general problems but some additional calculation may be required. For the fixed panel it is known that at the corners  $\epsilon_{xx} = \epsilon_{yy} = 0$  and the temperature is  $T_B$ . Substituting these values into equation (4.9) yields

$$C = -(1+\nu) \alpha T_B \quad (4.10)$$

For the free panel  $\epsilon_{xx}$  and  $\epsilon_{yy}$  are both equal to  $\alpha T_B$  at the corner and the temperature is  $T_B$ . Equation (4.9) then becomes

$$C = (1-\nu) \alpha T_B \quad (4.11)$$

The second part of the boundary value problem requires the evaluation of  $\psi$  at the boundaries. The general form of  $\psi(\bar{x}, \bar{y})$  is

$$\psi(\bar{x}, \bar{y}) = f_1(\bar{x}) + f_2(\bar{y}) + f_3(\bar{x}) f_4(\bar{y}) + C \quad (4.12)$$

For the free panel we have the requirement that the shear stresses, and thus the shear strains, are zero at the boundaries (equation (4.4b)).

$$\partial_{\bar{x}\bar{y}} \psi \bigg|_B = 0 \quad (4.13)$$

Substituting equation (4.12) into the above expression and evaluating this at the boundaries  $|\bar{x}| = 1$  and  $|\bar{y}| = 1$  we have the condition

$$\partial_{\bar{x}\bar{y}} \psi \bigg|_B = f'_3(1) f'_4(\bar{y}) = f'_3(\bar{x}) f'_4(1) = 0 \quad (4.14a)$$

which gives

$$f'_3(\bar{x}) \bigg|_{\substack{|\bar{y}|=1 \\ -1 < |\bar{x}| < 1}} = 0, \quad f'_4(\bar{y}) \bigg|_{\substack{|\bar{x}|=1 \\ -1 < |\bar{y}| < 1}} = 0 \quad (4.14b)$$

thus

$$\psi \bigg|_B = f_1(\bar{x}) + f_2(\bar{y}) + C \quad (4.14c)$$

At the boundary the normal stresses must be zero. In terms of the potential function equations (4.5) become

$$\frac{a}{b} \partial_{\bar{x}\bar{x}} \psi \bigg|_{|\bar{x}|=1} + \nu \frac{a}{b} \partial_{\bar{y}\bar{y}} \psi \bigg|_{|\bar{x}|=1} - (1+\nu) \alpha T(1, \bar{y}) = 0 \quad (4.15a)$$

$$\frac{a}{b} \partial_{\bar{y}\bar{y}} \psi \bigg|_{|\bar{y}|=1} + \nu \frac{b}{a} \partial_{\bar{x}\bar{x}} \psi \bigg|_{|\bar{y}|=1} - (1+\nu) \alpha T(\bar{x}, 1) = 0 \quad (4.15b)$$

Substituting equation (4.14c) into the above we have

$$\frac{a}{b} f''_1(1) + \nu \frac{a}{b} f''_2(\bar{y}) = (1+\nu) \alpha T(1, \bar{y}) \quad (4.16a)$$

$$\frac{a}{b} f''_2(1) + \nu \frac{b}{a} f''_1(\bar{x}) = (1+\nu) \alpha T(\bar{x}, 1) \quad (4.16b)$$

Solving equation (4.16) for  $f_1$  and  $f_2$  at the boundaries we have for the constant boundary temperature case

$$f_1(\bar{x}) = \left[ \frac{a(1+\nu)}{2b\nu} \alpha T(\bar{x}, 1) - \frac{f''_1(1)}{2\nu} \right] \bar{x}^2 + C_1 \bar{x} + C_2 \quad (4.17a)$$

$$f_2(\bar{y}) = \left[ \frac{b(1+\nu)}{2a\nu} \alpha T(1, \bar{y}) - \frac{f''_2(1)}{2\nu} \right] \bar{y}^2 + C_3 \bar{y} + C_4 \quad (4.17b)$$

where  $f''_1(1)$ ,  $f''_2(1)$ ,  $C_1$ , and  $C_3$  are unknown constants to be evaluated from the boundary conditions for the known temperature distributions.  $C_2$  and  $C_4$  are arbitrary since the potential is only known to within a constant. Solving equation (4.17) for the case of a square panel with a constant boundary temperature,  $T_B$ , we have upon substitution of the second derivatives into equation (4.15)

$$f''_1(1) = f''_2(1) = (1-\nu) \alpha T_B \quad (4.18)$$

Applying the condition of zero rigid body motion we have  $C_1 = C_3 = 0$  in equations (4.17). Thus the potential is

$$\bar{\psi}(\bar{x}, \bar{y}) \Big|_B = \alpha T_B (\bar{x}^2 + \bar{y}^2) \Big|_B + C_2 + C_4 \quad (4.19)$$

Since  $\bar{\psi}(\bar{x}, \bar{y})$  can only be known to within an arbitrary constant we can assign a value to a point. In this case we will assign a zero value to the midpoint on a boundary. This results in a value of  $-\alpha T_B/2$  for  $(C_4 + C_2)$ .

For the fixed panel the boundary conditions are that the displacements at the boundary are zero.

$$\frac{\partial \bar{\psi}}{\partial \bar{x}} \Big|_{|\bar{y}|=1} = \frac{\partial \bar{\psi}}{\partial \bar{y}} \Big|_{|\bar{x}|=1} = 0 \quad (4.20)$$

Applying these conditions to equation (4.12) we have

$$f'_1(\bar{x}) + f'_3(\bar{x}) f_4(1) = 0 \quad (4.21a)$$

$$f'_2(\bar{y}) + f_3(1) f'_4(\bar{y}) = 0 \quad (4.21b)$$

Integrating and combining like functions results in

$$f_1(\bar{x}) + f_4(1) f_3(\bar{x}) - C_1 = 0 \quad \therefore f_5(\bar{x}) = C_1 \quad (4.22a)$$

$$f_2(\bar{y}) + f_3(1) f_4(\bar{y}) - C_2 = 0 \quad \therefore f_6(\bar{y}) = C_2 \quad (4.22b)$$

where  $f_5(\bar{x}) = f_1(\bar{x}) + f_4(1)f_3(\bar{x})$  and similarly for  $f_6(\bar{y})$ . Since  $C_1$  and  $C_2$  are arbitrary constants they can be given zero value yielding

$$\bar{\psi}(\bar{x}, \bar{y}) \Big|_B = 0 \quad (4.23)$$

For the free and fixed square panel with constant boundary temperature we can now determine a function  $\psi$  which satisfies equation (4.4a) and the boundary conditions given by equations (4.10) and (4.23) or (4.11) and (4.19). From potential theory, it can be shown that with  $\psi$  known on the boundary, the function obtained under the above conditions is the unique solution.<sup>9</sup> There are several methods for the solution of equation (4.4a). For simple temperature distributions and classical boundary conditions, closed form analytical solutions are available. For general temperature distributions and various boundary conditions two other methods of solution seem preferable. One method is the numerical analysis of equation (4.4a). The other method consists of a combination of experimental, numerical, and statistical techniques.

Three techniques may be employed in the numerical analysis of equation (4.4a): numerical integration, finite elements, or finite differences. In the present study the finite difference technique was employed due to its compatibility with the low storage time sharing computers and the existence of several applicable algorithms for the solution of elliptic equations by finite differences. As shown in the literature,<sup>10</sup> the solution to the finite difference representation of the second order, elliptic equation converges uniquely to the solution of the partial differential equation. The finite difference solution is the superposition of the homogeneous and particular solutions. A description of the computer programs used in solving this equation by the finite difference technique is given in Appendix D. Once the program has been developed solutions may be obtained quickly and economically; however, each case requires an individual solution. It is often desirable to have an indication of the variation of the stress for a range of independent parameters. In this case a few computer and experimental solutions may be combined with any of several statistical techniques to yield design curves giving a reasonable approximation to the actual stress response.<sup>11</sup>

The form of  $T$  for the nonhomogeneous portion of equation (4.4a) will be taken as

$$T(\bar{x}, \bar{y}) = A_1 + A_2|\bar{x}| + A_3|\bar{x}^2| + A_4|\bar{x}^3| + A_5|\bar{x}^4|$$

$$-1 \leq \bar{x} \leq 1, \quad -|\bar{x}| \leq \bar{y} \leq |\bar{x}| \quad (4.24a)$$

$$T(\bar{x}, \bar{y}) = A_1 + A_2|\bar{y}| + A_3|\bar{y}^2| + A_4|\bar{y}^3| + A_5|\bar{y}^4|$$

$$-1 \leq \bar{y} \leq 1, \quad -|\bar{y}| \leq \bar{x} \leq |\bar{y}| \quad (4.24b)$$

This form of temperature distribution is symmetric with respect to the  $x$  and  $y$  axes and has a constant boundary temperature. Forming the dimensionless temperature ratio  $\bar{T}$  equation (4.24a) becomes

$$\bar{T}(\bar{x}, \bar{y}) = \bar{A}_2(\bar{x} - 1) + \bar{A}_3(\bar{x}^2 - 1) + \bar{A}_4(|\bar{x}|^3 - 1) + \bar{A}_5(|\bar{x}|^4 - 1)$$

$$-1 \leq \bar{x} \leq 1, \quad -|\bar{x}| \leq \bar{y} \leq |\bar{x}| \quad (4.25)$$

where  $\bar{A}_2 = A_2/A_1$ ,  $\bar{A}_3 = A_3/A_1$ , etc. A similar expression for equation (4.24b) can be written. The normalized center temperature is then

$$\bar{T}_c = -\bar{A}_2 - \bar{A}_3 - \bar{A}_4 - \bar{A}_5 \quad (4.26)$$

Since stress is the response parameter of interest we would like to find  $\sigma = \sigma(\bar{x}, \bar{y}, \bar{T})$ . Making the substitutions indicated in equation (4.1) in the expression for stress (equation (4.5)) we define a dimensionless response parameter as

$$\bar{\sigma}_{\bar{x}\bar{x}} = \frac{\sigma_{\bar{x}\bar{x}}}{\frac{\alpha ET}{1-\nu}} = \frac{\frac{b}{a} \frac{\partial^2 \bar{\psi}}{\partial \bar{x}^2} + \nu \frac{a}{b} \frac{\partial^2 \bar{\psi}}{\partial \bar{y}^2}}{(1+\nu) \alpha T} - 1 \quad (4.27)$$

with similar expressions for  $\bar{\sigma}_{\bar{y}\bar{y}}$ . Since  $\bar{\psi}$  depends on the coefficients of the non-homogeneous portion of equation (4.4a) and the boundary conditions, equation (4.27) can be written in parametric form as

$$\bar{\sigma} = \bar{\sigma}(\bar{A}_i, \frac{a}{b}, \nu, \text{boundary}) \quad (4.28)$$

Particular attention will be paid to the center stress parameter,  $\bar{\sigma}_C$ , as a function of  $\bar{A}_i$  for  $a/b = 1.0$ ,  $\nu = 0.27$ , for free and fixed boundaries.

The initial intent of this study was to apply the statistical technique known as Latin Squares to determine the relation between  $\bar{\sigma}$  and  $\bar{T}$ .<sup>12, 13</sup> However, a few solutions to the thermal stress problem indicated that for the above type of symmetric temperature distributions and boundary conditions,  $\bar{\sigma}_C$  varies linearly with each coefficient,  $\bar{A}_i$ . In this case the use of a tool as powerful as Latin Squares is not required. For problems where the functional relationships are more complicated the Latin Squares technique should be employed. The value of  $\bar{\sigma}_C$  for a temperature distribution which is a function of more than one coefficient is found by the superposition of the solutions to the various single coefficient problems. Computer solutions of  $\bar{\sigma}_C$  for various values  $\bar{A}_i$  for free and fixed panels are presented in Tables 3 and 4, respectively. The values and locations of the maximum stresses are also presented. For each case where the temperature distribution was purely linear, quadratic, cubic, or quartic a least squares polynomial fit of  $\bar{\sigma}_C$  vs  $\bar{A}_i$  was performed. In each case the form of the polynomial was  $\bar{\sigma}_C = C_i \bar{A}_i + D_i$ . For the case of a fixed plate the  $C_i$  are all 0.626 and the  $D_i$  are -1.0. For the free plate,  $C_i = -0.372$  and  $D_i = 0$ . As noted in equation (4.26),  $\bar{T}_C = \sum \bar{A}_i$  so each plot for  $\bar{T}$  having only one non-zero coefficient is also a plot of  $\bar{\sigma}_C$  vs  $\bar{T}$ . The  $\bar{\sigma}_C$  vs  $\bar{T}_C$  curve for both the free and fixed panel are presented in Figure 17. It should be noted that for  $\bar{T}_C = 0$ , the constant temperature case, there is zero stress in the free panel and  $\bar{\sigma}_C = -\alpha ET/(1-\nu)$  for the fixed panel. When  $\bar{T} = 1.0$ ,  $T_B = \text{ambient}$ , the panel responds as a fixed panel regardless of physical boundary conditions and  $\bar{\sigma}_C$  is  $-(1-\nu)/2$ . Cases 11 and 12, Table 4, for the fixed panel and cases 14 through 16, Table 3 for the free panel verify that applying  $\bar{T} = \sum \bar{A}_i$  and the equations for  $\bar{\sigma}$  vs  $\bar{T}$  yields the same  $\bar{\sigma}$  value as the solution of equation (4.5).

The results of the analytical studies shown in Tables 3 and 4 indicated that for temperature distributions of quadratic and higher order the maximum stress is not in the center. Temperature and stress distributions for the fixed and free panels for first through fourth order temperature distributions are presented in Figures 18 through 25. The shape of the stress distribution shown for the higher order distributions was also observed in the experimental investigations.

In addition to the analytical studies a thermal test was conducted on a 15-inch-square, stainless steel panel. The test setups used for the simulated free and fixed boundary tests are shown in Figures 26 and 27, respectively. Heat was applied to the panel by the quartz lamp and reflector arrangement shown in the figures.



TABLE 3  
THERMAL STRESS DATA FOR FREE PANEL

Case	$\bar{A}_1$	$\bar{A}_2$	$\bar{A}_3$	$\bar{A}_4$	$\bar{A}_5$	$T_C$	$T_B$	$\Delta T$	$\Delta T/T_C$	$\sigma_{Center}$ $\times 10^6$	$\sigma_{Center (i-u)}$ $\alpha ETC$	$\sigma_{max}$ $\times 10^5$	$x_{max}$	$y_{max}$	$\sigma_{Max (1-u)}$ $\alpha ETC$
1	1	-0.2499	0	0	0	400	300	100	0.25	-0.0099	-0.0095	-0.0099	0	0	0.0095
2	1	-0.8	0	0	0	500	100	400	0.80	-0.039	-0.296	-0.039	0	0	-0.296
3	1	-0.75	0	0	0	800	200	600	0.75	-0.058	-0.276	-0.058	0	0	-0.276
4	1	-0.333	0	0	0	1200	800	400	0.333	-0.039	-0.124	-0.039	0	0	-0.124
5	1	-0.8866	0	0	0	1200	400	800	0.666	-0.078	-0.246	-0.078	0	0	-0.246
6	1	-1.0	0	0	0	1200	0	1200	1.0	-0.115	-0.365	-0.115	0	0	-0.365
7	1	0	-0.2489	0	0	400	300	100	0.25	-0.00996	-0.0095	-0.01	0	-0.9	-0.0095
8	1	0	-0.7495	0	0	800	200	600	0.75	-0.058	-0.276	-0.059	0	-0.9	-0.276
9	1	0	-0.9998	0	0	1200	0	1200	1.0	-0.115	-0.365	-0.116	0	-0.9	-0.368
10	1	0	0	-0.4992	0	1200	600	600	0.5	-0.059	-0.185	-0.063	0	-2.8	-0.201
11	1	0	0	-1.002	0	1200	0	1200	1.0	-0.115	-0.365	-0.124	0	-2.8	-0.394
12	1	0	0	0	-0.4999	1200	600	600	0.5	-0.059	-0.185	-0.068	0	-3.7	-0.215
13	1	0	0	0	-1.9993	1200	0	1200	1.0	-0.118	-0.374	-0.137	0	-3.7	-0.427
14	1	-3	-1.249	0	0	400	-1300	1700	4.25	-0.163	-1.56	0.163	0	0	-1.56
15	1	-0.9833	-0.9164	0	0	1200	0	1200	1.0	-0.115	-0.365	-0.115	0	0	-0.365
16	1	0.5803	-3.974	7.635	-5.221	600	0	600	1.0	-0.058	-0.368	-0.068	0	-4.7	-0.431

TABLE 4  
THERMAL STRESS DATA FOR FIXED PANEL

CASE	$\bar{A}_1$	$\bar{A}_2$	$\bar{A}_3$	$\bar{A}_4$	$\bar{A}_5$	$T_C$	$T_B$	$\Delta T$	$\Delta T/T_C$	$\sigma_{\text{Center}} \times 10^6$	$\sigma_{\text{Center}} (1-\nu) / \alpha E T_C$	$\sigma_{\text{max}} \times 10^6$	$x_{\text{max}}$	$y_{\text{max}}$	$\sigma_{\text{Max}} (1-\nu) / \alpha E T_C$
1	1	-0.2499	0	0	0	400	300	100	0.25	-0.089	-0.848	-0.089	0	0	-0.848
2	1	-0.75	0	0	0	800	200	600	0.75	-0.112	-0.539	-0.112	0	0	-0.539
3	1	-1.0	0	0	0	1200	0	1200	1.0	-0.120	-0.388	-0.120	0	0	-0.388
4	1	0	-0.2499	0	0	400	300	100	0.25	-0.089	-0.848	-0.089	0	-0.9	-0.848
5	1	0	-0.75	0	0	800	200	600	0.75	-0.113	-0.539	-0.114	0	-0.9	-0.539
6	1	0	-0.998	0	0	1200	0	1200	1.0	-0.122	-0.389	-0.123	0	-0.9	-0.389
7	1	0	0	-0.507	0	1200	600	600	0.5	-0.220	-0.699	-0.224	0	-2.8	-0.71
8	1	0	0	-1.0	0	1200	0	1200	1.0	-0.117	-0.372	-0.126	0	-2.8	-0.400
9	1	0	0	0	-0.4999	1200	600	600	0.5	-0.220	-0.699	-0.229	0	-3.7	-0.727
10	1	0	0	0	-0.9993	1200	0	1200	1.0	-0.118	-0.374	-0.137	0	-3.7	-0.427
11	1	-0.1249	-0.6244	0	0	400	200	600	0.75	-0.113	-0.539	-0.113	0	0	-0.539
12	1	-3.0	-1.248	0	0	400	-1300	1700	4.25	0.171	1.63	0.171	0	0	1.63

FIGURE 17  
THERMAL STRESS RESPONSE

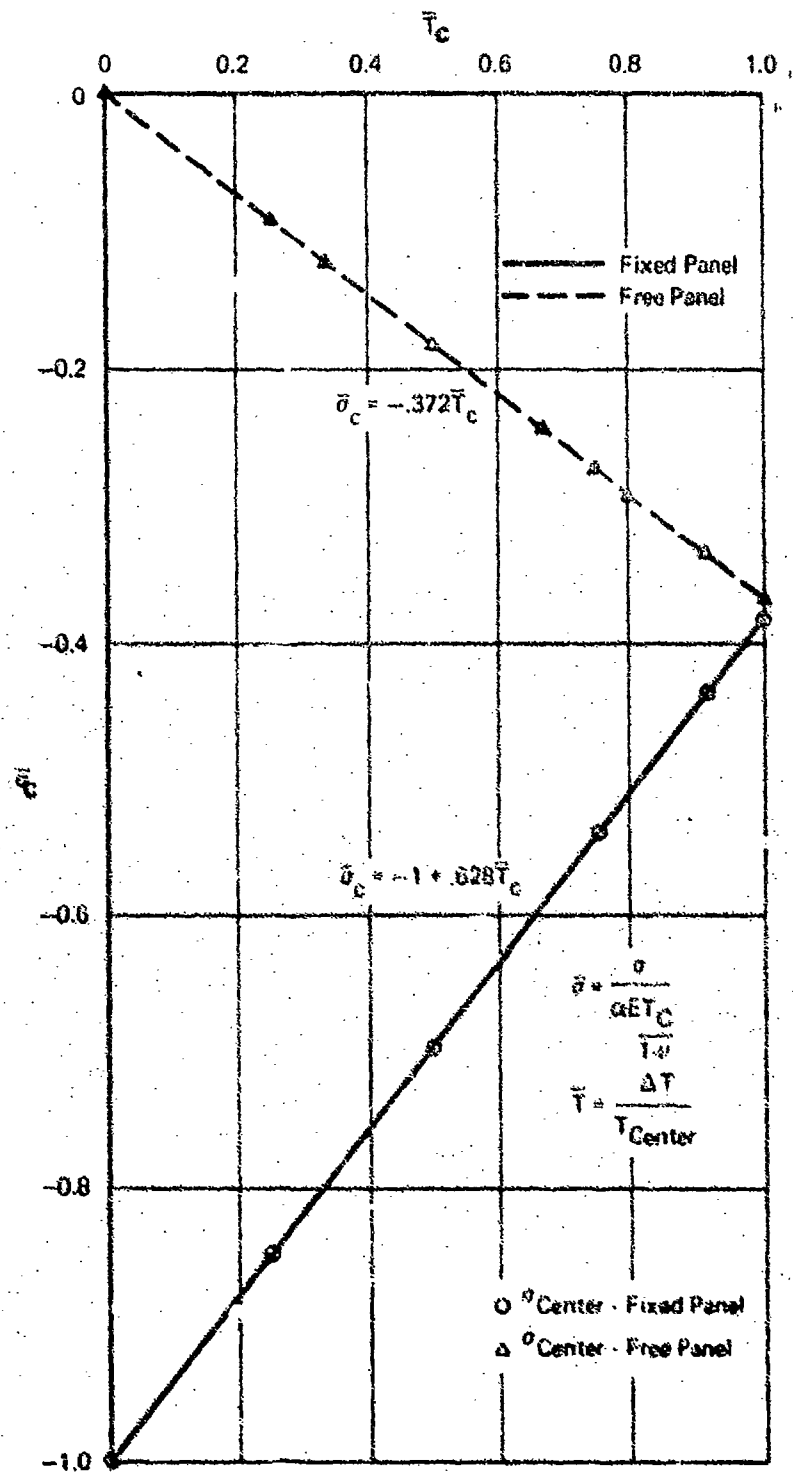


FIGURE 18  
THERMAL STRESS DISTRIBUTION  
FIXED BOUNDARY CONDITION  
1st Order Temperature Distribution

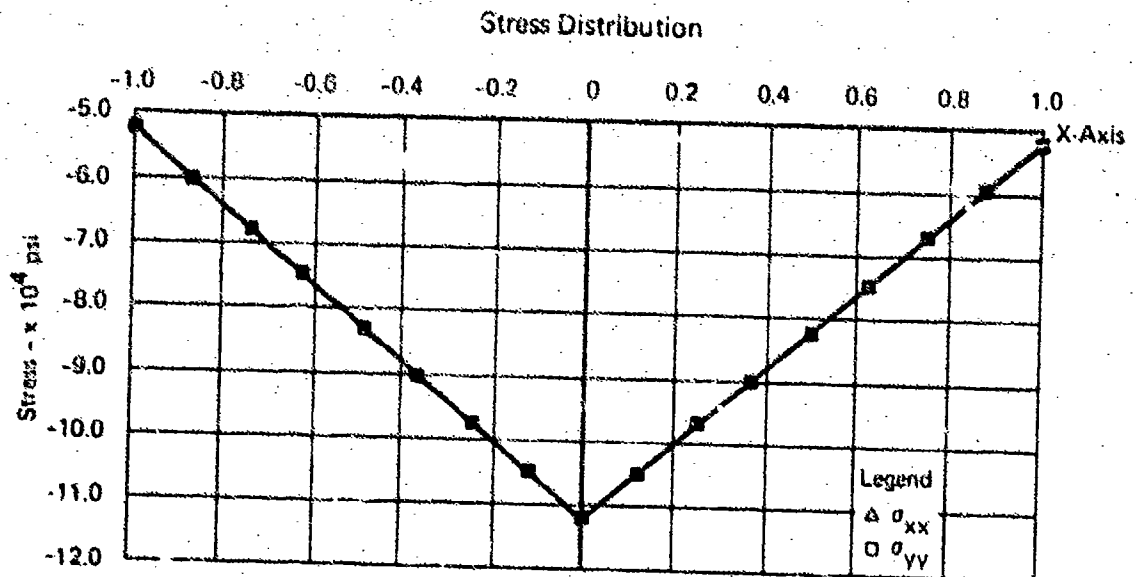
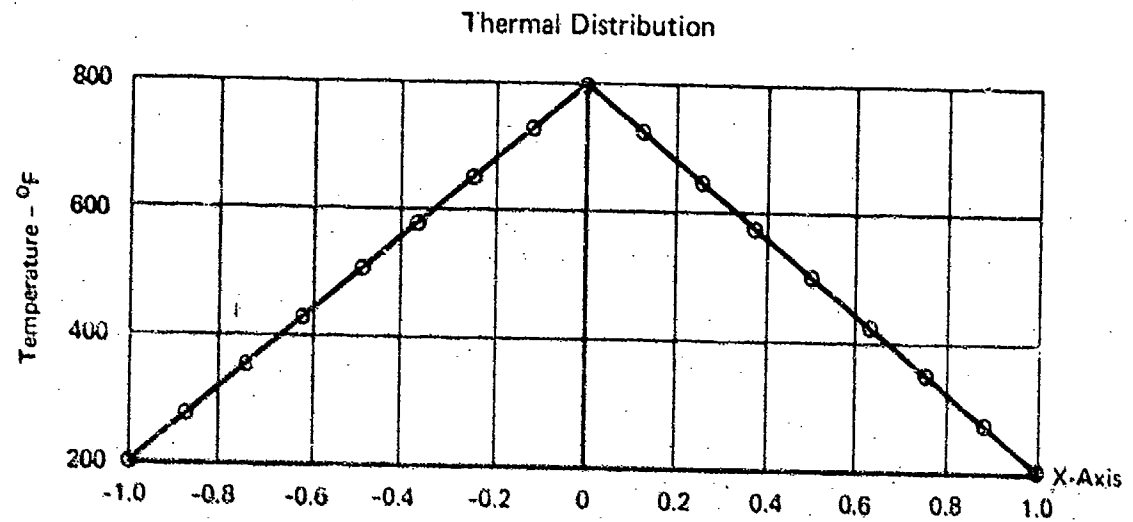


FIGURE 19  
THERMAL STRESS DISTRIBUTION  
FIXED BOUNDARY CONDITION  
2nd Order Temperature Distribution

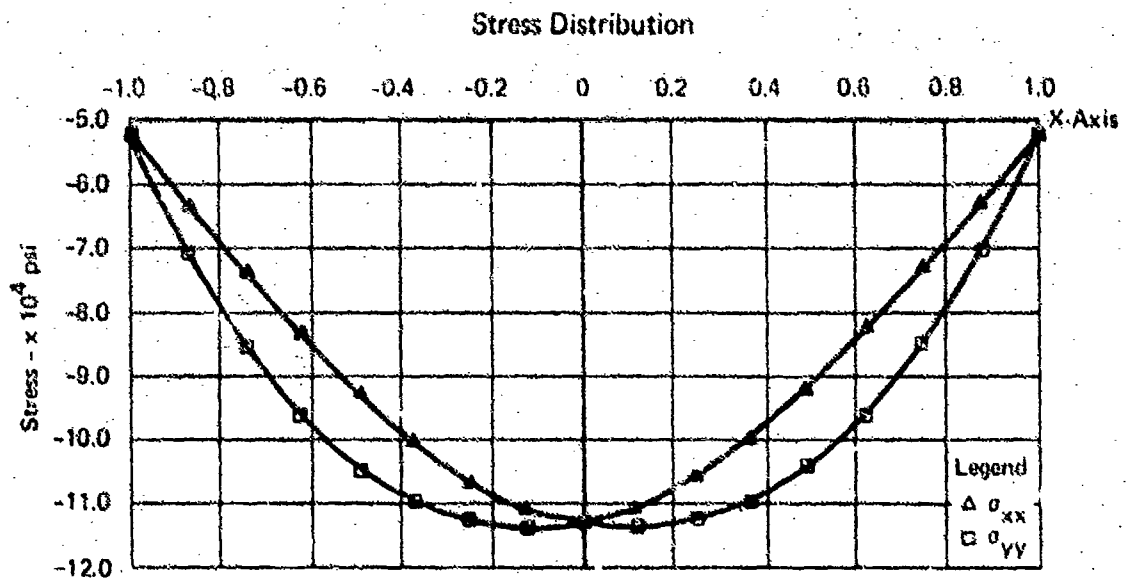
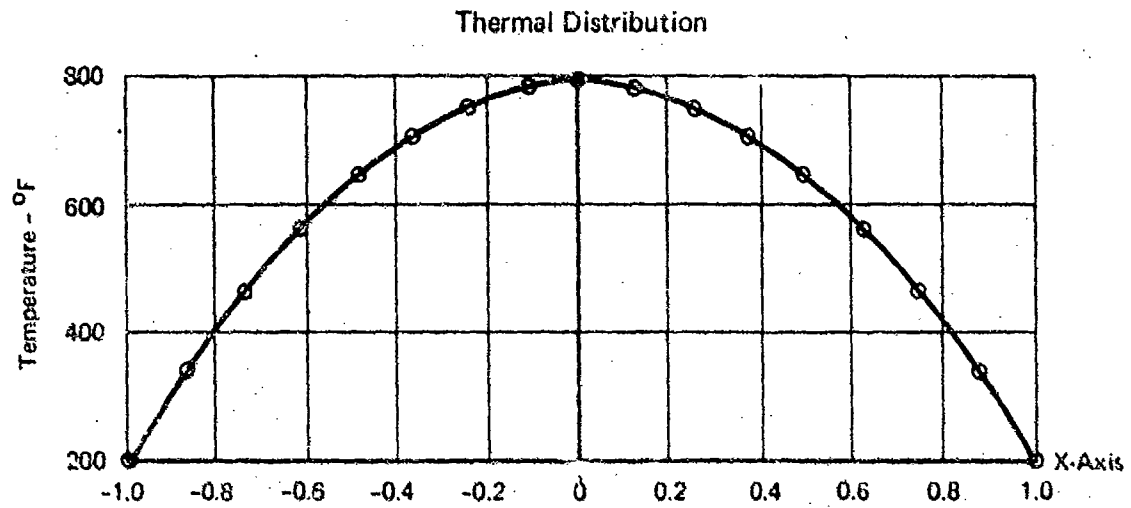


FIGURE 20  
THERMAL STRESS DISTRIBUTION  
FIXED BOUNDARY CONDITION  
3rd Order Temperature Distribution

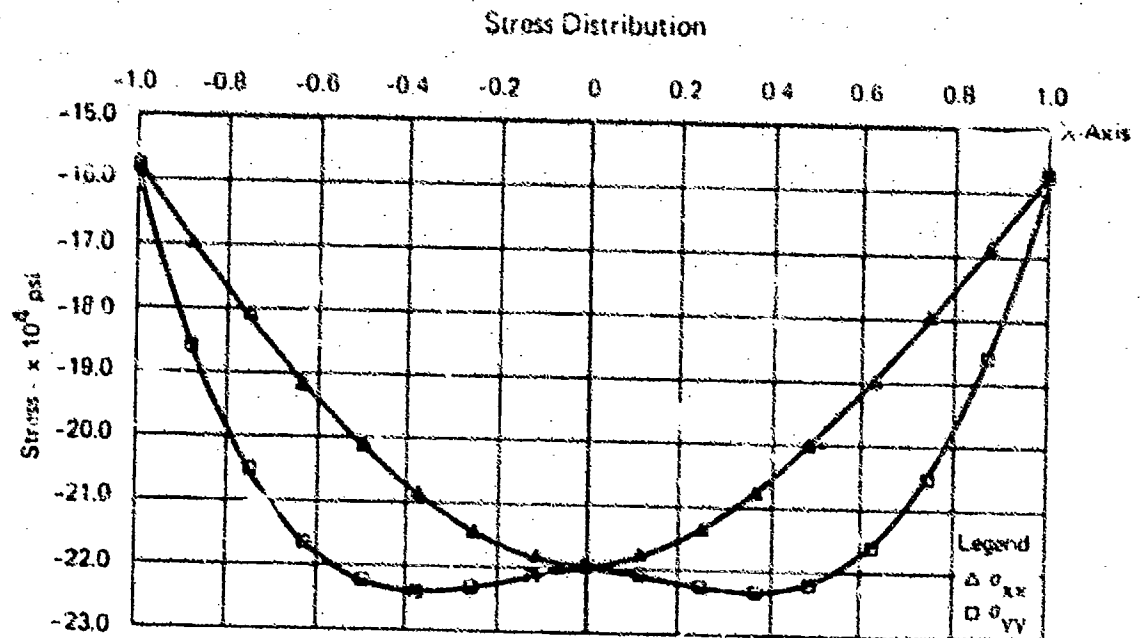
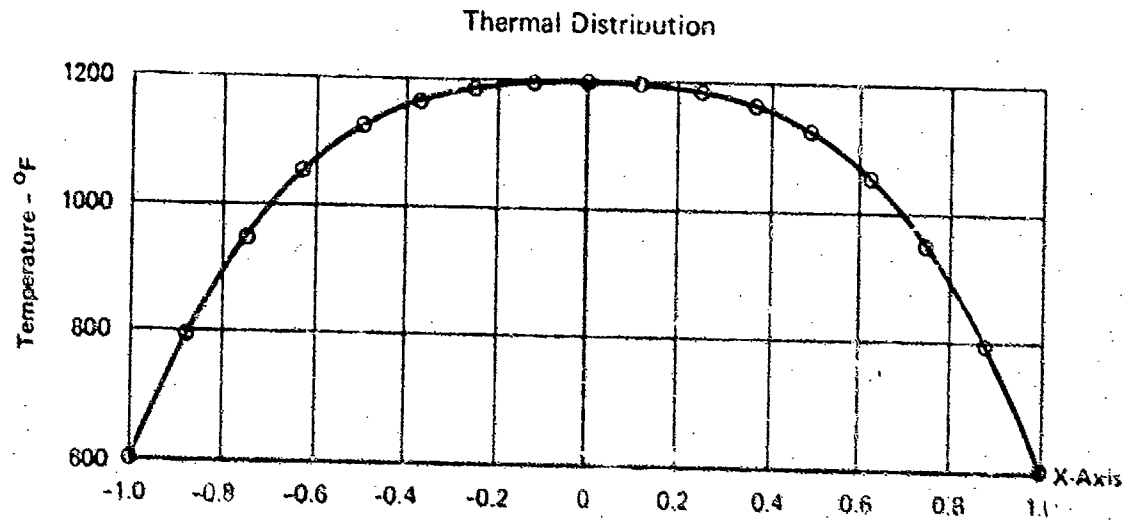


FIGURE 21  
THERMAL STRESS DISTRIBUTION  
FIXED BOUNDARY CONDITION  
4th Order Temperature Distribution

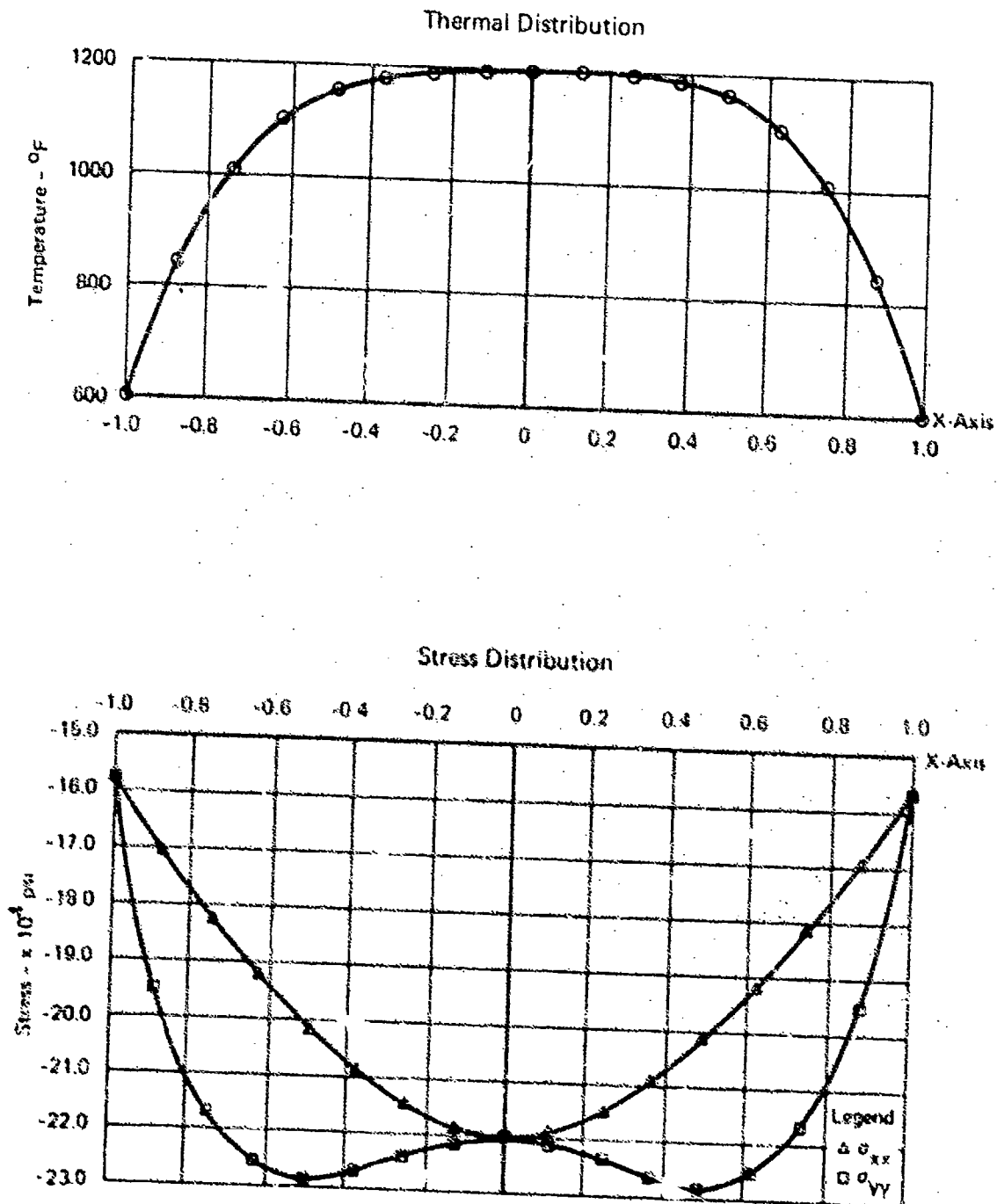


FIGURE 22  
THERMAL STRESS DISTRIBUTION  
FREE-FREE BOUNDARY CONDITION  
1st Order Temperature Distribution

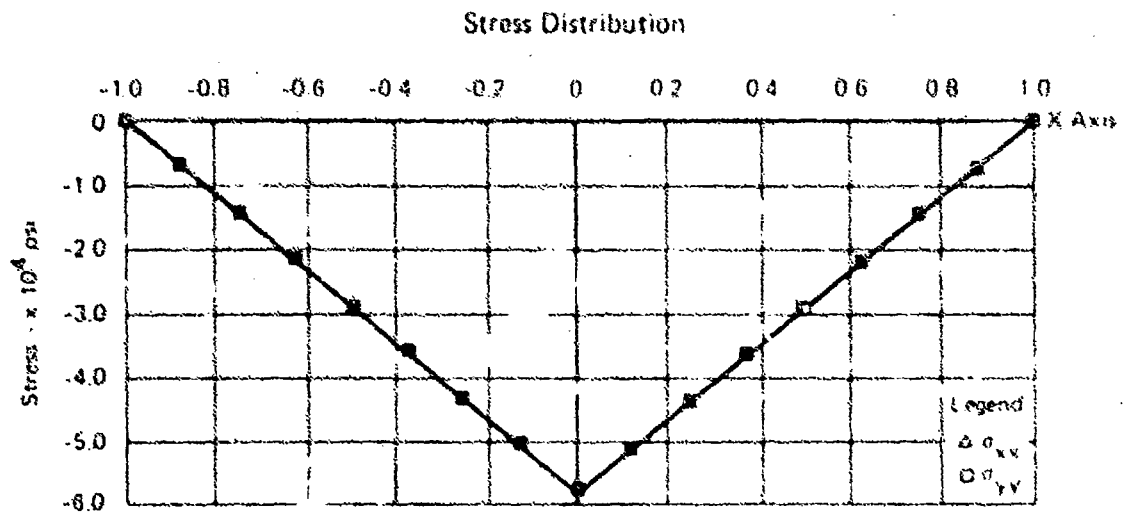
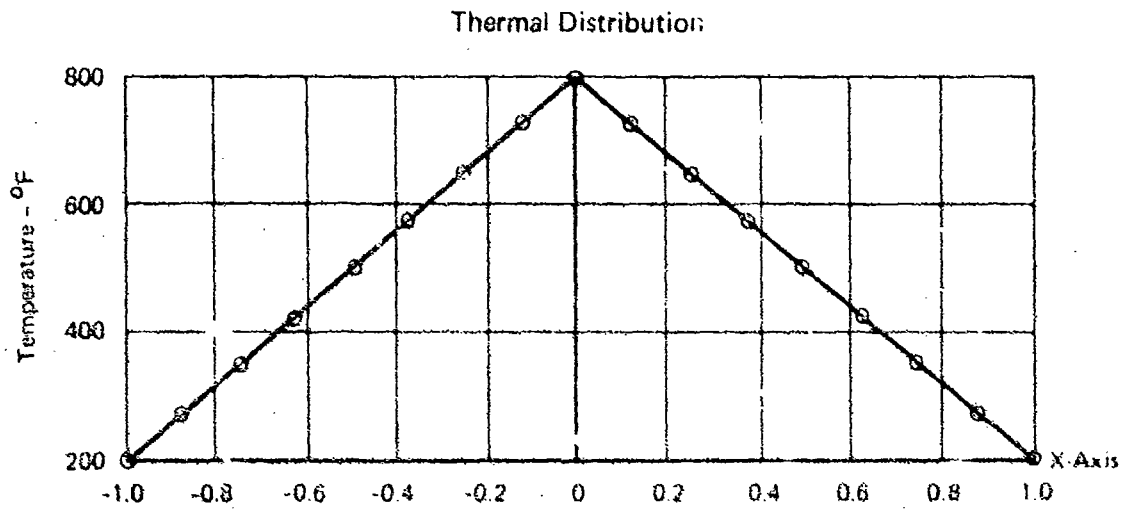




FIGURE 23  
THERMAL STRESS DISTRIBUTION  
FREE-FREE BOUNDARY CONDITION  
2nd Order Temperature Distribution

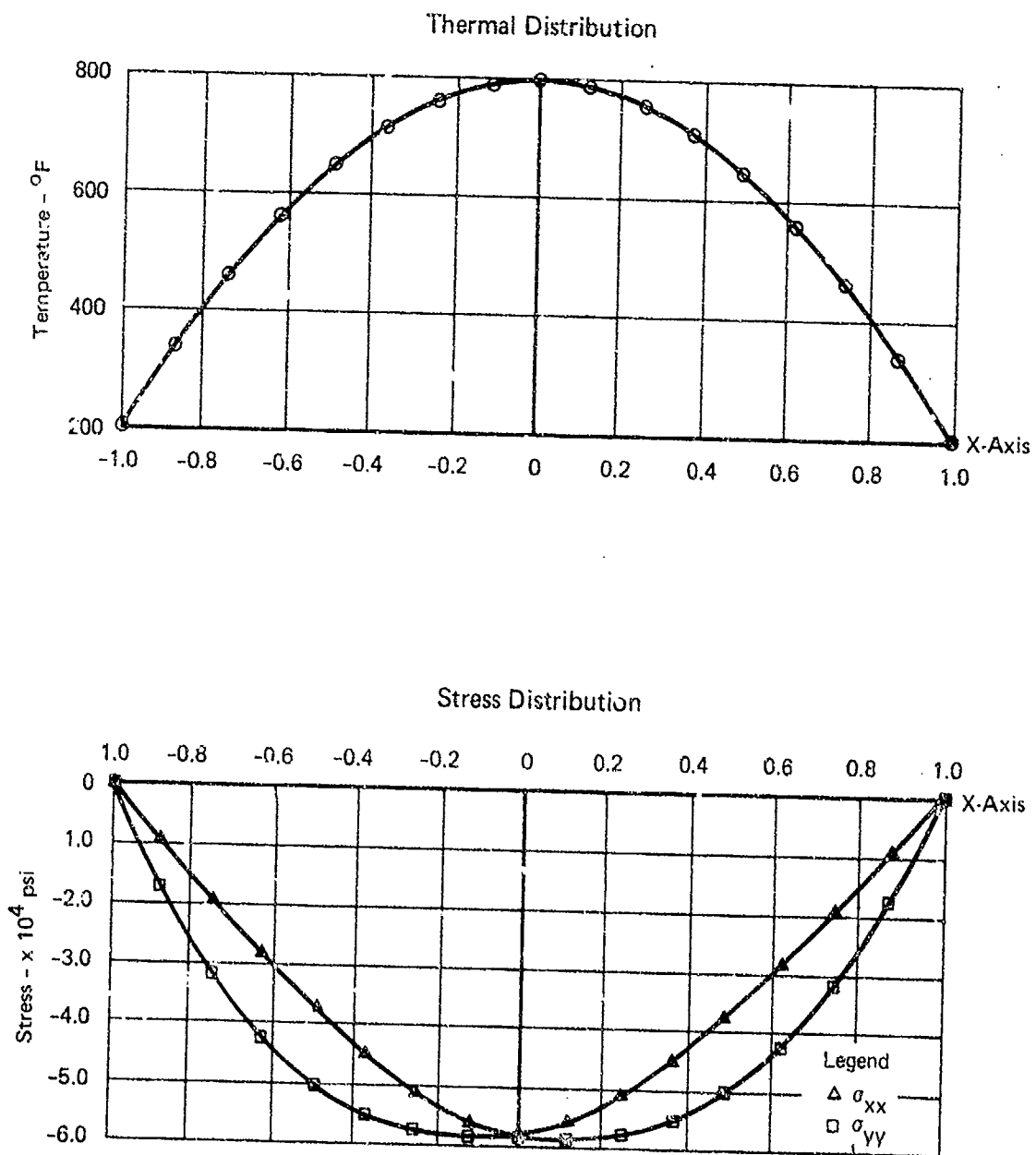


FIGURE 24  
THERMAL STRESS DISTRIBUTION  
FREE-FREE BOUNDARY CONDITION  
3rd Order Temperature Distribution

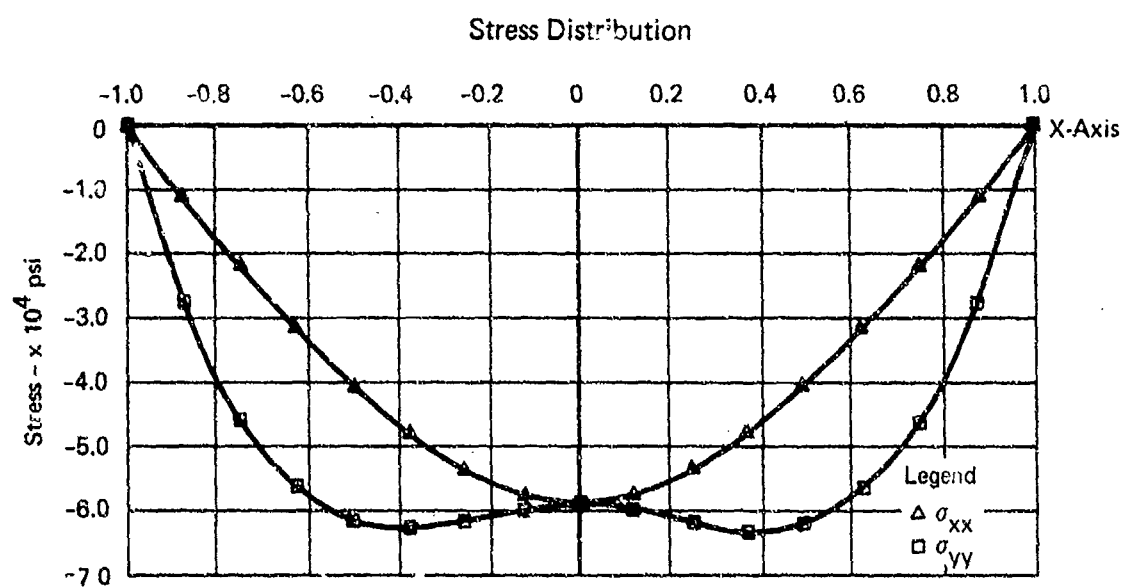
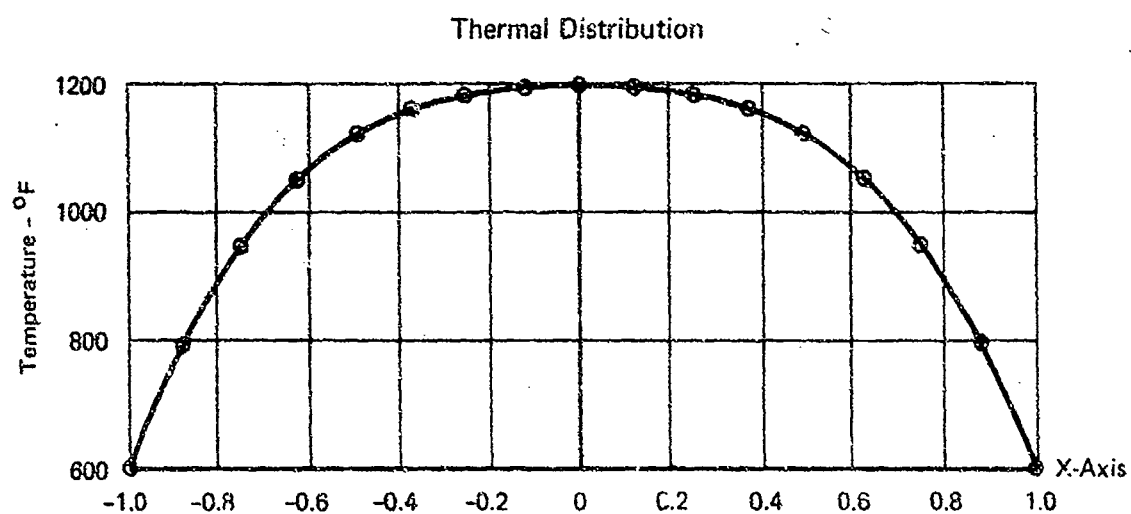


FIGURE 25  
THERMAL STRESS DISTRIBUTION  
FREE-FREE BOUNDARY CONDITION  
4th Order Temperature Distribution

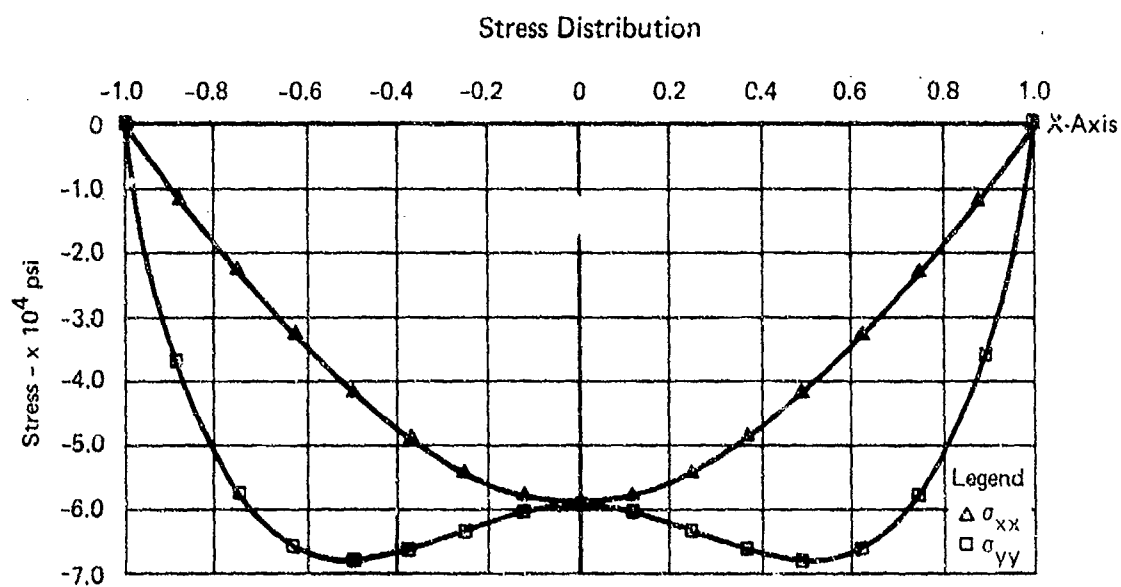
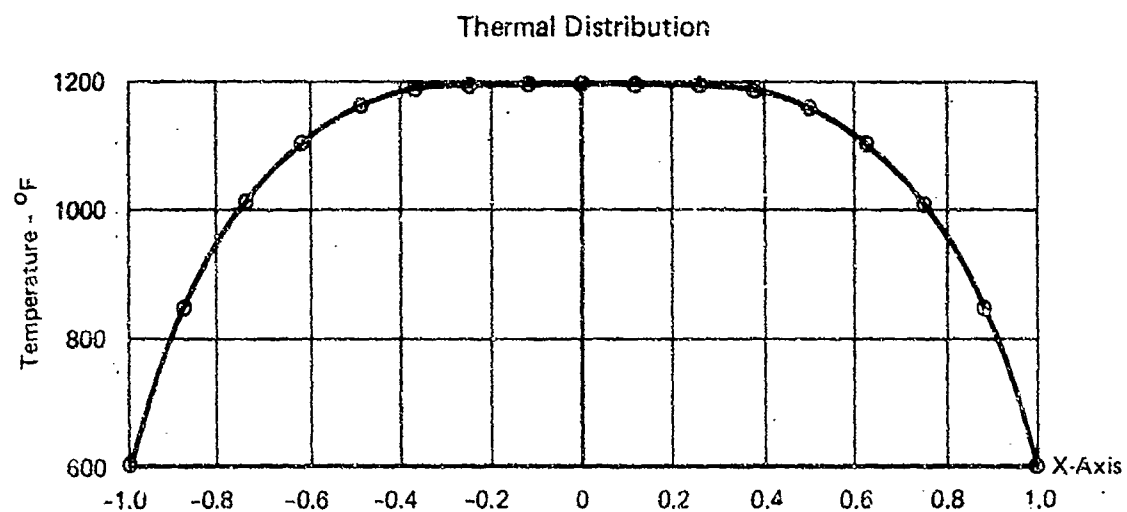


FIGURE 26  
TEST SET UP FOR FREE PANEL

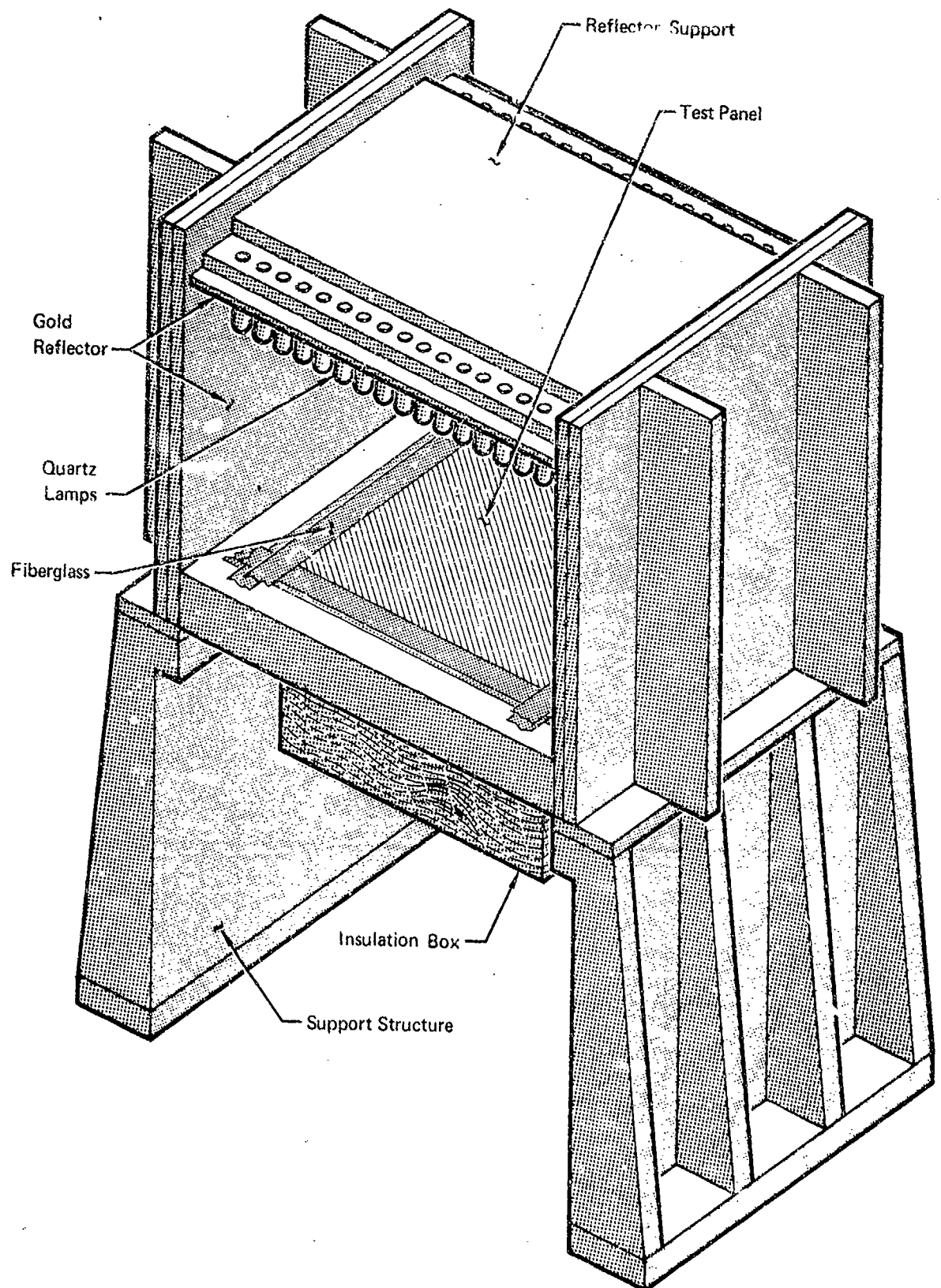
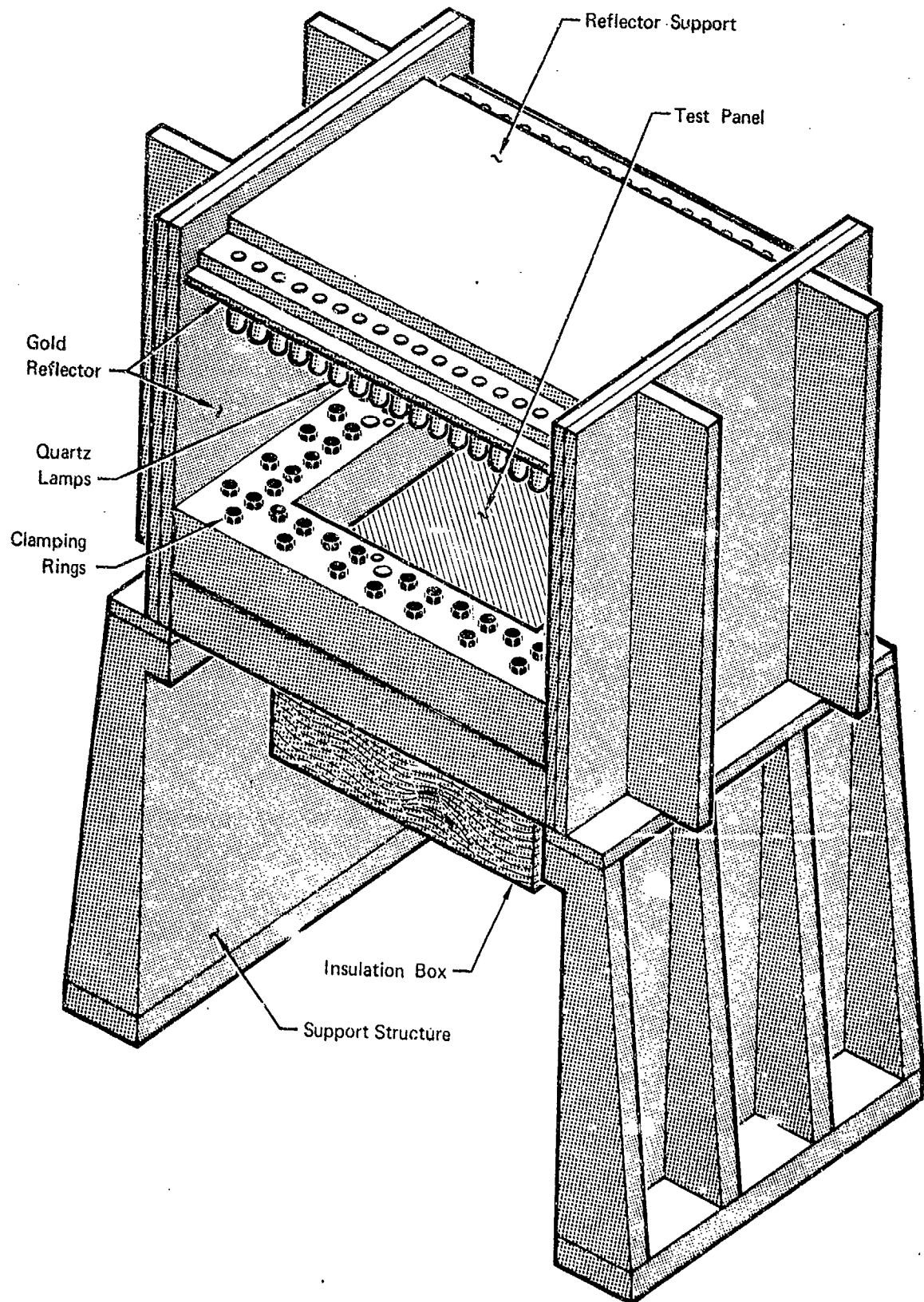


FIGURE 27  
TEST SET UP FOR FIXED PANEL



Temperature and strain data were obtained at several points on the fixed-edge test panel. A least squares polynomial fit was performed on the centerline temperatures and the coefficients were normalized to obtain the  $\bar{A}_i$  values described in equation (4.26). The  $\bar{T}_C$  value calculated in this manner is compared with  $\bar{T}_C$  obtained as  $(T_C - T_B)/T_C$  using an average boundary temperature. The results are summarized in Table 5. During the initial low temperature thermal tests the stress data for the experimental panel was consistent with the theoretical values shown in Figure 17. During the high temperature tests the experimental boundary was substantially less stiff than a fixed condition as shown by the fact that the strain at the boundary was approximately  $\alpha T_B/2$ . The boundary strain for a fixed panel would be zero while the boundary strain for a free panel would be  $\alpha T_B$ . A least squares analysis of  $\bar{\sigma}_C$  vs  $\bar{T}_C$  for the high temperature tests on the experimental panel is presented in Table 6. The results of this analysis are shown in Figure 28.

The techniques used in this section for determining the stress distribution due to thermal effects can be powerful tools in analyzing actual laboratory cases. As shown previously, for simple experimental cases, a good estimate of the actual stress experienced by the test panel can be obtained by utilizing normalized polynomial temperature distributions. A few experimental cases may then be run to determine  $\bar{\sigma}_C$  vs  $\bar{T}_C$ . For variable boundary temperatures and difficult boundary conditions equations (4.4a) and (4.9) must be solved for C and  $\psi_{\text{boundary}}$ , respectively and these values used in the computer programs shown in Appendix D. If, however, the boundary can be assumed to be close to one of the conditions studied here, Figure 28 may be used to give an approximate center stress. Tables 3 and 4 also give an indication of how maximum stress varies with increased order of temperature distribution.

To verify the accuracy of the technique described in this section a comparison was made between the closed form solution of the rectangular plate problem (shown in Figure 29 and described in reference 14) and the solution obtained by the finite difference solution of the strain potential equation. The plate in this case is free to expand in the y direction. The boundaries at  $x = \pm b/2$  are placed in the "free" condition by the application of a stress in the x direction of  $2\alpha ET_0/3$ , according to Timoshenko.

At the corners we have the conditions

$$\sigma_{xx} = 2\alpha ET_0/3, \sigma_{yy} = 0, T_{\text{corner}} = 0. \quad (4.29)$$

Solving equations (4.5a) and (4.5b) for  $\epsilon_{xx}$  and  $\epsilon_{yy}$  and substituting into (4.9) the constant, C, is found to be  $2(1-\nu)\alpha T_0/3$ . We assume  $\psi$  to be of the form given in equation (4.12). The values at the boundary then become

$$\psi \Big|_{x = \pm \frac{b}{2}} = f_1 \left( \frac{b}{2} \right) + f_2(y) + f_3 \left( \frac{b}{2} \right) f_4(y) \quad (4.30a)$$

$$\psi \Big|_{y = \pm \frac{a}{2}} = f_1(x) + f_2 \left( \frac{a}{2} \right) + f_3(x) f_4 \left( \frac{a}{2} \right) \quad (4.30b)$$

The boundary conditions are

$$\sigma_{xx} = 2\alpha ET_0/3, \sigma_{yy} = 0 \quad (4.31)$$

at

$$x = \pm \frac{b}{2}, y = \pm \frac{a}{2}$$

TABLE 5  
EXPERIMENTAL EVALUATION OF  $\bar{T}_c$

Axis	$T_B$		$T_C$	$\frac{T_B - T_C}{T_C}$	$\bar{T} = -\bar{A}_1$	$\bar{c}$
	+1.	-1.				
X	76	70	118	0.382	0.406	-0.301
X	83	73	118	0.322	0.354	-0.34
X	150	135	247	0.425	0.453	-0.390
Y	166	180	247	0.360	0.324	-0.401
X	220	186	400	0.488	0.528	-0.370
Y	342	316	400	0.425	0.460	-0.383

TABLE 6  
EXPERIMENTAL THERMAL STRESS DATA ANALYSIS

LEAST - SQUARES POLYNOMIALS

NUMBER OF POINTS = 7  
MEAN VALUE OF X = .513571  
MEAN VALUE OF Y = -.364286  
STD ERROR OF Y = 3.41258E-02

X =  $\bar{T}$   
Y =  $\bar{\sigma}$

POLYFIT OF DEGREE 1 INDEX OF DETERM = 8.41584E-03

TERM	COEFFICIENT			
0	-.357031			
1	-1.41261E-02			
X-ACTUAL	Y-ACTUAL	Y-CALC	DIFF	PCT-DIFF
.354000	-.340000	-.362032	2.20316E-02	-6.06554
.394000	-.401000	-.362597	-3.84034E-02	10.5912
.406000	-.301000	-.362766	6.17661E-02	-17.0264
.453000	-.390000	-.363430	-2.65699E-02	7.31088
.460000	-.383000	-.363529	-1.94710E-02	5.35612
.528000	-.370000	-.364490	-5.51047E-03	1.51183
1	-.365000	-.371157	6.15707E-03	-1.65889

STD ERROR & ESTIMATE FOR Y = 3.72253E-02



FIGURE 28  
THERMAL STRESS RESPONSE

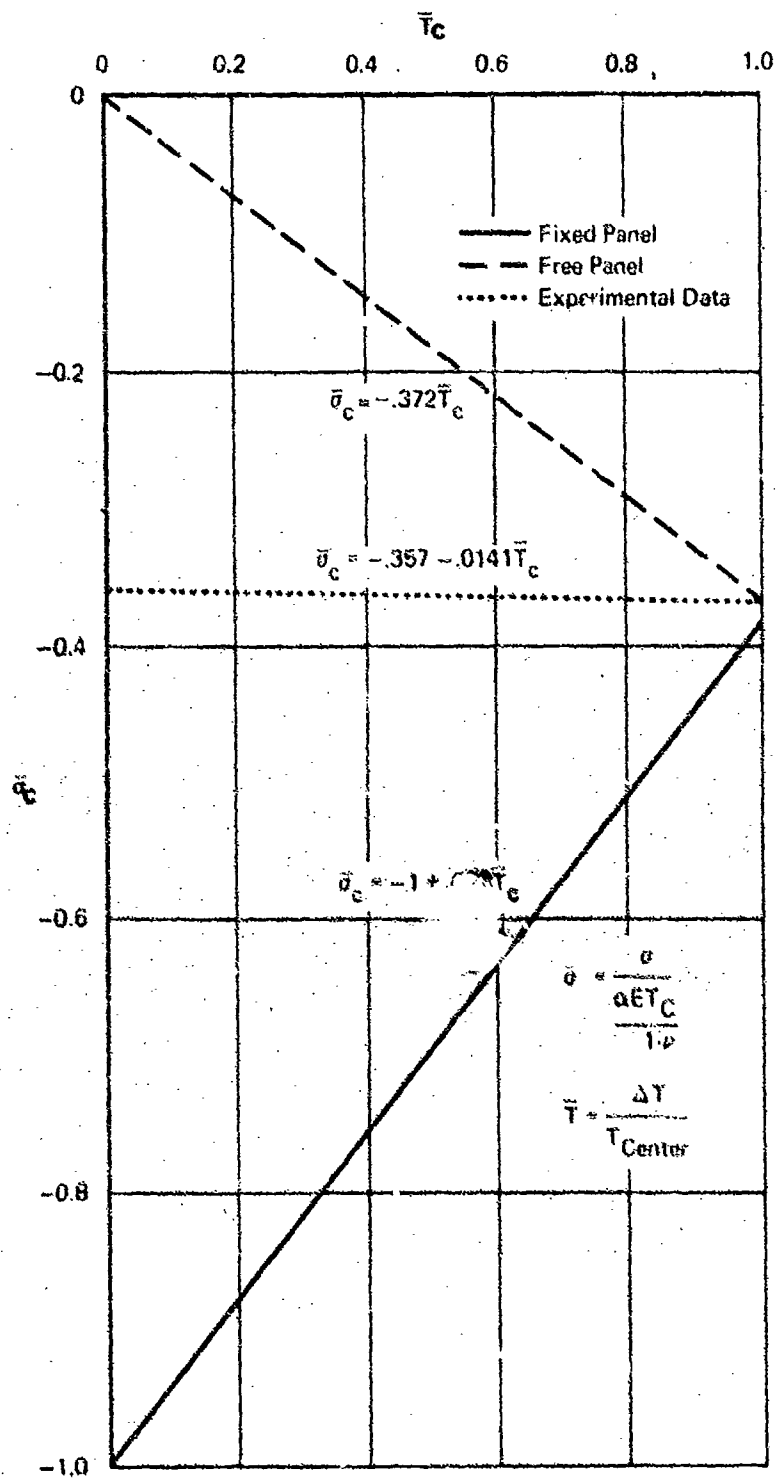
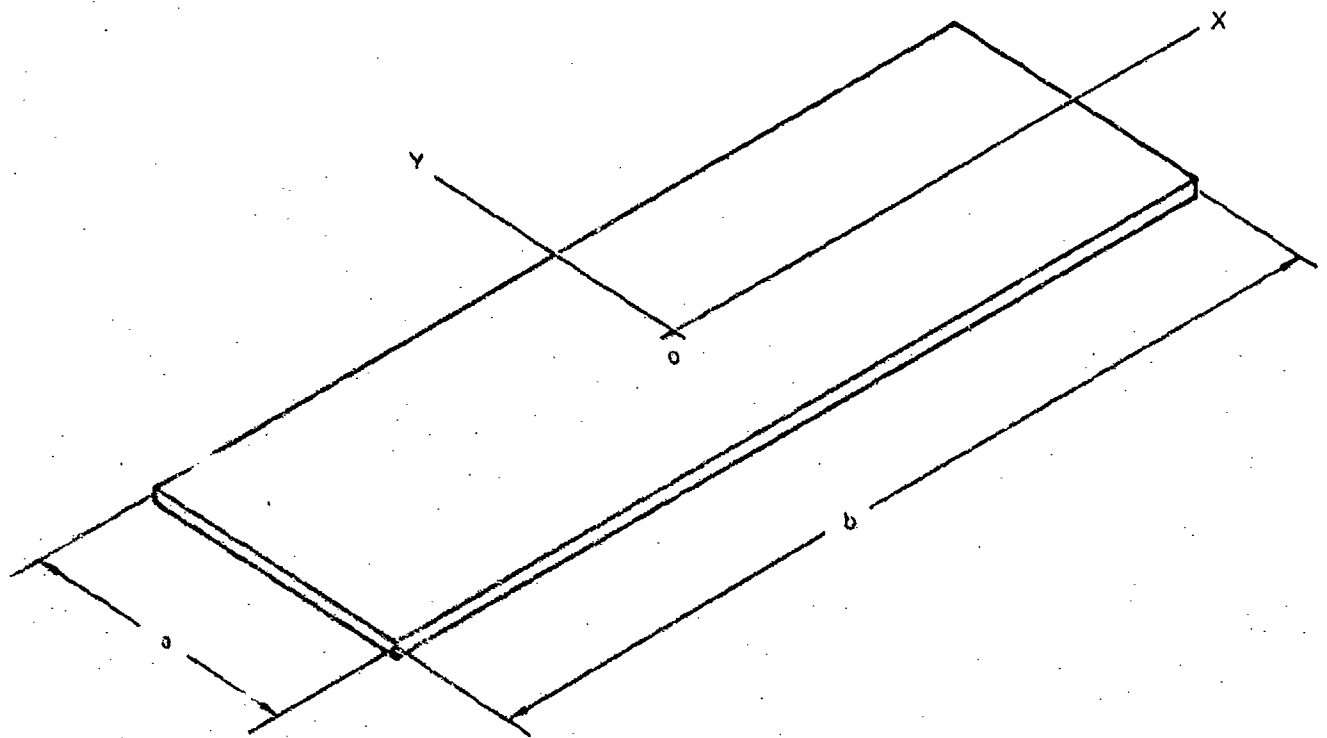


FIGURE 29  
RECTANGULAR PLATE MODEL  
CLOSED FORM - FINITE DIFFERENCE COMPARISON



$$T(x,y) = T_0 \left( 1 - \frac{4y^2}{a^2} \right)$$

$$\frac{a}{b} = 0.10$$

Substitution of equations (4.30) and (4.31) into (4.5a) and (4.5b) will allow solution for the functions  $f_1$ ,  $f_2$ ,  $f_3$ , and  $f_4$  to within a constant. Applying the requirement that the values of  $\psi$  given by equations (4.30a) and (4.30b) be the same at the corners allows evaluation of the arbitrary constants. The values of  $\psi$  at the boundaries are then given by

$$\psi \Big|_{x=\pm \frac{b}{2}} = \frac{(1+\nu)\alpha T_0}{2} y^2 \left(1 - \frac{2y^2}{3a^2}\right) - \frac{\nu\alpha T_0}{3} y^2 - \quad (4.32a)$$

$$\psi \Big|_{y=\pm \frac{a}{2}} = \frac{5(1+\nu)\alpha T_0 a^2}{48} + \frac{\nu\alpha T_0 a^2}{12} - \frac{\alpha T_0 x^2}{3} - \frac{\alpha T_0 b^2}{12} \quad (4.32b)$$

Solution of equations (4.4) through (4.5) subject to the constant in (4.4) being  $2(1-\nu)\alpha T_0/3$  was accomplished by use of the computer programs presented in Appendix D. Table 7 lists the results of this analysis compared to the closed form solution,

$$\sigma_{xx} = \frac{2}{3} \alpha E T_0 - \alpha E T_0 \left(1 - \frac{4y^2}{a^2}\right), \sigma_{yy} = 0 \quad (4.33)$$

In this case  $T_0$  was taken as 5387.9°F, thus for a steel panel  $\alpha E T_0$  becomes  $1.00 \times 10^6$ . The error in the values of  $\sigma_{xx}$  are obviously due to truncation of the decimal values of improper fractions. The error in  $\sigma_{yy}$  is due to the method of computing strain which results in taking the difference of large numbers. The accuracy, if required, can be improved by using double precision arithmetic, increasing the number of iterations in the potential program, and using a finer mesh in the finite difference routine.

Substituting the closed form solution (4.33) into equations (4.5a) and (4.5b) and solving for strain we find that the sum of the strains minus  $(1+\nu)\alpha T$  at any point in the plate is  $2(1-\nu)\alpha T_0/3$ . This is the constant of integration evaluated from equation (4.9) and the boundary conditions at the corners.

For commonly encountered boundary conditions and materials it is recommended that the techniques developed previously be used with a statistical method such as Latin Squares to extend the design information presented here. For details on the use of Latin Squares the reader is referred to references 11 and 13. It is suggested that a four level Latin Square plan be used to determine  $\bar{\sigma}_C$  and  $\bar{\sigma}_{Max}$  as a function of  $\bar{T}$ ,  $a/b$ , and boundary stiffness. The variation of  $\bar{\sigma}$  with the parameter  $\nu$  need not be considered since it is approximately the same for most engineering materials and  $E/(1-\nu^2)$  is contained in the parameter  $\bar{\sigma}$ . The boundary stiffness may be determined either qualitatively or quantitatively. The stiffness used in the analysis must be non-dimensionalized to an appropriate value. An example of a four level Latin Square design for determining  $\bar{\sigma}$  as a function of boundary,  $\bar{T}$ , and  $a/b$  is shown in Figure 30. This analysis requires  $4^2$  or 16 experiments as compared to  $4^3$  or 64 experiments for a conventional analysis of variance.

The values of  $\bar{\sigma}_{11}$ ,  $\bar{\sigma}_{12}$ , and  $\bar{\sigma}_{14}$  are obtained from Figure 28. The values of  $\bar{\sigma}_{21}$ ,  $\bar{\sigma}_{31}$ ,  $\bar{\sigma}_{41}$ ,  $\bar{\sigma}_{24}$ ,  $\bar{\sigma}_{34}$ , and  $\bar{\sigma}_{44}$  may be obtained by using computer programs presented in Appendix D. The remaining  $\bar{\sigma}_{ii}$  may be determined by experiment or numerical solution as described

**TABLE 7**  
**COMPARISON OF FINITE DIFFERENCE-CLOSED FORM**  
**SOLUTIONS FOR A RECTANGULAR PLATE**

Y	X	TEMP.	FINITE DIFFERENCE SOLUTION		CLOSED FORM SOLUTION	
			$\sigma_{yy}$	$\sigma_{xx}$	$\frac{\sigma_{yy}}{10^{-5}}$	$\frac{\sigma_{xx}}{10^{-5}}$
-5.00	-50.00	0.0	0.219E-01	0.667E+06	0	2/3
-5.00	-40.00	0.0	0.219E-01	0.667E+06		
-5.00	-30.00	0.0	0.219E-01	0.667E+06		
-5.00	-20.00	0.0	0.219E-01	0.667E+06		
-5.00	-10.00	0.0	0.219E-01	0.667E+06		
-5.00	.00	0.0	0.219E-01	0.667E+06		
-5.00	10.00	0.0	0.219E-01	0.667E+06		
-5.00	20.00	0.0	0.219E-01	0.667E+06		
-5.00	30.00	0.0	0.219E-01	0.667E+06		
-5.00	40.00	0.0	0.219E-01	0.667E+06		
-5.00	50.00	0.0	0.219E-01	0.667E+06		
-3.33	-50.00	2993.3	0.186E+00	0.111E+06	0	1/9
-3.33	-40.00	2993.3	-6.36E+03	0.111E+06		
-3.33	-30.00	2993.3	0.115E+03	0.111E+06		
-3.33	-20.00	2993.3	-1.40E+03	0.111E+06		
-3.33	-10.00	2993.3	0.282E+01	0.111E+06		
-3.33	.00	2993.3	0.115E+03	0.111E+06		
-3.33	10.00	2993.3	0.282E+01	0.111E+06		
-3.33	20.00	2993.3	-1.40E+03	0.111E+06		
-3.33	30.00	2993.3	0.115E+03	0.111E+06		
-3.33	40.00	2993.3	-6.36E+03	0.111E+06		
-3.33	50.00	2993.3	0.186E+00	0.111E+06		
-1.67	-50.00	4789.3	0.153E+00	-2.22E+06	0	2/9
-1.67	-40.00	4789.3	-9.16E+03	-2.22E+06		
-1.67	-30.00	4789.3	-1.00E+03	-2.22E+06		
-1.67	-20.00	4789.3	0.153E+03	-2.22E+06		
-1.67	-10.00	4789.3	-1.31E+03	-2.22E+06		
-1.67	.00	4789.3	0.181E+02	-2.22E+06		
-1.67	10.00	4789.3	-1.31E+03	-2.22E+06		
-1.67	20.00	4789.3	0.153E+03	-2.22E+06		
-1.67	30.00	4789.3	-1.00E+03	-2.22E+06		
-1.67	40.00	4789.3	-9.16E+03	-2.22E+06		
-1.67	50.00	4789.3	0.153E+00	-2.22E+06		
.00	-50.00	5387.9	0.142E+00	-3.33E+06	0	1/3
.00	-40.00	5387.9	-1.08E+04	-3.33E+06		
.00	-30.00	5387.9	-3.94E+02	-3.33E+06		
.00	-20.00	5387.9	-3.94E+02	-3.33E+06		
.00	-10.00	5387.9	0.163E+03	-3.33E+06		
.00	.00	5387.9	-3.94E+02	-3.33E+06		
.00	10.00	5387.9	0.163E+03	-3.33E+06		
.00	20.00	5387.9	-3.94E+02	-3.33E+06		
.00	30.00	5387.9	-3.94E+02	-3.33E+06		
.00	40.00	5387.9	-1.08E+04	-3.33E+06		
.00	50.00	5387.9	0.142E+00	-3.33E+06		
1.67	-50.00	4789.3	0.153E+00	-2.22E+06	0	2/9
1.67	-40.00	4789.3	-9.16E+03	-2.22E+06		
1.67	-30.00	4789.3	-1.00E+03	-2.22E+06		
1.67	-20.00	4789.3	0.153E+03	-2.22E+06		
1.67	-10.00	4789.3	-1.31E+03	-2.22E+06		
1.67	.00	4789.3	0.181E+02	-2.22E+06		
1.67	10.00	4789.3	-1.31E+03	-2.22E+06		
1.67	20.00	4789.3	0.153E+03	-2.22E+06		
1.67	30.00	4789.3	-1.00E+03	-2.22E+06		
1.67	40.00	4789.3	-9.16E+03	-2.22E+06		
1.67	50.00	4789.3	0.153E+00	-2.22E+06		
3.33	-50.00	2993.3	0.186E+00	0.111E+06	0	2/5
3.33	-40.00	2993.3	-6.36E+03	0.111E+06		
3.33	-30.00	2993.3	0.115E+03	0.111E+06		
3.33	-20.00	2993.3	-1.40E+03	0.111E+06		
3.33	-10.00	2993.3	0.282E+01	0.111E+06		
3.33	.00	2993.3	0.115E+03	0.111E+06		
3.33	10.00	2993.3	0.282E+01	0.111E+06		
3.33	20.00	2993.3	-1.40E+03	0.111E+06		
3.33	30.00	2993.3	0.115E+03	0.111E+06		
3.33	40.00	2993.3	-6.36E+03	0.111E+06		
3.33	50.00	2993.3	0.186E+00	0.111E+06		
5.00	-50.00	0.0	0.219E-01	0.667E+06	0	2/3
5.00	-40.00	0.0	0.219E-01	0.667E+06		
5.00	-30.00	0.0	0.219E-01	0.667E+06		
5.00	-20.00	0.0	0.219E-01	0.667E+06		
5.00	-10.00	0.0	0.219E-01	0.667E+06		
5.00	.00	0.0	0.219E-01	0.667E+06		
5.00	10.00	0.0	0.219E-01	0.667E+06		
5.00	20.00	0.0	0.219E-01	0.667E+06		
5.00	30.00	0.0	0.219E-01	0.667E+06		
5.00	40.00	0.0	0.219E-01	0.667E+06		
5.00	50.00	0.0	0.219E-01	0.667E+06		

FIGURE 30  
4 LEVEL LATIN SQUARE

$$\bar{\sigma} = f(\text{boundary}, \bar{Y}, \frac{a}{b})$$

$$\frac{a}{b} = 1$$

$$\frac{a}{b} = .75$$

$$\frac{a}{b} = .5$$

$$\frac{a}{b} = .25$$

Boundary 1  
Fixed

$$\bar{Y} = 0$$
  

$$\bar{\sigma}_{11}$$

$$\bar{Y} = .25$$
  

$$\bar{\sigma}_{21}$$

$$\bar{Y} = .5$$
  

$$\bar{\sigma}_{31}$$

$$\bar{Y} = .75$$
  

$$\bar{\sigma}_{41}$$

Boundary 2  
Experimentary

$$\bar{Y} = .25$$
  

$$\bar{\sigma}_{12}$$

$$\bar{Y} = .5$$
  

$$\bar{\sigma}_{22}$$

$$\bar{Y} = .75$$
  

$$\bar{\sigma}_{32}$$

$$\bar{Y} = 0$$
  

$$\bar{\sigma}_{42}$$

Boundary 3

$$\bar{Y} = .5$$
  

$$\bar{\sigma}_{13}$$

$$\bar{Y} = .75$$
  

$$\bar{\sigma}_{23}$$

$$\bar{Y} = 0$$
  

$$\bar{\sigma}_{33}$$

$$\bar{Y} = .25$$
  

$$\bar{\sigma}_{43}$$

Boundary 4  
Free

$$\bar{Y} = .75$$
  

$$\bar{\sigma}_{14}$$

$$\bar{Y} = 0$$
  

$$\bar{\sigma}_{24}$$

$$\bar{Y} = .25$$
  

$$\bar{\sigma}_{34}$$

$$\bar{Y} = .5$$
  

$$\bar{\sigma}_{44}$$

in references 11 and 13. The partial responses  $\bar{\sigma}_C = f(\bar{T})$ ,  $\bar{\sigma}_C = f(\bar{K}_T)$ ,  $\bar{\sigma}_C = f(a/b)$ , and the total response  $\bar{\sigma}_C = f(\bar{T}, \bar{K}_T, a/b)$  can be determined from statistical techniques. If it is desired to find  $\bar{\sigma}_{Max}$  as a function of  $\bar{T}$ ,  $\bar{K}_T$ , and  $a/b$  the form of  $\bar{T}$  may be another independent parameter in which case a Greco-Latin Square would be used. This would require  $4^3$  or 64 experiments instead of 256 for the conventional analysis of variance.

The results of the above analysis would provide the design curves necessary for the selection of boundary stiffness to induce the proper stress level. For a given boundary an estimate of the center and maximum stress for a given temperature distribution could also be obtained from the design curves.

### 4.3 DYNAMIC EFFECTS

The solution of the dynamic stress problem requires the solution of the following equations:

$$\sigma_{\bar{x}\bar{x}} = \frac{E}{2(1-\nu^2)} \left[ \left(\frac{c}{a}\right)^2 \bar{x}\bar{x} \bar{w}_s + \nu \left(\frac{c}{b}\right)^2 \partial_{\bar{y}\bar{y}} \bar{w}_s \right] \quad (4.34a)$$

$$\sigma_{\bar{y}\bar{y}} = \frac{E}{2(1-\nu^2)} \left[ \left(\frac{c}{b}\right)^2 \partial_{\bar{y}\bar{y}} \bar{w}_s + \nu \left(\frac{c}{a}\right)^2 \partial_{\bar{x}\bar{x}} \bar{w}_s \right] \quad (4.34b)$$

$$\sigma_{\bar{x}\bar{y}} = 2G \left(\frac{c}{a}\right) \left(\frac{c}{b}\right) \partial_{\bar{x}\bar{y}} \bar{w}_s \quad (4.34c)$$

Thus for known material properties the stress can be determined when the deflection,  $\bar{w}_s$ , is known.

The first step in obtaining the deflection,  $\bar{w}_s$ , requires the solution of the dynamic plate equation (4.7). The values of  $N_{xx}$ ,  $N_{yy}$ ,  $N_{xy}$  are given by equations (4.5) and (4.6). It is evident that the thermal stress problem must be solved prior to solving the combined dynamic and thermal problems. From equation (4.7) the parameters that affect the undamped mode shape for free vibrations,  $\bar{w}$ , are boundary conditions,  $a/b$ ,  $a/c$ ,  $\alpha T$ ,  $\nu$ , and  $(\rho a^4 \omega_n^2 / gE C^2)$ . This last parameter is of special interest due to the  $\omega_n^2$  term. In general  $\omega_n^2$  is not known and in fact may be considered as a dependent variable which is a function of the mode shape, in-plane forces, boundary conditions, geometric and material properties. It will be convenient to multiply the dimensionless parameter containing  $\omega_n^2$  by  $12(1-\nu^2)$  to yield  $\omega_n^2 [gE C^2 / 12(1-\nu^2) \rho a^4]$ . The term in brackets can be considered as the natural frequency of the panel at ambient temperature divided by a constant. Thus we write this dimensionless parameter as  $\omega_n^2 / C^2 \omega_n^2 \text{ ambient}$ . The value of  $C^2$  for various boundary conditions, materials, and  $a/b$  ratios is readily available in the literature.<sup>15,16</sup>

For zero in-plane forces  $\omega_n$  is the frequency given by equation (C19) and for increasing compressive loads  $\omega_n$  is decreased to zero at the first critical buckling load. Since equation (4.7) is a homogeneous equation the previously employed finite difference technique yields only the trivial solution  $w = 0$ . However, a number of computer programs are available in the industry for computing  $\omega_n$  and  $w$  for various structural modes. Most of these programs require only the geometry and material properties as input. A lumped parameter mass and stiffness matrix is then generated using techniques such as the finite element technique. The values of  $w$  are then obtained as the eigenvectors and  $\omega_n$  as the eigenvalues of the dynamic matrix by one of several numerical techniques.

The main problem with this type of solution is accounting for the thermal loads. Equation (C20), Appendix C, rewritten in the form  $M\ddot{w} + Kx = 0$  becomes

$$\rho \frac{c}{g} \ddot{w} + \left\{ D \left[ \partial_{xxxx} w + 2\partial_{xxyy} w + \partial_{yyyy} w \right] - \left[ N_{xx} \partial_{xx} w - 2N_{xy} \partial_{xy} w + N_{yy} \partial_{yy} w \right] \right\} = 0 \quad (4.35)$$

From this it is apparent that the expression in braces is a stiffness term. Thus it would be necessary to modify finite element programs such as the McDonnell Douglas Automation Company dynamic analysis program to provide for a reduction of the terms in the stiffness matrix to a matrix determined from the terms involving  $N_{ij} \partial_{ij} w$ . It may also be possible to use a modified form of the current popular NASTRAN program.<sup>17</sup>

Although the above modified programs would provide a solution to the dynamic equation including in-plane loads, it would still be necessary to use a large number of elements to obtain reasonable accuracy.<sup>18</sup> In the experimental 15 inch square panel, if elements are taken every inch (fairly large increments) the stiffness and mass matrices are  $15 \times 15$  for only one degree of freedom. The size of the matrix is increased by 15 per side for each additional degree of freedom. It is obvious that the storage limitations and cost soon become limiting factors. Single runs of the above mentioned programs, not modified to include thermal loading, may cost several hundred dollars.

The cost involved in the numerical solution and the lack of closed form solutions for equation (4.7) indicates that either experimental solutions or combined experimental and numerical solutions should be employed. Mapping mode shapes in the combined thermal/acoustic environment can be an expensive and time-consuming process, thereby making experimental determination of  $w$  difficult. One possible, low cost method of obtaining design curves for  $\omega_n^2/C^2\omega_n^2$  ambient vs the independent parameters is to experimentally determine the values of  $\omega_n$  for various high temperature cases. In some cases, such as simply supported polygonal plates with constant in-plane forces, the mode shape is independent of the magnitude of the in-plane load. Thus a computer solution or experimental mode mapping is not necessary. In cases where the mode shape is not known from the literature it may be necessary to perform a ground vibration test to determine the modal response. Normalized mode shapes can then be computed from the measured data and the mass matrix. Equations (A4) and (A5) relate the normalized mode shapes and the natural frequencies to the mass and stiffness matrices. It is these matrices which must be known for the elevated temperature case. The generalized mass and stiffness matrices are then given by

$$[M] = [\Phi]^T [\Phi] \quad (4.36a)$$

$$[K] = [\Phi]^T [-\omega_n^2] [\Phi] \quad (4.36b)$$

It should be noted here that two important assumptions have been made; first, it is assumed that the method of excitation and measurement does not effect the normal modes; second, the damping must be small so that the mode shape computed from the measured data is the same as the undamped normal mode. It is recommended that measured modes be checked for orthogonality to test the accuracy of the above assumptions.

Once the system characteristics have been determined either by one of the finite element computer programs or the experimental methods described above the deflection can be determined for a given forcing function and damping value by the methods presented in section 2.2. This section presents methods for determining the deflections which must be substituted into equations (4.34) to obtain stress in terms of the coupling between the structure and the given acoustic field.

In the present experimental study a plate with both free and fixed boundary conditions was subjected to acoustic loads at ambient temperature and at a nominal 450°F plate center temperature.<sup>19</sup> The experimental test setups for the free and fixed panels are the same as those for the static thermal tests (Figures 26 and 27). Mathematical models used in the ambient temperature modal analysis for the free and fixed panels are shown in Figure 31. The mode shapes and natural frequencies from the analysis and experiment at ambient temperature are presented in Figure 32 for the fixed and free panel. The experimental frequencies shown are the results of vibration excitation since some modes could not be excited acoustically and mode mapping was not convenient in the acoustic environment. However, these results give an indication of the quality of the dynamic boundary conditions. Frequency shifts during acoustic testing from ambient to 450°F center temperature are shown in Figures 33 and 34 for the free panel and Figures 35 and 36 for the fixed panel. Table 8 summarizes the frequency changes and the percentage frequency shifts. As shown in the table the average reduction in natural frequencies was 3.4% for the free panel and 9.4% for the fixed panel. A reduction of 5.0% in Young's Modulus due to temperature would account for a 2.2% reduction in natural frequency. Thus a 1.2% and 7.2% decrease in frequency in the free and fixed panels can be attributed to the effect of in-plane forces.

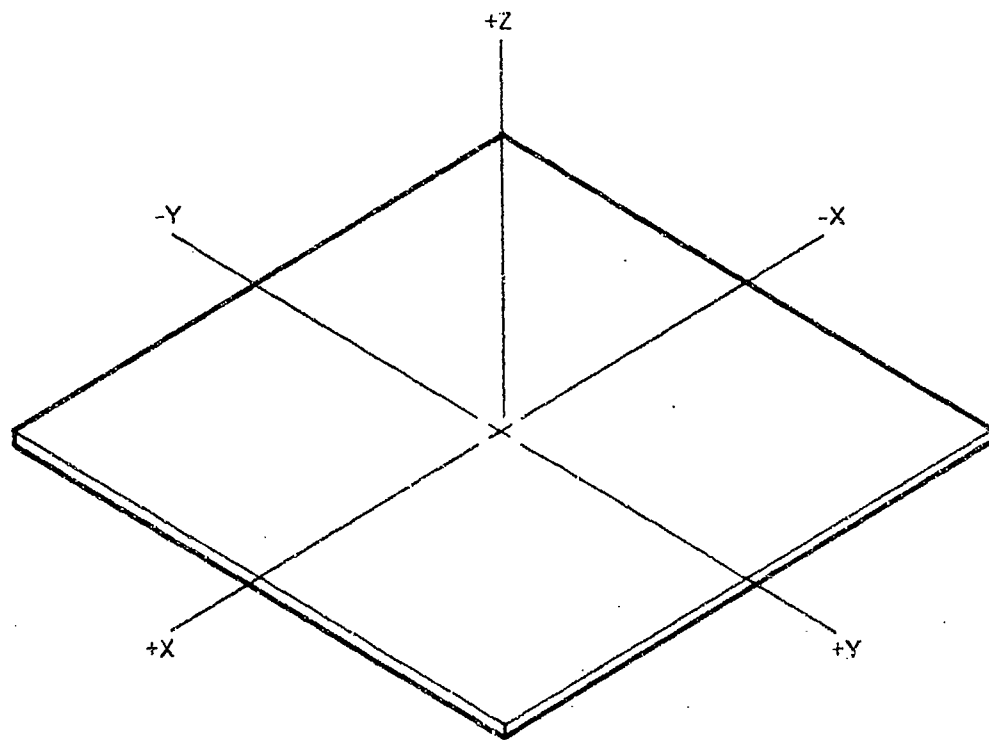
#### 4.4 THERMAL/ACOUSTIC MOUNTING

The preceding sections have shown how thermal stresses and dynamic stresses can be analytically evaluated in a sonic fatigue test specimen. The importance of the support structure for combined thermal/acoustic loading is apparent from the governing equations. In designing a mounting for testing panels in the combined environment, one must consider both the thermal conditions at the boundary of the panel, and the mechanical restraint imposed on the edges of the panel. The remainder of this section will discuss specimen mounting designs, starting with the thermal aspect of the problem. After the method for controlling the boundary temperature has been established, one may proceed to the design of a mechanical boundary that will produce the desired thermally-induced in-plane loads. Finally, attention may be directed to the design of panel edge restraints that will result in the proper panel frequencies and mode shapes.

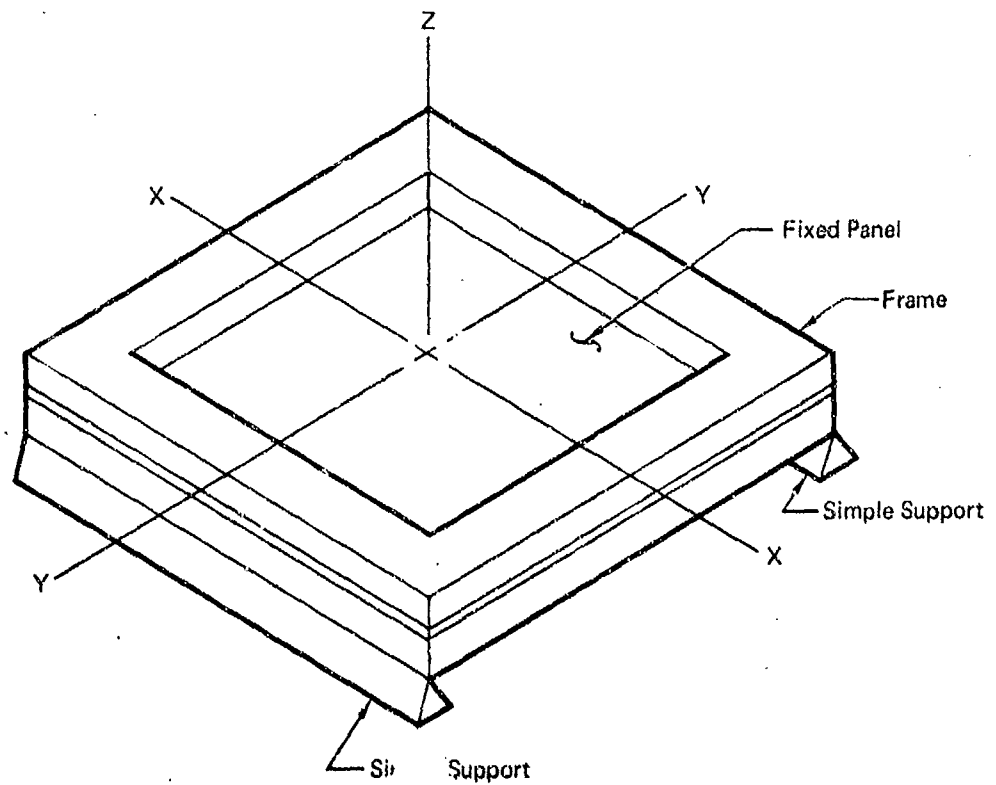
The first part of the boundary synthesis problem is the design of the thermal boundary. The specification of boundary temperature and  $\dot{q}$  will determine the temperature distribution. Maintaining the proper boundary temperature may be as important as the physical stiffness of the boundary. As described in section 4.2, even a free panel with boundaries maintained at ambient temperature will have the same thermal stress as a fixed panel.



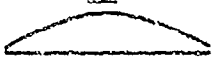
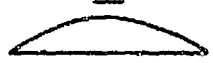


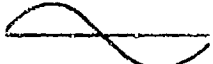
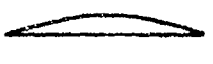
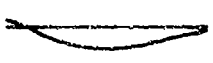
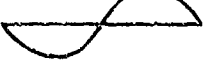
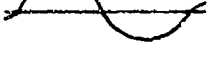
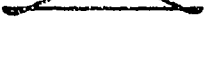




FIGURE 31  
FREE-PANEL CONFIGURATION FOR ANALYTICAL STUDIES



FIXED PANEL CONFIGURATION FOR ANALYTICAL STUDIES



**FIGURE 32  
FIXED PANEL MODAL CHARACTERISTICS**

Mode	Analytical Frequency	Experimental Frequency	Computed Mode Shape Axis	
			X	Y
1	576.7	585		
2	838.4	833		
3	1104.0	1083		
4	1256.8	-		
5	1360.2	-		
6	1830.9	-		
7	2017.2	-		

**FREE PANEL MODAL CHARACTERISTICS**

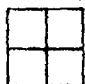






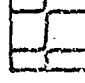

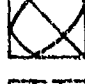

Computed		Measured	
Frequency (Hz)	Mode Shape	Frequency (Hz)	Mode Shape
209		190	
294		279	
391		392	
508		512	
541			
922			
930			

FIGURE 33  
ACCELERATION RESPONSE  
FREE-PANEL

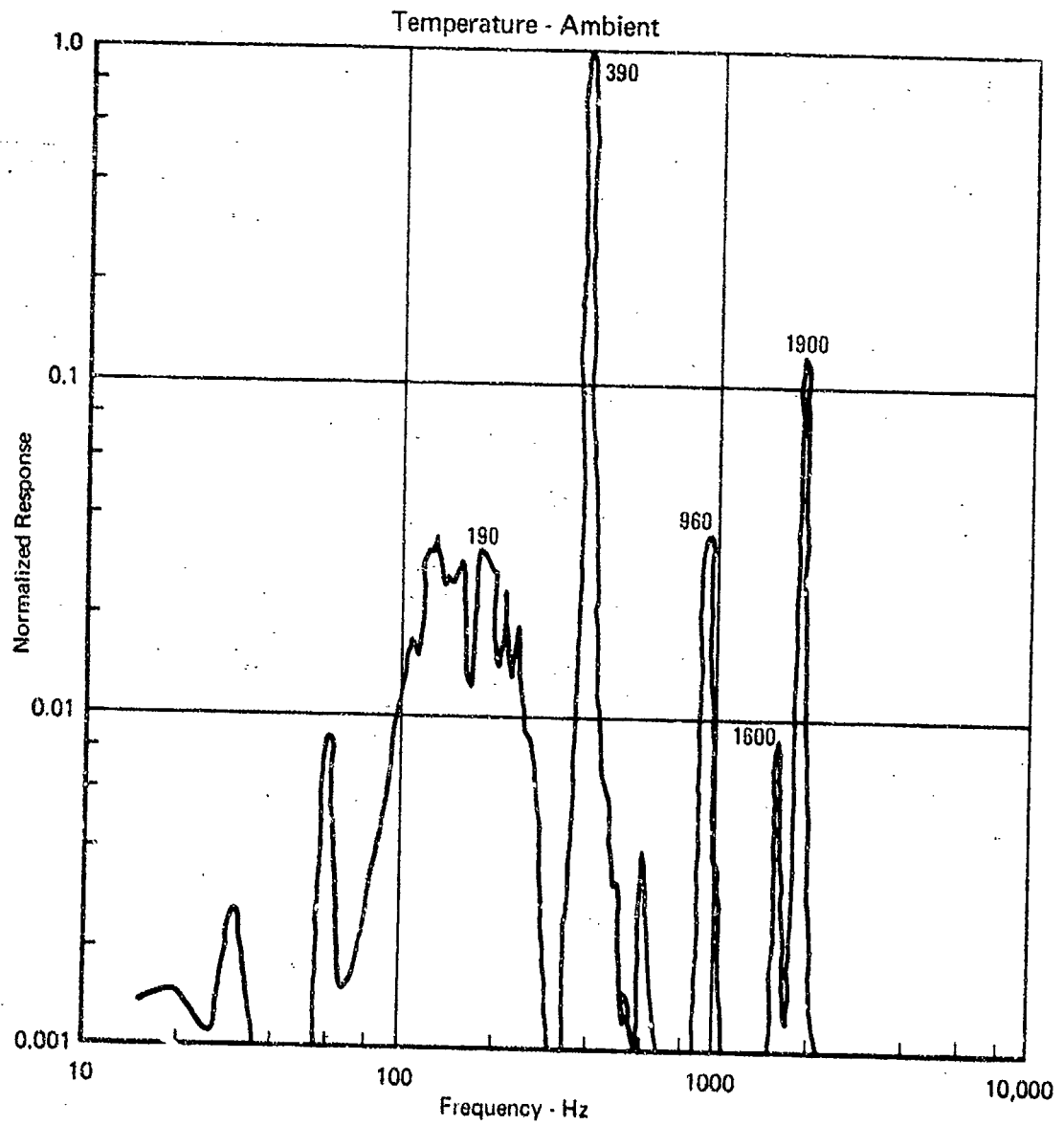


FIGURE 34  
ACCELERATION RESPONSE  
FREE-PANEL

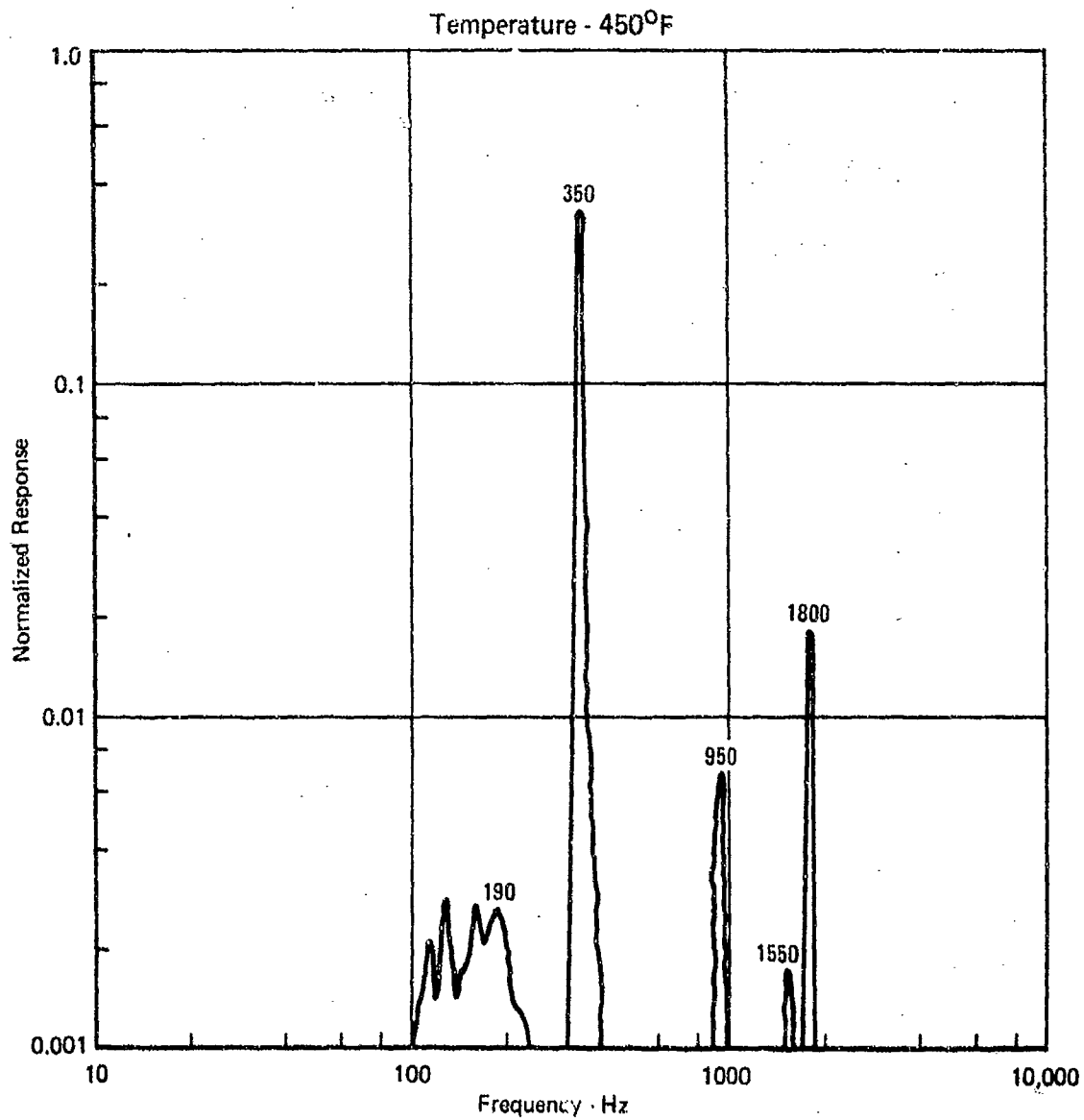


FIGURE 35  
ACCELERATION RESPONSE  
FIXED PANEL

Temperature - Ambient

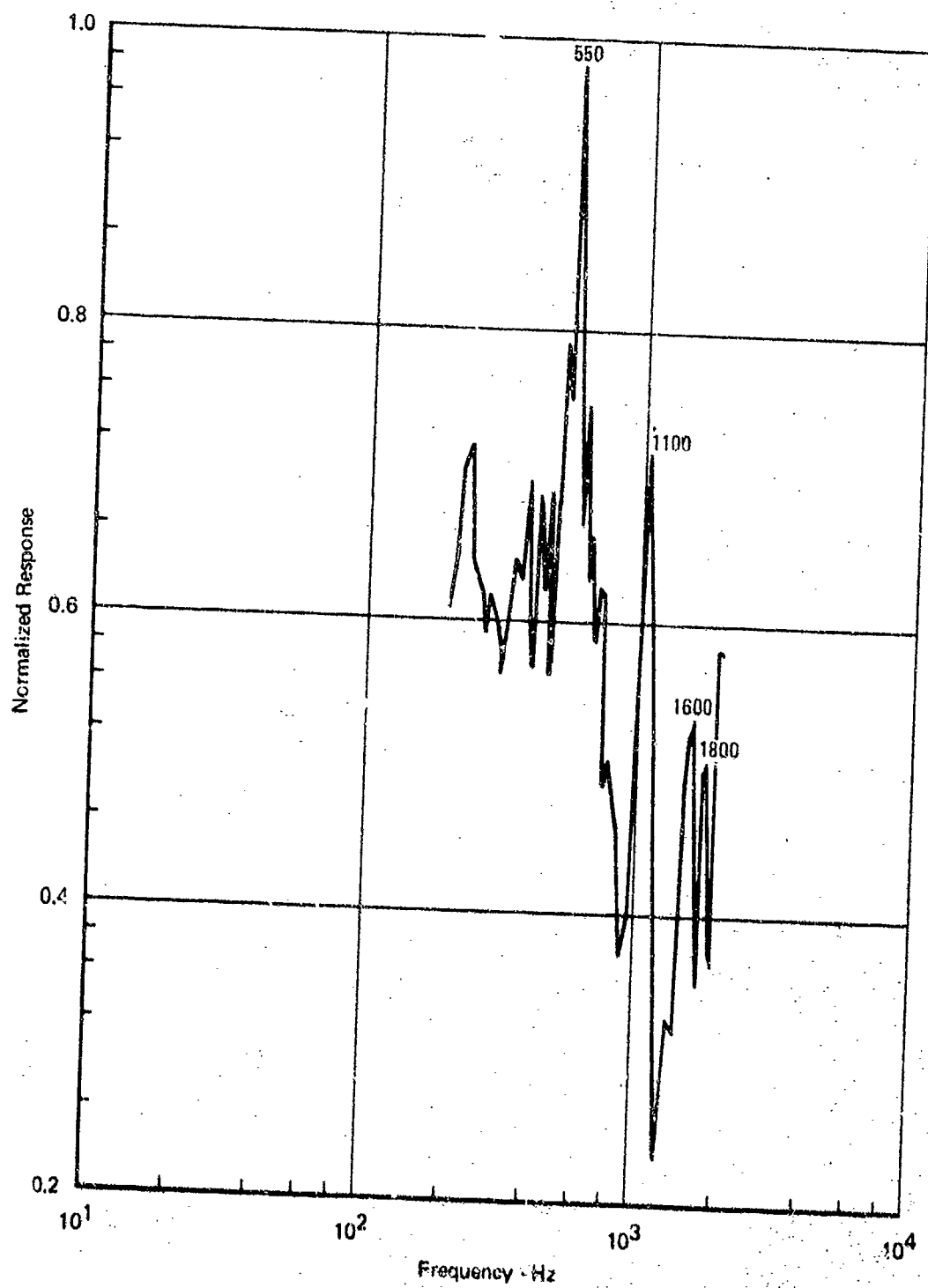
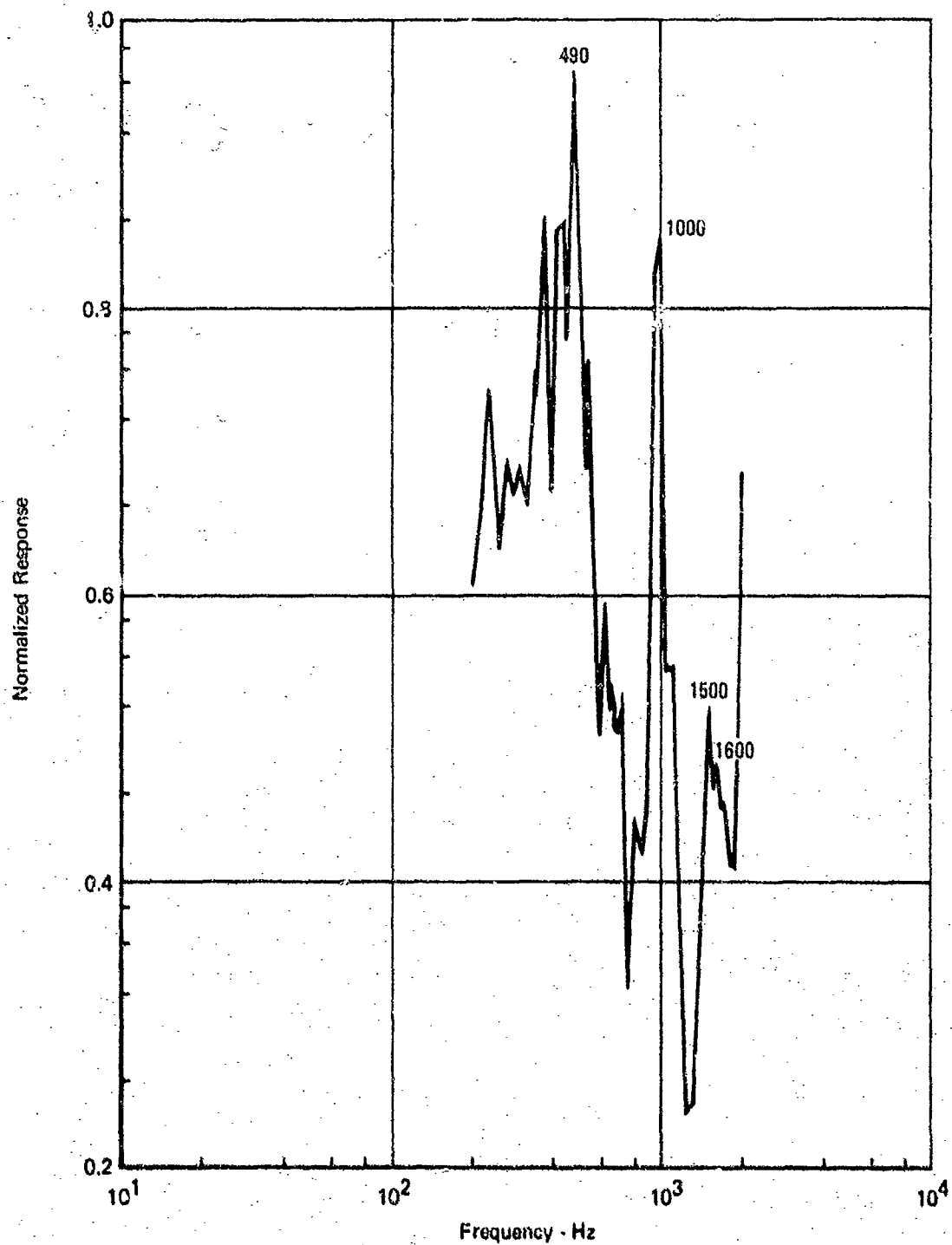


FIGURE 36  
ACCELERATION RESPONSE  
FIXED PANEL

Temperature - 480°F



**TABLE 8**  
**CHANGE IN NATURAL FREQUENCY OF PANEL DUE TO THERMAL EFFECTS**

Free Panel			Fixed Panel		
Ambient Frequency (Hz)	450°F Frequency (Hz)	Percent Change	Ambient Frequency (Hz)	450°F Frequency (Hz)	Percent Change
190	190	0	550	490	10.9
390	360	7.7	1100	1000	9.1
960	950	1.0	1600	1500	6.3
1600	1550	3.1	1800	1600	11.1
1900	1800	5.3			
Average		3.4			9.4

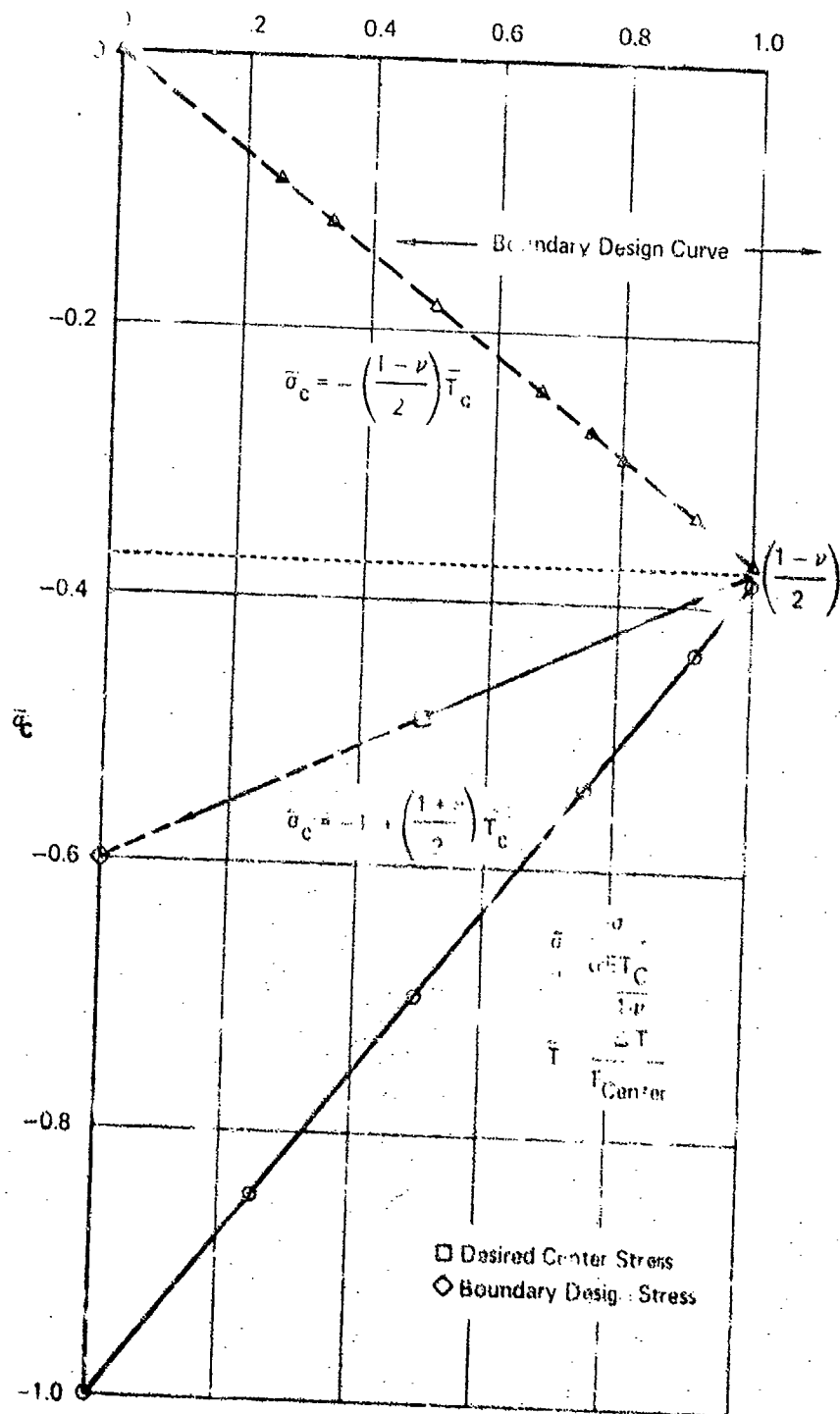
There are several methods available for controlling boundary temperatures. A massive fixture with good thermal conductivity will act as a heat sink which maintains ambient boundary temperatures. This method of controlling boundary temperature is particularly applicable when dynamically fixed boundaries are required to be maintained at ambient temperature. Convective cooling or heating, where a gas or liquid is forced to flow over the boundary, may also be used. This method requires a good analysis of the convective heat transfer problem to determine proper flow rates, contact areas and fluid temperature. Care must also be exercised in the attachment of hardware to control the fluid flow since the in-plane and bending stiffness of the boundary may be affected. A third method of controlling boundary temperature is electrical resistance heating of the boundary. In this case the specimen must be electrically isolated from the boundary but have good thermal contact. Several materials with these properties are available commercially, such as cupric oxide cements. In each case, boundary heating due to radiation from the specimen, lamp banks, and reflectors must be accounted for or the boundary must be insulated against radiation from these sources.

Once  $T(x, y)$  has been established with the boundary controlled at a constant temperature  $T_B$ , the value of  $\bar{T}_C$  (Figure 37) may be computed. As shown in section 4.2, if small gradients exist along the boundary, use of an average boundary temperature yields satisfactory results. The next problem is to design a mounting such that the in-plane stiffness at the boundaries produces the desired static stress. To examine the possible stresses which may be developed in the panel we observe the stress limits shown in Figure 37. As mentioned in section 4.2, when the boundary temperature is ambient ( $\bar{T}_C = 1.0$ ), the center stress is independent of the in-plane boundary loads. The value of the center stress for the ambient boundary temperature case is given by  $-(1-\nu)/2$ . Thus for a given value of  $\nu$ , a plot such as the one in Figure 37 can be constructed. The points on the  $\bar{\sigma}_C$  axis have the range  $-1.0 \leq \bar{\sigma}_C \leq 0$ . These points represent the possible in-plane boundary stiffnesses from infinite to zero (fixed to free). As shown in the figure for values of  $\bar{\sigma}_C > -(1-\nu)/2$  a gradient ( $\bar{T}_C > 0$ ) will increase the magnitude of the center stress. For values of  $\bar{\sigma}_C < -(1-\nu)/2$  a gradient will result in a decrease of the center stress. As shown in Figures 18 through 25 the stress at points other than the center is a function of the order of  $T(x, y)$ . The curves in these figures show two significant characteristics: the form of the stress distribution is independent of the boundary condition, and the magnitude of the stress at a point is related to the stress at the same point in the free-boundary case by an additive constant. This constant depends on the in-plane stiffness of the boundary.

Figure 37 can be used to design the mechanical boundary to produce a given thermal stress in a panel. The value of  $\bar{\sigma}_C$  as a function of  $\bar{T}_C$  for a given boundary is determined by a straight line which lies between the lines  $\bar{\sigma}_C = -((1-\nu)/2)\bar{T}_C$  and  $\bar{\sigma}_C = -1.0 + ((1+\nu)/2)\bar{T}_C$ . Since each line must pass through the common point ( $\bar{\sigma}_C = -(1-\nu)/2, \bar{T}_C = 1.0$ ) the line for a given mechanical boundary is completely determined by the specification of  $\bar{\sigma}_C$  at  $\bar{T}_C = 0$ . The value  $\bar{\sigma}_C$  at  $\bar{T}_C = 0$  establishes the center stress for the constant temperature case. This stress, however, is the stress at every point in the panel including the boundary. Thus, if we are given  $\bar{T}_C = 0.5$ , a desired center stress of  $-0.48 \alpha E T_C / (1-\nu)$ , and wish to design a boundary which will produce this result, we proceed as follows: A line is drawn through the points  $\bar{T}_C = 0.5, \bar{\sigma}_C = -0.48$ , and  $\bar{T}_C = 1.0, \bar{\sigma}_C = -(1-\nu)/2$ . The point where



FIGURE 37  
STAT C BOUNDARY DESIGN



this line intersects the  $\bar{T}_C = 0$  axis then found. In this case the intercept has the value  $\bar{\sigma}_C = -0.6$ . Substitution of  $\sigma_{xx} = \sigma_{yy}$  Boundary =  $-0.6 \alpha E T_C / (1 - \nu)$  into the generalized Hooke's law (equations 4.5) yields a value of  $0.4 \alpha T_C$  for the strain at the boundary. Thus 60% of the free boundary strain,  $\alpha T_C$ , must be suppressed. To do this a load per unit length,  $P$ , must be applied to each boundary where

$$P = \int_{-\frac{C}{2}}^{\frac{C}{2}} \sigma dz = .6 \alpha E T_C c / (1 - \nu) \quad (4.37)$$

One method of accomplishing this loading is to spring load the panel edges. Keeping the spring at ambient temperature the spring constant may be determined from the load and deflection. In this case the deflections,  $u$  and  $v$ , for zero panel rotation or translation, are  $0.2 \alpha T_C a$ . The spring constant per unit length must then be  $0.3 E c / a (1 - \nu)$ . The problems involved in designing such springs for combined environment testing will be discussed later in this section. If the temperature distributions are not of the form discussed in section 4.2 it is suggested that the computer analysis described in that section be used to check the stress distribution for the designed boundary.

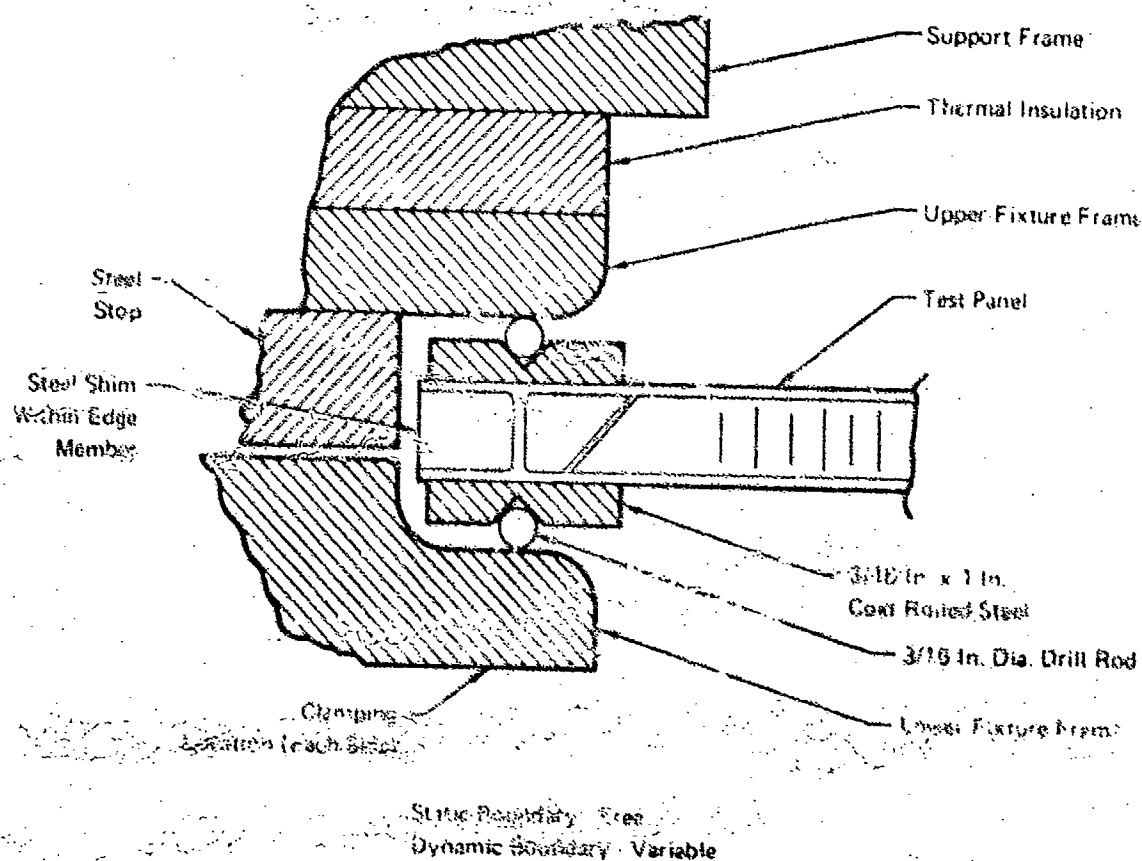
The problem of designing a mechanical boundary to control the dynamic response of a panel is not as straightforward as the static case. While the boundary problem is one of producing a given bending stiffness at the boundary, the dynamic response is dependent on the in-plane thermal loading, damping, and coupling with the acoustic field. The designer has the option of controlling the panel mounting, the acoustic field or both to produce the desired dynamic stress.

The basic problem in direct boundary synthesis (and analysis) is the determination of stress as a function of mode shape and frequency. Thus control of the acoustic field is generally the easier method of producing a desired dynamic stress level. If the acoustic field is to be the controlled variable, a dynamic boundary may be selected on the basis of convenience and ease of analysis.

In the present study, fixed and free boundaries were designed. The design of the fixed boundary was based on the information presented in Reference 19. The free boundary was simulated by laying the panel on thermal insulating material with low damping and low translational stiffness. The panel was kept from rotating or translating as a rigid body by the application of fiberglass tape to the panel edges. The tape also prevented the thermal insulation from being disturbed by the air flow from the acoustic source. In both cases, the experimental boundaries resulted in frequencies and mode shapes closely approximating the analytical predictions.

Another mounting technique which proved successful is the application of loading restraint (dynamic boundaries) after the test specimen is at the desired temperature. The specimen in this case is allowed to expand on rollers placed at the boundary. After the desired temperature is reached the edges may be restrained by tightening the bolt on a picture frame type mounting. A mounting of this type is shown in Figure 38. Some control over the dynamic response can be achieved by using the variable dynamic restraint (amount of torque on picture frame bolts) to tune the damped natural frequencies at the high temperature condition. These frequencies would be tuned to produce the acoustic coupling required for the given stress level.

FIGURE 38  
THERMAL/ACOUSTIC SPECIMEN MOUNTING



Although the design of specimen mountings has been approached as the superposition of three independent boundary designs it is obvious that the three boundaries do interact. In some cases the interaction of the three boundary conditions can be used to the designers advantage. For example if the boundary is to be at ambient temperature and both the bending and in-plane stiffness is to be large, one massive mounting fixture would satisfy all three conditions. In other cases it is difficult to obtain certain combinations of the three boundary conditions. It is, for example, difficult to obtain a statically fixed and dynamically free boundary since physical methods of in-plane loading usually introduce some bending stiffness. Two design considerations should be included in most combined environment mountings. First the static and dynamic boundaries should either be isolated from the thermal environment or maintained at a constant, known temperature. Second, where interaction between the static and dynamic boundaries is a problem, priority should be given to proper static boundary simulation since the dynamic stress can often be controlled by control of the acoustic field.

## SECTION 5

### SONIC FATIGUE INSTRUMENTATION AND MEASUREMENTS

Simulation of the thermal/acoustic environment and proper mounting of the specimen within this environment are predominant factors in elevated temperature sonic fatigue testing. Measurement of the test conditions and monitoring the response of the test specimen are matters of no less importance. Consequently, one phase of this program was to study methods to measure the parameters of interest in combined environment tests. The study consisted of determining the availability of instruments to make the various measurements, and indicating the advantages and limitations of different types of devices. The following parts of this section discuss sonic fatigue environment and response measurements, and methods for detecting sonic fatigue cracks.

#### 5.1 SONIC FATIGUE MEASUREMENTS

Elevated temperature sonic fatigue tests require a number of measurements. The most basic parameter is the acoustic field itself. Of almost equal importance are the temperature conditions and the response of the specimen undergoing test. Surveys of devices to make these measurements were conducted as part of this study program. The results of these surveys are summarized below.

##### 5.1.1 Acoustic Field Measurements

A number of good transducers are available to measure high intensity acoustic noise fields. The transducers operate on a variety of principles, including piezoelectric, strain gage, capacitive, inductive, magnetostrictive, and pressure-sensitive semi-conductors. Each of these devices has a metallic diaphragm upon which the acoustic pressure impinges, and the resultant force is converted into an electrical signal through one of the above principles. In selecting a pressure transducer for a specific application, the user must recognize that high sensitivity and wide frequency range will be difficult to obtain in a single instrument. High sensitivity results from a low stiffness diaphragm, but low stiffness also contributes to a low resonant frequency. Therefore, a trade-off between upper frequency range and sensitivity must be made in all types of pressure transducers.

Piezoelectric and capacitive transducers are generally usable to temperatures in the 500°F range without external cooling. The change of sensitivity with temperature is reliably predicted in this temperature range, so the transducers can be used with confidence. Above 500°F, external cooling of the transducer is generally required. Some devices are being developed with materials that can sustain higher temperatures, but the use of cooled transducers is more reliable at the present time.

Several methods of cooling pressure transducers are employed. The most common method requires that a coolant fluid be circulated within the transducer to maintain the sensing element at some specified temperature. Another scheme is to build the transducer into a heat sink which is then cooled. Some transducers are mechanically isolated from mechanical members that experience high temperatures, and are cooled by a flow of air or some other gas between the transducer and the high temperature environment. When a cooled transducer is used, special attention should be given to the noise generated by the cooling system. Likewise, the amplifier used with the pressure transducers must have a noise level that is sufficiently low to permit measurement of the required acoustic levels.

Another concept evaluated during this study was that of coupling the acoustic field to a pressure transducer through a small tube. In the case of elevated temperature sonic fatigue tests, this method would permit the pressure transducer to be located away from the elevated temperature environment. A reliable room temperature transducer could then be used to measure the high temperature acoustic field. Some cooling of the coupling tube might be required, but this could be easily accomplished.

The limiting factor in the use of a coupling tube is the frequency response of the tube. The behavior of the tube can be analyzed by considering the pressure transducer to be an infinitely stiff termination of the tube, as shown in Figure 39. Such an arrangement is similar to the closed-end tube discussed in Section 2.1. The pressure at any point  $x$  in the tube (with the  $x=\ell$  point taken as the "input" to the tube) is given by

$$p(x) = \frac{P_0}{\sin k\ell} \cos kx \quad (5.1)$$

Although equation (5.1) neglects losses, it is adequate to show the limitations of the coupling tube. The equation is readily evaluated at the termination and input points,  $x=0$  and  $x=\ell$  respectively. Finally, the gain of the tube is found by taking the ratio of the pressure at the transducer to the pressure at the input, yielding

$$\frac{p(0)}{p(\ell)} = \frac{1}{\cos k\ell} \quad (5.2)$$

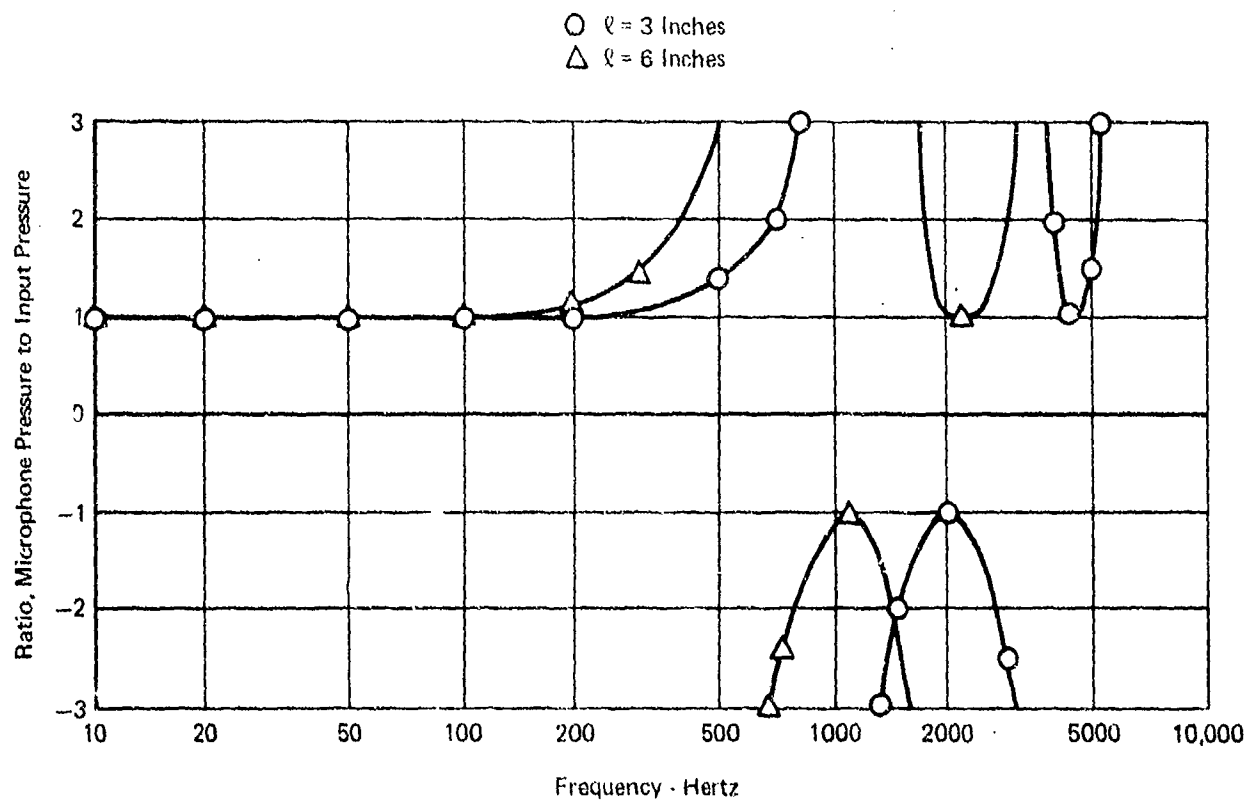
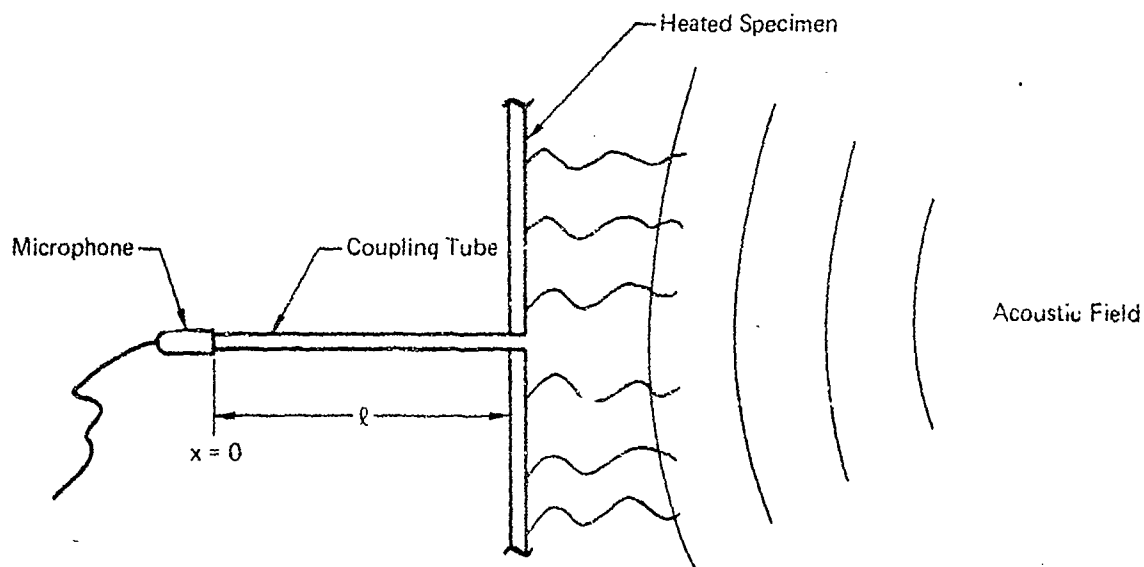
where

$$k = \frac{2\pi}{\lambda} = \frac{\omega}{c} \quad (5.3)$$

At sufficiently small values of  $k\ell$ ,  $\cos k\ell \approx 1$ , and the transducer pressure is approximately equal to the input pressure. These conditions are only met, however, for frequencies at which the tube length,  $\ell$ , is much smaller than the acoustic wavelength. The variation of gain in the tube is plotted in Figure 39 for two representative tube lengths. At frequencies where  $k\ell$  equals odd multiples of  $90^\circ$ , equation (5.2) indicates that the ratio approaches infinity. The losses in an actual tube, however, will always limit the pressure ratio to a finite value. Even with some losses in the tube, it is apparent that the use of coupling tubes should be limited to low frequencies. This restriction reduces the usefulness of coupling tubes for sonic fatigue tests, since signals up to several kilohertz must ordinarily be measured.

Calibration of pressure transducers for use on elevated temperature sonic fatigue tests can be accomplished in several ways. The reciprocity technique yields the most accurate results, because it requires only the measurement of electrical quantities and distances. This method can also be used at elevated temperatures, since the variation in the physical properties of air can be determined for elevated temperatures. Comparison calibrations, using a known "reference" transducer, are also suitable and widely used. A less common calibration method is the use of a shock tube, in which a pressure step-function is applied to the transducer. For those transducers whose bandwidth extends down to zero frequency, a static pressure calibration can be used to establish the transducer's sensitivity. Knowledge of the transducer's resonant frequency and damping are then needed to extend the frequency range of the calibration.

FIGURE 39  
COUPLING ACOUSTIC FIELD TO A MICROPHONE  
THROUGH A TUBE



Measurement of the acoustic field in elevated temperature sonic fatigue tests can be accomplished with currently available transducers. At temperatures above 500°F, transducers with external cooling should be employed. Properly selected and controlled cooling methods will result in reliable acoustic field measurements throughout the temperature range of sonic fatigue tests. As transducer manufacturers continue to develop materials that will sustain higher temperatures, pressure transducers will become available that can be used, uncooled, beyond the temperature limits of current instruments.

#### 5.1.2 Sonic Fatigue Strain Measurements

A knowledge of the state of strain in a sonic fatigue test specimen is a basic factor in evaluating test results. The measurement of such data is difficult in the combined high temperature/acoustic environment because this environment imposes detrimental elevated temperatures and dynamic acceleration loads on the strain gages. To determine the availability of strain gages for sonic fatigue applications, a survey was made of strain gages currently on the market. Significant findings regarding the properties and applications of strain gages are summarized below.

The use of strain gages at elevated temperatures is subject to errors from several sources. As one example, the resistance of the strain gage material may change as a function of temperature. In addition, there is usually a difference between the thermal coefficients of expansion of the strain gage material and the material which is being measured. The elastic moduli of the test material and the strain gage material are also subject to change as a function of temperature. To account for errors from these and other factors, strain gages must be compensated for temperature variations, according to the specific materials on which the gage is installed. An alternative to compensation is calibration of the strain sensing system throughout the load and temperature range of intended usage.

Several methods of temperature compensation may be employed. A common method employs a second strain gage (dummy gage) which is exposed to the same temperature environment as the gage of interest (active gage) without applying the actual strain conditions to the dummy gage. The temperature-dependent output of the dummy gage can thus be used to cancel out the apparent strain indicated by the active gage. For sonic fatigue applications, this method is limited by the difficulties in locating the dummy gage in precisely the same temperature as the active gage, and yet assuring that the dummy gage does not experience any load.

Another method of temperature compensation is the use of a 3-wire system. This method requires that an additional lead be attached to one of the strain gage terminals, and be routed out along with the two normal gage leads. The additional lead is used to identify thermally-induced changes in lead resistance, which might otherwise be mistaken for changes in gage resistance and read out as strain.

Self-compensating gages are also available for temperatures up to 800°F. These gages are manufactured with known temperature characteristics that can be used to correct the indicated strain levels. Corrections depend on an accurate knowledge of the temperature at the gage, and the gage manufacturer's compensation data for the type of material being tested. Some gages are supplied with the gage factor variation as a function of temperature. This information is useful when the dynamic component of strain is being measured, since static drift or apparent strain can be zeroed, and the time-varying strain may be determined by using the correct gage-factor value at a given temperature.



The method of attachment of the gage to the specimen must also be considered in selecting gages for sonic fatigue tests. The most common method is bonding, with the choice of bonding agent depending primarily on the temperature range of the gage. Bonding materials range from low temperature epoxy cements to high temperature ceramic cements which are used at temperature of 1200 to 1400°F. For even higher temperatures, flame spraying is used to attach strain gages to the material being measured. Some gages are encapsulated in metal sheaths which are spot welded directly to the test specimen.

The selection of a gage attachment method must also consider the compatibility of the method with the material being tested. Spot welding, for example is likely to reduce the fatigue life of some materials, and therefore may not be suitable for sonic fatigue test applications. Bonding materials have different thermal conductivities than the test specimen materials and may cause sharp thermal gradients when the specimen is heated.

In sonic fatigue testing, a strain gage attached to a panel experiences high dynamic accelerations as the panel is tested. This motion is perpendicular to the strain gage surface and lead wires, and tends to throw the wiring and strain gage connections away from the test panel. Published strain gage data dealing with "dynamic" loads is derived from repeated loading as applied by fatigue testing machines. A high speed machine of this type may operate at 10 to 20 Hz, frequencies that are low compared to acoustic excitation frequencies. The resultant low accelerations do not present the lead retention problem that is experienced on sonic fatigue tests, where it has become necessary to bond or otherwise attach the leads securely to the specimen.

In summary, it is concluded that strain measurement methods for high temperature sonic fatigue tests require much additional development. Problem areas include the following:

- a. Accuracy of gages at elevated temperatures is questionable.
- b. Specimens undergoing sonic fatigue tests experience high stress levels, and require gages with good fatigue life at high strains.
- c. Attachment of gages, whether by bonding, flame spraying, or welding, can cause localized thermal gradients in the specimen. The same problem applies to the attachment of lead-out wires.

Manufacturers of strain gages are continually improving the temperature characteristics of their products. However, as long as it is necessary to physically attach a device to an elevated temperature/sonic fatigue specimen, there will be uncertainties related to the thermodynamic, chemical, and dynamical effects of the attached device. Therefore, other means of estimating the stress level in a sonic fatigue panel should be pursued. Concepts that have potential for this purpose include optical methods, and accurate specimen deflection measurements from which the stress can be calculated.

### 5.1.3 Displacement Measurements

Measurement of the dynamic displacement of a specimen undergoing sonic fatigue testing provides a good indication of the dynamic properties of the specimen. The wide range of amplitudes and broad frequency range of sonic fatigue specimens place severe requirements on devices used to make displacement measurements. As part of this program, a survey was made to identify devices that might be used to make displacement measurements on sonic fatigue specimens at elevated temperatures. Several types of devices, along with their limitations, are described in the following paragraphs.

Devices to measure displacement were considered to fall in two broad categories: devices which must be attached to the specimen being tested, and devices which do not make physical contact with the specimen. The former type includes accelerometers, potentiometric devices, and linear variable differential transformers (LVDT's). The disadvantage of contacting devices is that they add mass to the test specimen. In the case of thin sonic fatigue test specimens, even light-weight accelerometers can affect the response characteristics of the test specimen. Another disadvantage is that, in the combined thermal/acoustic environment, devices attached to the specimen produce undesirable temperature gradients in the area of the attachment.

The frequency range of accelerometers is generally adequate for sonic fatigue work. Other types of contacting devices have more limited frequency response. For example, LVDT's depend on modulation of the signal applied to the fixed windings of the device. Since the excitation frequencies are generally a few kilohertz, the frequency of the motion being measured is limited to several hundred Hertz. This type of device is not suitable for measuring motion at the higher frequencies encountered in sonic fatigue testing.

Potentiometric devices are limited because of the mechanical problems associated with their operation. Coupling of the specimen motion to the resistive elements is cumbersome, and requires special precautions to avoid free-play. If the potentiometric device incorporates a wire-wound resistive element, resolution is limited by the size of the wire. Continuous resistive elements have their resolution limited by the wiping element in the device. All potentiometric devices are subject to wear and noise problems, and are not recommended for sonic fatigue specimen displacement measurements.

Noncontacting displacement measuring devices operate on one of several principles. The noncontacting transducers may be subdivided into two general categories: electrical and optical devices.

The electrical devices depend on either capacitive or inductive measurements to determine the motion of a specimen. In both types, a probe is moved to within a specified distance of the test specimen, which is referred to as the "target". Then, motion of the target relative to the fixed probe is read out as a change in capacitance or inductance, or as a change in capacitive or inductive coupling between elements of the measuring system. Displacement can therefore be measured without physically contacting the moving specimen. The frequency range and resolution of these systems are adequate for sonic fatigue test requirements. A basic problem with systems of this type is one of linearity. Since the electrical quantities being measured are not truly linear functions of the distance between the probe and target, it is necessary that the range of operation be limited. The device can, of course, be calibrated over a larger range than the linear range. High temperature operation of these devices is usually limited by the temperature characteristics of the probe unit. Since the measurements involve some electrical property of the target, the resistivity, permeability, and/or permittivity of the target material can affect the accuracy at high temperature.

An increasingly important type of noncontacting transducer is the optical device. Some optical devices focus a beam of light on a prescribed spot on the target materials, and track the spot as the target moves. Other types include laser interferometers, which produce alternate light and dark lines on a detector as the target specimen moves through small distances. Optical devices have a common advantage with the electrical noncontacting devices, in that neither type mass-loads the specimen or affects the thermal properties in any

way. The optical devices may be located farther from the material than electrical devices - typically, several feet rather than several inches. For sonic fatigue tests at elevated temperatures, however, optical methods presently have practical limitations. For one, the location of the test specimen in a progressive wave tube or other enclosure may restrict the optical path between the specimen and the measuring device. If the test is being conducted at elevated temperature, the heat lamps and their reflectors tend to further complicate the optical path problem. Another problem present at elevated temperature is the radiation from the test specimen. Optical displacement measuring devices have their own light sources, and specimen radiation would appear as noise to the optical detector.

In summary, several types of devices to measure the motion of sonic fatigue specimens are available. Those devices which must be physically attached to the specimen add mass, and thereby distort the thermal and dynamic properties of the specimen. To circumvent these disadvantages, noncontacting electrical and optical devices are more desirable. The use of noncontacting transducers requires recognition of the physical limitations of the devices, particularly at elevated temperatures. Thermal effects related to the sonic fatigue test specimen, the measuring device, and the medium between the specimen and measuring device can all cause errors in the use of noncontacting instruments.

Additional development work is needed on noncontacting electrical and optical displacement measuring devices. The use of these devices in the thermal/acoustic environment should be fully evaluated. Noncontacting devices are the most promising instruments for measuring sonic fatigue specimen displacements.

#### 5.1.4 Temperature Measurement

Temperature measurements in the range of sonic fatigue tests - up to about 2000°F - are a well established procedure under static conditions. In the high intensity acoustic noise environment, however, the motion of the test specimen causes difficulties with those temperature transducers which must make physical contact with the specimen. It is fortunate that noncontacting devices are becoming available which promise to make sonic fatigue temperature measurements a more routine operation.

The most widely used type of temperature transducer is the accurate, low cost, thermocouple. This device operates on the temperature-dependent change in contact potential between two dissimilar metals. A number of materials are commonly used for thermocouples - copper, constantan, chromel, iron, platinum, and rhodium are examples. The proper combinations of materials and alloys provide thermocouples for use at temperatures well in excess of 3000°F.

The difficulty in the use of thermocouples for sonic fatigue applications results from the requirement that the thermocouple junction make direct contact with the test specimen. Common practice is to spot-weld the thermocouple junction in place. The thermocouple wires must also be attached to the specimen, either with cement or with metal tabs which are spot welded in place. The thermocouple must then sustain the large dynamic motions that the test specimen experiences when it responds to the acoustic excitation. The use of thermocouples on sonic fatigue specimens thus becomes a question of how well the user can physically attach the thermocouple to the test specimen. Another deleterious result of a thermocouple, and its associated attachment mechanism, is that thermocouples represent materials with different thermal properties than the test specimen. Undesirable thermal gradients in the test specimen are a consequence of this situation.

Radiation transducers largely circumvent the difficulties inherent in thermocouples because radiation-sensitive devices do not make physical contact with the device being measured. The transducer can be located remote from the specimen at a distance ranging from several inches to many feet, depending on the individual device.

Some radiation-detecting devices, generally known as optical pyrometers, measure the brightness temperature of a specimen. Such instruments are useful only for measuring temperature in excess of about 1000°F, since the measured object must be at a sufficiently high temperature that its brightness can be measured.

Other types of radiation detectors operate over a wider range of temperatures. The thermal radiation from a small area of the test specimen can be focused on a heat-sensitive detector whose output is calibrated to indicate the temperature of the radiating surface. Radiation-sensing devices can be used with specimens whose temperature ranges from 100°F to several thousand degrees.

A highly advanced form of radiation detector is the infrared scanning system. This system continuously scans the surface being measured, detects the infrared radiation from the surface, and presents a video display of the thermal gradient of the surface. When the temperature of a single point on the surface is known, the thermal gradient display is calibrated, and the temperature distribution is completely defined. The advantages of this system are immediately apparent. First, the infrared scanning system does not have any physical contact with the specimen. Also, this single instrument provides complete temperature information for the entire surface, eliminating the need to measure the temperature at a number of points, and then estimating the temperature between measured locations.

The use of radiation detectors in high intensity acoustic environments is subject to some restrictions. The detectors must first be able to view the specimen. The detection devices must also be sufficiently rugged to survive the acoustic environment. Both of these limitations are minimized by the small size of some devices. The infrared scanning system requires a satisfactory optical path between the measured surface and the scanning camera. Since the system operates at infrared wavelengths, special optical components may be required to provide the required viewing conditions.

Measurement of test specimen temperatures during sonic fatigue tests can be accomplished with either thermocouples or radiation-sensing devices. The familiar thermocouples have several problems when used for measuring specimens undergoing dynamic motions, as discussed above. Modern radiation detectors have been developed for temperature measurements without making any physical contact with the specimen. Further evaluation of radiation detectors under actual sonic fatigue test conditions is needed, to establish special techniques for operation in the acoustic environment. The future for temperature measurement of sonic fatigue specimens clearly lies in the use of noncontacting radiation detectors.

## 5.2 SONIC FATIGUE CRACK DETECTION

The detection of cracks in sonic fatigue test specimens presents a number of challenges to the experimentalist. The complicated configuration of a representative aerospace test structure usually does not suggest that any single area is most likely to fail. Therefore, the entire structure should be monitored for failure. The locations of crack-detection devices would have to cover all zones where failure is considered likely to occur. The addition of elevated temperature conditions further complicates the problem.

Several methods of sonic fatigue crack detection were evaluated as part of this program. Direct crack detection methods, using devices whose electrical continuity was interrupted when a crack occurred, were considered first because of the success with these devices on static and low-frequency tests.

One type of crack detection material that was evaluated was a conductive copper tape with a dielectric adhesive backing. This tape is available commercially in a nominal thickness of 0.002 inches, in widths as small as 0.015 inches. Use of the tape as a crack-detecting device requires that the tape be applied to the specimen in an area where a crack is likely to occur. The tape is then wired into an electrical circuit, and the continuity of this circuit is monitored. When the specimen cracks in the designated area, the crack will propagate through the tape, and the resulting discontinuity is detected.

Evaluation of the conductive tape on a stylized aluminum panel disclosed that the copper tape was cracking before the test panel, giving false indications of failures. The test tape was made from relatively pure copper, which has poor fatigue characteristics. To be useful as a fatigue detection device, tape with better fatigue properties would be required. Material such as beryllium copper might be suitable. Present dielectric adhesives are stable to about 400°F, and so a different adhesive material would be needed at higher temperatures.

Another type of crack detecting material is conductive paint. This paint consists of finely powdered silver suspended in a fast drying carrier. The paint is applied to the test specimen in narrow strips along areas most likely to be cracked during sonic fatigue tests. The paint must be insulated from specimens which are themselves conductive. Copper foil solder tabs are located at the ends of the stripes for convenience in attaching leads to the conductive paint. Continuity of the conductive stripe is monitored, and a break in continuity is interpreted as an indication of a crack at some point along the painted stripe.

A special panel was designed to evaluate this fatigue crack detection method. The panel, as shown in Figure 40, is clamped at each end and subjected to vibration excitation. The notches in the panel result in stress concentrations at the notches, and cracks are initiated in the panel after only a few minutes of excitation.

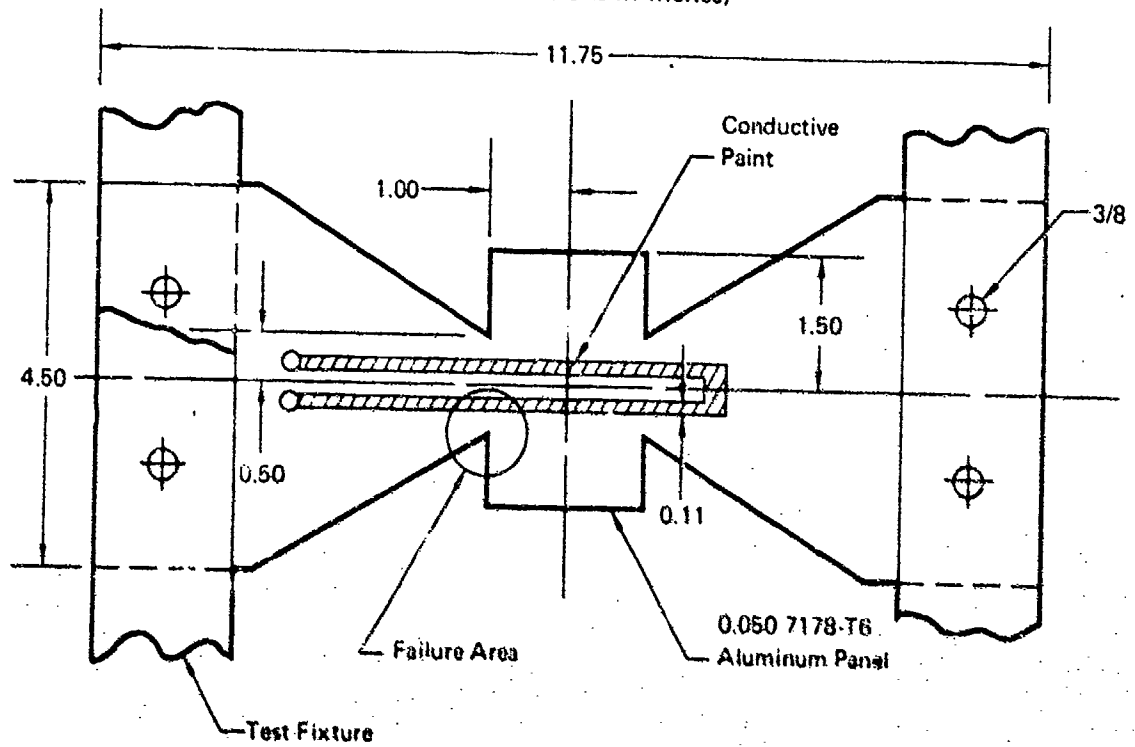
Figure 41 shows the display that results when a crack propagates through the conductive paint. During that part of a vibration cycle when the painted surface is in tension, the conductive path opens, and, when the surface is in compression, the conductive path is closed. It was also noted that continuity was restored when the vibration was stopped, indicating that the cracked edges of the painted stripe maintain good electrical continuity when the panel is undeflected.

The carrier material used in the conductive paint evaluated here is suitable for use to 300°F. Within this temperature range, these tests indicate that conductive paints are a satisfactory method of detecting sonic fatigue failure in specimens where the failure location can be predicted. Development of carrier materials that are stable at higher temperatures would extend the use of this method.

There are other schemes for observing sonic fatigue failures that do not detect the failure directly, but rather monitor some parameter which is, in turn, influenced by the existence of a crack. One such parameter is the strain at some point on the panel. A strain gage location should be selected based on the predominant normal mode shapes of the panel under test. A change in stress distribution in the panel, resulting from a fatigue crack, will then be detected by that strain gage.

FIGURE 40  
CRACK DETECTION PANEL DESIGN

(All Dimensions in Inches)



CRACK MONITORING CIRCUIT

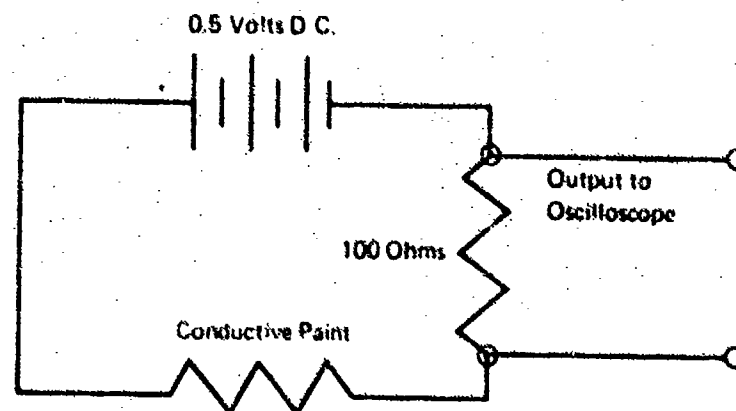
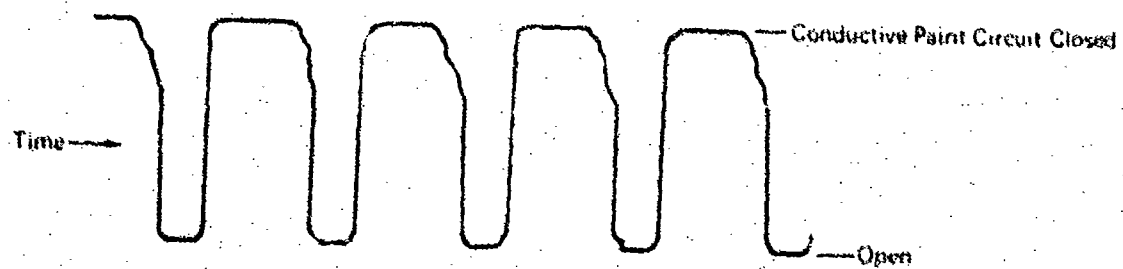


FIGURE 41  
OSCILLOSCOPE TRACE AT FAILURE



An experiment to demonstrate the above effect was conducted as part of this program. A multiple-bay panel was tested, with a strain gage attached to the panel near one of the rows of fasteners on the panel. Since the excitation was random acoustic noise, the output of the strain gage was normalized with respect to the output of the microphone in the acoustic field. By observing the ratio of the two signals, small changes in strain gage output resulting from small changes in acoustic excitation would not be mistaken for a change in specimen characteristics. When an abrupt change in the ratio was observed, the test was stopped and the panel was inspected. A section of the panel was found to have buckled, causing the reduction in the output of the observed strain gage. While this method is subject to the usual limitations of applying strain gages to high temperature sonic fatigue specimens, it has the sensitivity to detect panel changes caused by buckling or cracking.

Another means of detecting failure-induced changes in the dynamic properties of a panel is by use of a microphone. In this application, a panel undergoing tests was enclosed on the side that was not exposed to the acoustic excitation. The enclosure consisted of a rigid walled box, lined with material that had high acoustic absorption. A microphone was placed inside the enclosure, and its output was dominated by the fundamental response frequency of the panel. As the panel edges cracked, small changes were observed in both the amplitude and frequency of the microphone signal. The use of a microphone does not physically contact the specimen. High temperatures on the panel would cause no problems, because the temperature of the microphone could be controlled independent of the specimen. In addition, the microphone has no effect on either the thermodynamic or structural dynamic properties of the test panel.

A more sophisticated method of monitoring sonic fatigue cracks would be through the use of the infrared scanning device described in Section 5.1.4. Even a small crack in a heated specimen would represent a sharp thermal discontinuity in the test specimen. A discontinuity of this type would be clearly and immediately evident on the video display of the infrared scanning system.

Based on the results of this study, the use of a microphone to monitor the response of a panel is recommended as a reliable, low cost technique for detecting specimen failure. This method is most suitable for simple, single-bay panels in which the response is dominated by one or two panel resonances. For more complex structures, the use of conductive paint shows promise for monitoring several potential failure areas simultaneously. Additional development work is needed to identify paint materials usable at temperatures in excess of 300°F.

Only one method - the infrared scanning system - has the ability to continuously monitor a full structural surface for fatigue cracks. The high cost and optical path requirements of this system may limit its application. Nevertheless, the feature of this method will merit consideration on sonic fatigue tests where a precise knowledge of fatigue crack initiation is of prime importance.



## SECTION 6

### SUMMARY AND RECOMMENDATIONS

Tasks described in this report covered four major areas related to high temperature sonic fatigue tests. These areas are the acoustic environment, thermal environment, effects of specimen mounting on thermal and dynamic response, and instrumentation and measurements. The results in each area are briefly summarized, and recommendations for further study are indicated.

The studies of acoustic fields have shown that, in cases where the acoustic field is not diffuse, simple trigonometric functions can be used to describe pressure distributions. Although these functions do not represent exact equations for the pressure field, they are useful in estimating the response of a structure by the participation factor concept. It was also determined that the air flow from air stream modulator noise sources is sufficient to preclude sharp rises in the air temperature during elevated temperature tests. The properties of air are such that under the flow conditions described here, there is low heat transfer to the air from the heat sources and the test specimen. Therefore, the usual ambient values of air density and speed of sound can be used.

Additional experimental studies would be desirable to show the effect of acoustic field directional properties on structural response. As a first step, an existing progressive wave and reverberant test enclosure should be mapped to determine the pressure distributions in these enclosures. Then, a stylized panel could be designed with a high participation factor in the progressive wave test section. The panel would be tested in both enclosures, to show the difference in response level for different excitation fields.

For thermal environment simulation, a computer program has been written to calculate the two-dimensional temperature distribution in a panel that is heated by a quartz lamp-bank. Work has also been reported on lampbank design considerations for a combined thermal/acoustic environment. Methods for introducing damping into the reflectors and for improving the quartz lamp supports were discussed.

A needed extension to the thermal environment studies is the addition of temperature gradients along the thickness of the test panel. This would permit prediction of temperature in honeycomb structures and other sonic fatigue specimens where temperature variations normal to the surface may be expected. Additional work on quartz lamp holders is also needed to improve the reliability of quartz lamps in the high intensity acoustic noise environment. Still another area for work would be a detailed study of the mechanism by which quartz lamps deliver heat to a test specimen. This effort would require an experimental determination of the variation of the heat transfer process at different temperatures, and identification of all thermal losses that occur in heating sonic fatigue specimens. Empirical data of this kind are needed to provide a realistic estimate of what fraction of the power in quartz lamps is available for heating test specimens.

Considerable work has been done on the thermal and dynamic response of a test specimen as influenced by the specimen mounting. In a large number of cases, the thermal and dynamic problems can be treated separately and then combined, according to the principles of superposition. Computer programs were developed for the plane stress response to a thermal field. Basic equations were also presented to show how thermal in-plane loads enter into the dynamic equations. Experimental data was presented to illustrate the thermal effect on the dynamic properties of a panel.

A logical continuation of the panel thermal stress studies would be to extend the stress analysis to the three-dimensional problem. Even in the plane stress analysis, however, other length-to-width ratios, boundary conditions, and material properties could be evaluated to supplement the temperature-stress curves given in this report.

The determination of stress in a panel from a knowledge of the panel geometry, material, and deflection is indicated by the dynamic equations. Evaluation of the stress would first require a response test on the panel to identify and map the first few normal modes of the panel. Then, the panel should be subjected to a specific thermal/acoustic environment and the deflection should be measured at two or three points on the panel. From these deflection measurements, the modes in which the panel is responding can be determined and amplitudes assigned to the mode shapes. The deflection of the panel can also be calculated from the measured mode shapes if the coupling with the acoustic field is known. Determination of bending stresses in the panel can then be obtained by carrying out the differentiation operations in the dynamic equations.

A survey of devices to make high temperature/sonic fatigue measurements was made. Currently available instruments to measure the acoustic pressures and specimen temperatures appear to be adequate for the ranges currently encountered in thermal/acoustic testing. Measurement of specimen deflections and strains, however, are definite problem areas in the combined environment. Because of inherent shortcomings in strain-measuring devices that must be physically attached to the specimen, indirect methods for measuring strain should be pursued, as discussed above. Deflection measurements with noncontacting optical and electrical devices are potentially suitable for combined thermal/acoustic testing, although individual devices should be thoroughly evaluated to determine corrections that must be added in the thermal/acoustic environment.

## APPENDIX A

### STRUCTURAL COUPLING AND ACOUSTIC FIELD

#### A.1 STRUCTURAL RESPONSE - PERIODIC FORCING FUNCTION

The structural response to periodic forcing functions will be determined and the results will be presented in terms of the participation factor and the single-degree-of-freedom system functions.

The coupled dynamic equations of equilibrium will be written and the equations will be decoupled by rotation into normal coordinates. The Fourier Transform of the response in normal coordinates will be performed to show the relation between the response, the participation factor, and single-degree-of-freedom system functions.

Dynamic Equation:

$$[M] \{\ddot{w}\} + [C] \{\dot{w}\} + [K] \{w\} = \{p(x, t)\} \quad (A1)$$

Dynamic Equation - Undamped Case Homogeneous Solutions

$$[M] \{\ddot{w}\} + [K] \{w\} = \{0\} \quad (A2)$$

$$([D] - \omega^2 [I]) \{w\} = \{0\} \quad (A3)$$

Eigenvalue Solution and Modal Matrix

$\omega = \omega_{ni}$   $i = 1, 2, 3, \dots$  natural frequencies

$[\Phi]$  Modal matrix - each column represents an eigenvector. The matrix is also normalized such that

$$[\Phi]^T [M] [\Phi] = [I] \quad (A4)$$

$$[\Phi]^T [K] [\Phi] = [-\omega_n^2] \quad (A5)$$

Dynamic Equation - Dampened Cases

$$[\Phi] \{\delta\} = \{w\} \quad (A6)$$

$$[\Phi]^T [M] [\Phi] \{\ddot{\delta}\} + [\Phi]^T [C] [\Phi] \{\dot{\delta}\} + [\Phi]^T [K] [\Phi] \{\delta\} = [\Phi]^T \{p(x, t)\} \quad (A7)$$

Let  $[C]$  be diagonal or proportional to  $[M]$  and/or  $[K]$

$$\{\ddot{\delta}\} + [-2\zeta \omega_n] \{\dot{\delta}\} + [-\omega_n^2] \{\delta\} = [\Phi]^T \{p(x, t)\} \quad (A8)$$

Let

$$\{p(x, t)\} = P_o \{p(x)\} p(t)$$

$$\{\ddot{\delta}\} + [-2\zeta \omega_n] \{\dot{\delta}\} + [-\omega_n^2] \{\delta\} = P_o [\Phi]^T \{p(x)\} p(t) \quad (A9)$$

Let

$$\{\Gamma\} = [\Phi]^T \{p(x)\} \quad (A10)$$

$$\{\hat{p}(x, t)\} = P_o \{\Gamma\} p(t) \quad (A11)$$

Participation Factor is  $\Gamma$ . The Participation factor depends on the product of the spatial distribution of pressure, and the structural mode shape of the panel.

The Fourier transform of Equation (A9) results in a solution of the equation in terms of its system characteristics (system function) and the forcing function (Participation Factor).

Let the Fourier transform of  $\delta(t)$  for the  $i$ th equation be<sup>20</sup>

$$\Delta_i(mF_o) = \frac{1}{T_o} \int_{-T_o/2}^{T_o/2} \delta(t) e^{-jm\omega_o t} dt \quad (A12)$$

The Fourier transform of (A9) is

$$\left\{ [\omega_{ni}^2 - (m\omega_o)^2] + j 2\zeta \omega_{ni} m\omega_o \right\} \Delta_i(mf_o) = P_o \Gamma_i P(mf_o) \quad (A13)$$

$$\Delta_i(mf_o) = \frac{P_o \Gamma_i P(mf_o)}{\omega_{ni}^2 \left[ 1 - \left( \frac{m\omega_o}{\omega_{ni}} \right)^2 + j 2\zeta \left( \frac{m\omega_o}{\omega_{ni}} \right) \right]} \quad (A14)$$

where the system function ( $H_i(mf_o)$ ) is expressed as

$$H_i(mf_o) = \frac{1}{\left[ 1 - \left( \frac{m\omega_o}{\omega_{ni}} \right)^2 + j 2\zeta \left( \frac{m\omega_o}{\omega_{ni}} \right) \right]} \quad (A15)$$

The response is expressed in terms of the participation factor and the single-degree-of-freedom system function.

$$\Delta_i(mf_o) = H_i(mf_o) \Gamma_i \left[ \frac{P_o P(mf_o)}{\omega_{ni}^2} \right] \quad (A16)$$

## A.2 STRUCTURAL RESPONSE - RANDOM FORCING FUNCTION.

The cross-correlation of the pressure field in normal coordinates will be expressed in terms of the cross-correlation of the pressure field in the original coordinate system. The cross-power spectral density for the pressure field in the normal coordinates will be expressed in terms of the cross-power spectral density and the modal matrix. This expression will permit the transfer of any known cross-power spectra for the pressure field from the original coordinate system to normal coordinates, where structural response can be determined. An expression which transfers the response cross-power spectra from normal coordinates to the original coordinate system also is presented.

The cross-correlation function is expressed as<sup>21</sup>

$$R_{p_i p_j}(\tau) = \lim_{T \rightarrow \infty} \frac{1}{2T} \int_{-T}^T p_i(t) p_j(t+\tau) dt \quad (A17)$$

Rotation of the pressure  $p_i(t)$  into normal coordinates can be accomplished by

$$\hat{p}_n(t) = \sum_{i=1}^N \Phi_{ni}^T p_i(t) \quad (A18)$$

$$\hat{p}_m(t) = \sum_{j=1}^N \Phi_{mj}^T p_j(t) \quad (A19)$$

$$R_{\hat{p}_m \hat{p}_m}(\tau) = \sum_{i=1}^N \sum_{j=1}^N \Phi_{ni}^T \Phi_{mj}^T \lim_{T \rightarrow \infty} \frac{1}{2T} \int_{-T}^T p_i(t) p_j(t+\tau) dt \quad (A20)$$

$$R_{\hat{p}_m \hat{p}_m} = \sum_{i=1}^N \sum_{j=1}^N \Phi_{ni}^T \Phi_{mj}^T R_{p_i p_j}(t) \quad (A21)$$

The Fourier transform of the cross-correlation is the cross-power spectral density.

$$S_{\hat{p}_n \hat{p}_m}(f) = \int_{-\infty}^{\infty} R_{\hat{p}_n \hat{p}_m}(t) e^{-j\omega t} dt \quad (A22)$$

$$S_{\hat{p}_n \hat{p}_m}(f) = \sum_{i=1}^N \sum_{j=1}^N \Phi_{ni}^T \Phi_{mj}^T S_{p_i p_j}(f) \quad (A23)$$

In matrix form this equation is

$$[S_{\hat{p}}] = [\Phi]^T [S_p] [\Phi] \quad (A24)$$

Equation (A24) transforms the cross-power spectral density of a known pressure field into normal coordinates. The cross-correlation of response in normal coordinates is

$$R_{\delta_n \delta_m}(\tau) = \lim_{T \rightarrow \infty} \frac{1}{2T} \int_{-T}^T \delta_n(t) \delta_m(t+\tau) dt \quad (A25)$$

The transfer of a response parameter from normal coordinates to the original coordinate system can be accomplished by

$$w_i(t) = \sum_{n=1}^N \Phi_{in} \delta_n(t) \quad (A26)$$

Therefore, the cross-correlation of the response is

$$R_{w_i w_j}(\tau) = \sum_{n=1}^N \sum_{m=1}^N \Phi_{in} \Phi_{jm} \lim_{T \rightarrow \infty} \frac{1}{2T} \int_{-T}^T \delta_n(t) \delta_m(t+\tau) dt \quad (A27)$$

$$R_{w_i w_j}(\tau) = \sum_{n=1}^N \sum_{m=1}^N \Phi_{in} \Phi_{jm} R_{\delta_n \delta_m}(\tau) \quad (A28)$$

The Fourier transform of the cross-correlation is the cross-power spectral density.

$$S_{w_i w_j}(f) = \sum_{n=1}^N \sum_{m=1}^N \Phi_{in} \Phi_{jm} S_{\delta_n \delta_m}(f) \quad (A29)$$

In matrix form this expression is

$$[S_w] = [\Phi] [S_g] [\Phi]^T \quad (A30)$$

Equation A30 transfers the structural response parameter from normal coordinates to the original coordinate system.

### A.3 POWER SPECTRA FOR TYPICAL ACOUSTIC ENCLOSURES

Normal acoustic test enclosures have progressive wave or reverberant fields. Both of these cases can normally be considered single input multiple output systems. The acoustic enclosure, in a large majority of cases, is excited by a single or a group of sources which have the same pressure amplitude and phase. For this type of system the source can be considered single. The pressures at the structural test panel will have a variation in amplitude and phase which is distributed spatially across the panel. The pressures at these points ( $p_{oj}$ ) for this study will be considered to be multiple outputs from the single pressure source ( $p_{i1}$ ).

We will investigate first multiple input-output systems. The multiple output of a multiple input system can be described as a function of the conjugate system function, input cross-power spectral density and the system function. In matrix notation the expression is

$$[S_{p_o}] = [H^*] [S_{p_i}] [H]^T \quad (A31)$$

The cross-power spectral density between the  $i$ th and  $j$ th location is<sup>22</sup>

$$S_{p_{oi}p_{oj}}(f) = \sum_{n=1}^N \sum_{m=1}^N H_{in}^*(f) H_{jm}(f) S_{p_{in}p_{im}} \quad (A32)$$

If we assume that we have a single input system, that is, the enclosure is excited by a single source or a group of sources which can be considered as a single source, the cross-power spectrum for the pressure between the  $i$ th and  $j$ th location is

$$S_{p_i p_j}(f) = H_{i1}^* H_{j1} S_{p_1 p_1}(f) \quad (A33)$$

Let the normalized cross-power spectrum be

$$C_{p_i p_j}(f) = H_{i1}^* H_{j1}(f) \quad (A34)$$

Equation (A34) gives the normalized cross-power spectral density in terms of system functions which are characteristics of the acoustic enclosure. If these system functions for various types of acoustic fields can be determined, then forcing functions in normal coordinates can be estimated by Equation (A24).

### A.4 SYSTEM FUNCTION - ANECHOIC TERMINATION

In Section A.3 we have shown that the cross-power spectrum for a pressure field is a function of the system functions for the enclosure. In this section the system functions for an enclosure with an anechoic termination will be developed. A system function by definition is the Fourier transform of the unit impulse response. The response of a one-dimensional pressure field with anechoic termination to a unit impulse is

$$p(x, t) = P_o \delta(ct-x) \quad (A35)$$

The Fourier transform of Equation (A35) is

$$P(x, f) = \int_{-\infty}^{\infty} p(x, t) e^{-j\omega t} dt \quad (A36)$$

$$P(x, f) = P_0 e^{-j \frac{\omega x}{c}} = P_0 e^{-j \left( \frac{2\pi x}{\lambda_p} \right)} \quad (A37)$$

$$P(x, f) = P_0 \left( \cos \left( \frac{2\pi x}{\lambda_p} \right) - j \sin \left( \frac{2\pi x}{\lambda_p} \right) \right) \quad (A38)$$

The normalized system function ( $H(x, f)$ ) is

$$H(x, f) = \cos \left( \frac{2\pi x}{\lambda_p} \right) - j \sin \left( \frac{2\pi x}{\lambda_p} \right) \quad (A39)$$

The system function of Equation (A39) describes the pressure field as a function of frequency and distance from the source. Equation (A39) is Equation 2.2, the pressure distribution in a tube with anechoic termination.

#### A.5 RESPONSE TO RANDOM ACOUSTIC FIELD-ANECHOIC TERMINATION

The normalized cross-power spectra for the  $i$ th and  $j$ th location in an acoustic field with anechoic termination is

$$C_{\hat{p}_i \hat{p}_j}(f) = H_{i1}^*(f) H_{j1}(f) \quad (A40)$$

$$C_{\hat{p}_i \hat{p}_j}(f) = \left( \cos \left( \frac{2\pi x_i}{\lambda_p} \right) + j \sin \left( \frac{2\pi x_i}{\lambda_p} \right) \right) \left( \cos \left( \frac{2\pi x_j}{\lambda_p} \right) - j \sin \left( \frac{2\pi x_j}{\lambda_p} \right) \right) \quad (A41)$$

Transforming the above equation into normal coordinates gives

$$C_{\hat{p}_n \hat{p}_m}(f) = \sum_{i=1}^N \sum_{j=1}^N \Phi_{ni}^T \Phi_{mj}^T \left( \cos \left( \frac{2\pi x_i}{\lambda_p} \right) + j \sin \left( \frac{2\pi x_i}{\lambda_p} \right) \right) \left( \cos \left( \frac{2\pi x_j}{\lambda_p} \right) - j \sin \left( \frac{2\pi x_j}{\lambda_p} \right) \right) \quad (A42)$$

Equation (A42) is the normalized cross-power spectrum in normal coordinates and it is separable in  $i$  and  $j$ . Equation (A42) can be rewritten in terms of the participation factor.

$$C_{\hat{p}_n \hat{p}_m}(f) = \Gamma_n^* \Gamma_m \quad (A43)$$

The normalized power spectrum for the case  $n$  equals  $m$  in normal coordinates is

$$C_{\hat{p}_n \hat{p}_n}(f) = |\Gamma|^2 \quad (A44)$$

Equations (A43) and (A44) indicate that the cross-power spectrum in normal coordinates for pressure field with an anechoic termination is a function of the participation factors which were developed for periodic functions. The normalized cross-power spectra for the pressure field in matrix form is

$$[C_{\hat{p}}] = [\Gamma_n^* \Gamma_m] = \{\Gamma^*\} [\Gamma] \quad (A45)$$

The response of structures in normal coordinates is

$$[S_\delta] = [H^*] [ \Gamma_n^* \Gamma_m ] [H] S_{p_i p_i}(f) \quad (A46)$$

The system function  $H$  in Equation (A46) is the single degree-of-freedom-system function in normal coordinates for the structure. For structural damping, which is normally less than 5 percent, the following approximation can be written at the normal mode frequencies.

$$|H_{ii}(f)|^2 \gg H_{ii}^* H_{jj} \quad (A47)$$

$$[S_\delta] \approx [ \Gamma ]^2 |H|^2 S_{p_i p_i}(f) \quad (A48)$$

The above expression is a diagonal matrix and is approximately true for cases when the modal frequencies are separated by at least 10 percent.

Equation (A48) indicates that the response to a random acoustic field in an enclosure with an anechoic termination is a function of the participation factors,  $\Gamma_i$ . The response to a random acoustic field is similar to the response to periodic functions since the forcing function in normal coordinates is the participation factor. The effect of participation factor on response will therefore be the same for both random and periodic acoustic pressure.

#### A.6 RESPONSE OF STRUCTURES TO RANDOM ACOUSTIC FIELD-ABRUPT TERMINATION

The response of a structure to a random acoustic field will depend on the cross-power spectra of the pressure within the enclosure. Equation (A45) indicated that the normalized cross-power is a function of the system function for the enclosure. The system functions for an enclosure with a particular type of an abrupt termination will be determined. The results of this analysis will be extended to the other types of terminations and to fields with three-dimensional properties. The system function is the Fourier transform of the unit impulse response. The termination to be examined will be an open tube. The unit impulse response will be found by applying boundary conditions to the wave equation. The wave equation for particle displacement in terms of unit impulses is

$$\beta(x, t) = \beta_+ \delta(ct - x) + \beta_- \delta(ct + x) \quad (A49)$$

The Fourier transform of Equation (A49) is

$$\beta(x, f) = \int_{-\infty}^{\infty} \beta(x, t) e^{-j\omega t} dt \quad (A50)$$

$$\beta(x, f) = \beta_+ e^{-j\frac{\omega x}{c}} + \beta_- e^{j\frac{\omega x}{c}} \quad (A51)$$

The boundary conditions for the open tube are

$$x = 0, \beta(0, t) = \beta_0 \delta(t) \quad (A52)$$

$$x = L, \dot{\beta}(L, t) = 0 \quad (A53)$$

The relation between particle displacement and pressure is

$$p(x, t) = -\rho_0 c^2 \partial_x \beta(x, t) \quad (A54)$$

$$P(x, f) = -j\rho_0 c^2 \left( \frac{\omega}{c} \right) \left[ \beta_- e^{j\frac{\omega x}{c}} - \beta_+ e^{-j\frac{\omega x}{c}} \right] \quad (A55)$$



Applying boundary conditions of (A52) and (A53)

$$\beta_0 = \beta_+ + \beta_- \quad (\text{A56})$$

$$0 = \beta_- e^{\frac{j\omega L}{c}} - \beta_+ e^{-\frac{j\omega L}{c}} \quad (\text{A57})$$

$$\beta_+ = \frac{\beta_- e^{\frac{j\omega L}{c}}}{e^{-\frac{j\omega L}{c}}} \quad (\text{A58})$$

$$\beta_- = \beta_0 \left[ \frac{e^{-\frac{j\omega L}{c}}}{e^{\frac{j\omega L}{c}} + e^{-\frac{j\omega L}{c}}} \right] \quad (\text{A59})$$

$$\beta_- = \frac{\beta_0 e^{-\frac{j\omega L}{c}}}{2 \cos\left(\frac{\omega L}{c}\right)} \quad (\text{A60})$$

$$\beta_+ = \frac{\beta_0 e^{\frac{j\omega L}{c}}}{2 \cos\left(\frac{\omega L}{c}\right)} \quad (\text{A61})$$

The particle displacement for an open tube is

$$\beta(x, t) = \frac{\beta_0 \left[ \cos\left(\frac{\omega}{c}(L-x)\right) \right]}{\cos\left(\frac{\omega L}{c}\right)} \quad (\text{A62})$$

The pressure is

$$P(x, t) = \frac{\beta_0 \rho_0 c^2}{\cos\left(\frac{\omega L}{c}\right)} \left( \frac{\omega}{c} \right) \left[ \sin\left(\frac{\omega}{c}(L-x)\right) \right] \quad (\text{A63})$$

$$P(x, t) = \beta_0 \rho_0 c \omega \left[ \tan\left(\frac{\omega L}{c}\right) \cos\left(\frac{\omega x}{c}\right) - \sin\left(\frac{\omega x}{c}\right) \right] \quad (\text{A64})$$

The normal mode frequency of the tube,  $\omega_n$ , is given by  $\omega_n = 2\pi(nc/4L)$ . Then,  $\tan(\omega_n L/c) = \tan(n\pi/2) = \infty$ , although the small losses present in the tube will limit the pressure amplitude to a finite value. The pressure distribution in the tube can then be approximated by

$$P(x, t) = P_0 \cos\left(\frac{2\pi x}{\lambda_p}\right) \quad (\text{A65})$$

Equation (A65) is the system function for an open tube and corresponds to Equation 2.3 in Section 2.1. The same procedure used in Section A.5 will result in a similar expression for the response. That is, the response will be a function of the single-degree-of-freedom system functions of the structure and the participation factor,  $\Gamma_i$ .

For a three-dimensional structure the system function for a large room is

$$H(x, y, z, f) = \left[ \cos\left(\frac{2\pi x}{\lambda_{p_x}}\right) \cos\left(\frac{2\pi y}{\lambda_{p_y}}\right) \cos\left(\frac{2\pi z}{\lambda_{p_z}}\right) \right] \quad (A66)$$

Sections A.2 through A.6 indicate that the acoustic-structural coupling for random functions can be estimated in a manner similar to the acoustic structural coupling for periodic functions. The response will be a function of the structural single-degree-of-freedom system functions and the participation factors.

## APPENDIX B

### TEMPERATURE PREDICTION COMPUTER PROGRAM

The program described here is used to solve for the temperature distribution  $T_{i,j}$  as defined by Equation (3.16) in Section 3.1. This example is for a stainless steel panel, symmetrical about a centerline. The half-panel has been divided into 50 segments (10x5), with this division appearing as 11x6 in the dimension statements. The 11x6 dimension accounts for the temperature being calculated at corners rather than centers of the segments.

The quantity A is the original assumed temperature, from which T is calculated. B is the difference between A and T for each iteration. Initially, 10 iterations are programmed. The user may request additional groups of 10 iterations, as indicated in line 440.

In the program, the constant R (line 60) is the same as K in Equation (3.14). Likewise,  $R_1$  (line 130) is the same as  $K_1$  in Equation (3.15).

The constant S (line 70) is initially assigned a value of zero. This term is later computed as the value of  $T_R$  (Equation (3.9)).

The program presented here is designed for use on a conversational, time-sharing computer system. Therefore, different computers will require different input (output) formats.

# PLATEM

```

10 DIMENSION A(11,6),T(11,6),B(11,6)
20 DATA B/66*0./
30 DATA T/66*0./
40 DATA A/12*80.,9*400.,80.,80.,9*400.,80.,80.,9*400.,80.,80.,
50&9*400.,80.,80.,9*400.,80./
60 READ, R
70 S=0.
80 X=0.
90 DO 1 I=1,11
100 DO 1 J=1,6
110 A(I,J)=A(I,J)+460.
120 1 CONTINUE
130 R1=8.8E-3
140 R2=R1/300.
150 25 DO 2 I=2,10
160 DO 3 J=2,5
170 T(I,J)=(A(I,J-1)+A(I-1,J)+A(I,J+1)+A(I+1,J)+R)/4.
180 T(I,J)=(4.*T(I,J)+100.*R2*S+R1*(A(I,J)/100.))**4)
190 3 T(I,J)=T(I,J)/(4.*(1.+R2*(A(I,J)/100.))**3))
200 J=6
210 T(I,J)=(2.*A(I,J-1)+A(I-1,J)+A(I+1,J)+R)/4.
220 T(I,J)=(4.*T(I,J)+100.*R2*S+R1*(A(I,J)/100.))**4)
230 2 T(I,J)=T(I,J)/(4.*(1.+R2*(A(I,J)/100.))**3))
240 DO 4 I=2,10
250 DO 4 J=2,6
260 4 B(I,J)=(T(I,J)-A(I,J))/4.
270 DO 8 I=2,10
280 DO 9 J=2,5
290 9 T(I,J)=T(I,J)+B(I-1,J)+B(I+1,J)+B(I,J-1)+B(I,J+1)
300 J=6
310 8 T(I,J)=T(I,J)+B(I-1,J)+B(I+1,J)+2.*B(I,J-1)
320 IF(X.LT.10.) GO TO 63
330 Z=0.
340 DO 5 I=2,10
350 DO 5 J=2,6
360 IF(ABS(B(I,J)).LE.2) GO TO 5
370 Z=ABS(B(I,J))
380 5 CONTINUE
390 Z1=4.*Z
400 PRINT 100,Z1
410 100 FORMAT("THE MAXIMUM DIFFERENCE IS",F7.3," DEG. F. ")
420 PRINT,
430 PRINT,
440 PRINT,"IF REITERATION DESIRED, TYPE 1; 0 TO PRINT OUT"
450 READ, Z2
460 IF(Z2.EQ.0.) GO TO 57
470 GO TO 62
480 57 CONTINUE
490 PRINT,
500 PRINT,

```

PLATEM CONTINUED

```
510 D0 6 I=2,10
520 D0 6 J=2,6
530 6 T(I,J)=T(I,J)-460.
540 PRINT200,(T(I,2),T(I,3),T(I,4),T(I,5),T(I,6),I=2,10)
550 200 F0RMAT(5F14.3)
560 G0 T0 73
570 62 X=0.
580 63 CONTINUE
590 X=X+1.
600 S=0.
610 D0 7 I=2,10
620 D0 7 J=2,6
630 S=S+(T(I,J)/100.)*4
640 7 A(I,J)=T(I,J)
650 S=S/45.
660 G0 T0 25
670 73 CONTINUE
680 END
```

## APPENDIX C

### DERIVATION OF GOVERNING EQUATIONS

The complete solution to the problem of specimen response to a combined thermal and dynamic loading requires the evaluation of eleven parameters (in Cartesian coordinates). These parameters are  $T$ ,  $\rho$ ,  $V_x$ ,  $V_y$ ,  $V_z$ ,  $\sigma_{xx}$ ,  $\sigma_{yy}$ ,  $\sigma_{zz}$ ,  $\sigma_{xz}$  and  $\sigma_{yz}$  (due to symmetry of the stress tensor  $\sigma_{xy} = \sigma_{yx}$ , etc.)<sup>2,3</sup>

To determine the above parameters eleven equations must be solved. The solution of these equations with the associated boundary conditions is usually quite difficult and often can only be accomplished by approximate numerical methods. Fortunately in many engineering problems the number of equations and the complexity of the equations may be reduced by the use of certain simplifying assumptions. The following are the eleven basic equations and the simplifying assumptions which can often be applied.

The first of the eleven equations is the equation of continuity. This equation expresses the conservation of mass and can be written

$$\partial_t \rho + \partial_x (\rho V_x) + \partial_y (\rho V_y) + \partial_z (\rho V_z) = 0 \quad (C1)$$

Under the assumption of a constant and known density we can reduce the number of required equations and unknowns by one.

The next three equations can be derived from conservation of momentum. These equations state that the acceleration of a body is equal to the sum of the forces and the specific surface forces. This can be written as:

$$\begin{aligned} \rho (\partial_t V_x + V_x \partial_x V_x + V_y \partial_y V_x + V_z \partial_z V_x) = \\ \rho F_x + \partial_x \sigma_{xx} + \partial_y \sigma_{xy} + \partial_z \sigma_{xz} \end{aligned} \quad (C2a)$$

$$\begin{aligned} \rho (\partial_t V_y + V_x \partial_x V_y + V_y \partial_y V_y + V_z \partial_z V_y) = \\ \rho F_y + \partial_x \sigma_{xy} + \partial_y \sigma_{yy} + \partial_z \sigma_{yz} \end{aligned} \quad (C2b)$$

$$\begin{aligned} \rho (\partial_t V_z + V_x \partial_x V_z + V_y \partial_y V_z + V_z \partial_z V_z) = \\ \rho F_z + \partial_x \sigma_{xz} + \partial_y \sigma_{yz} + \partial_z \sigma_{zz} \end{aligned} \quad (C2c)$$

The fifth equation to be dealt with is the energy equation. This equation states that the rate of change of kinetic energy plus the rate of change of internal energy must equal the rate of nonechanical energy loss plus the power of the surface and body forces acting on the continuum.

$$\begin{aligned}
& [\partial_t \rho + \partial_x \rho V_x + \partial_y \rho V_y + \partial_z \rho V_z] \left( \frac{1}{2} V_x V_x + \frac{1}{2} V_y V_y + \frac{1}{2} V_z V_z + e \right) + \\
& [\partial_t e + V_x \partial_x e + V_y \partial_y e + V_z \partial_z e] + \\
& \left\{ V_x \rho [\partial_t V_x + V_x \partial_x V_x + V_y \partial_y V_x + V_z \partial_z V_x] + \right. \\
& V_y \rho [\partial_t V_y + V_x \partial_x V_y + V_y \partial_y V_y + V_z \partial_z V_y] + \\
& V_z \rho [\partial_t V_z + V_x \partial_x V_z + V_y \partial_y V_z + V_z \partial_z V_z] \left. \right\} = \\
& \left\{ V_x [\rho F_x + \partial_x \sigma_{xx} + \partial_y \sigma_{xy} + \partial_z \sigma_{xz}] + \right. \\
& V_y [\rho F_y + \partial_x \sigma_{xy} + \partial_y \sigma_{yy} + \partial_z \sigma_{yz}] + \\
& V_z [\rho F_z + \partial_x \sigma_{xz} + \partial_y \sigma_{yz} + \partial_z \sigma_{zz}] \left. \right\} + \\
& \sigma_{xx} \partial_x V_x + \sigma_{xy} \partial_x V_y + \sigma_{xz} \partial_x V_z + \sigma_{xy} \partial_y V_x + \sigma_{yy} \partial_y V_y + \\
& \sigma_{yz} \partial_y V_z + \sigma_{xz} \partial_z V_x + \sigma_{yz} \partial_z V_y + \sigma_{zz} \partial_z V_z \\
& - \partial_x q_x - \partial_y q_y - \partial_z q_z
\end{aligned} \tag{C3}$$

From Equation (C1), the first term in brackets on the left side of (C3) is zero. From Equations (C2) it can be shown that the expressions in braces on the left and right side of (C3) cancel term for term. By definition  $\partial_i V_j = \dot{\epsilon}_{ij}$ . Equation (C3) can now be written as

$$\begin{aligned}
& \rho (\partial_t e + V_x \partial_x e + V_y \partial_y e + V_z \partial_z e) = \\
& \sigma_{xx} \dot{\epsilon}_{xx} + \sigma_{yy} \dot{\epsilon}_{yy} + \sigma_{zz} \dot{\epsilon}_{zz} + 2(\sigma_{xy} \dot{\epsilon}_{xy} + \\
& \sigma_{xz} \dot{\epsilon}_{xz} + \sigma_{yz} \dot{\epsilon}_{yz}) - \partial_x q_x - \partial_y q_y - \partial_z q_z
\end{aligned} \tag{C4}$$

The last six of the eleven required equations are the constitutive equations, better known in this case as the generalized Hooke's law.

$$\sigma_{xx} = \frac{E}{(1+\nu)(1-2\nu)} [(1-\nu)\epsilon_{xx} + \nu(\epsilon_{yy} + \epsilon_{zz}) - (1+\nu)\alpha T] \tag{C5a}$$

$$\sigma_{yy} = \frac{E}{(1+\nu)(1-2\nu)} [(1-\nu)\epsilon_{yy} + \nu(\epsilon_{xx} + \epsilon_{zz}) - (1+\nu)\alpha T] \tag{C5b}$$

$$\sigma_{zz} = \frac{E}{(1+\nu)(1-2\nu)} [(1-\nu)\epsilon_{zz} + \nu(\epsilon_{xx} + \epsilon_{yy}) - (1+\nu)\alpha T] \tag{C5c}$$

$$\sigma_{xy} = G \gamma_{xy} \tag{C5d}$$

$$\sigma_{xz} = G \gamma_{xz} \tag{C5e}$$

$$\sigma_{yz} = G \gamma_{yz} \tag{C5f}$$

The term in parentheses on the left of Equation (C4) is the total time derivative of the nonmechanical internal energy,  $e$ . This energy is  $J c_F T$  where  $c_F$  is the specific heat at constant deformation. We apply Equation (C5) to replace  $\sigma$  in Equation (C4) in terms of strain and note that if we consider zero input forces,  $\gamma_{xy}$ ,  $\gamma_{xz}$ , and  $\gamma_{yz}$  are zero since they are not a function of temperature. Further, we assume a purely conductive heat transfer mechanism. Equation (C4) then becomes:

$$\rho c_F \dot{T} = \left( \frac{E}{1-2\nu} \right) \alpha T (\dot{\epsilon}_{xx} + \dot{\epsilon}_{yy} + \dot{\epsilon}_{zz}) + k(\partial_{xx}T + \partial_{yy}T + \partial_{zz}T) \quad (C6)$$

The term involving  $\dot{T}$  represents the rate of change of temperature due to the motion of the body. If this temperature rise is small (as it is in most cases) then  $\dot{T} \approx 0$ . Similarly the terms involving  $\dot{\epsilon}_{ii}$  represent the mechanical vibrations due to thermal changes and can in general be neglected.<sup>24</sup> The energy equation in this case degenerates to the well known Laplace Equation<sup>25</sup>

$$\partial_{xx}T + \partial_{yy}T + \partial_{zz}T = 0 \quad (C7)$$

Equation (C7) shows that the temperature can be calculated without mechanical considerations. This represents the quasi-static thermoelastic theory. Before turning to the calculations of the velocity components from the equations of motion and the stress components from Equations (C5), we will examine the calculation of the temperature field in more detail.

Equation (C7) is the general expression for the three dimensional steady state temperature distribution with zero heat sources and losses. In the current discussion the specimen will be a thin structure ( $\partial_z T \approx 0$ ) that has reached steady state. It is assumed that the heat is applied from a quartz lamp reflector system in such a way that we can assume uniform heat generation within the specimen. The absorbed radiation is of such a magnitude that all convective and radiative heat losses are accounted for and the required temperature distribution is achieved. Equation (C7) is then written as

$$k(\partial_{xx}T + \partial_{yy}T) = \dot{q} \quad (C8a)$$

and

$$\dot{q} = \dot{q}_{\text{radiation loss}} + \dot{q}_{\text{convective}} - \dot{q}_{\text{absorbed}} \quad (C8b)$$

A description of the computer program used to calculate the temperature distribution is presented in Appendix B. For the remainder of this discussion it will be assumed that the temperature distribution is known.

The analysis of the thermal-dynamic problem now requires only the solution of the equations of motion and the constitutive equations. This is still not an easy task, but through the use of certain assumptions further simplifications may be made. We first make use of the theory of superposition and assume that all deflections are small. Two problems are then treated separately, one thermal problem and one dynamic problem. The components of the static and dynamic stress tensors add linearly. We will consider the thermal problem first.

The thermal stress problem is a static problem. The left-hand sides of Equations (C2) represent the total time derivatives of the velocity components which for the static case are zero. In this analysis, since  $T(z)$  is constant and we deal with thin panel structures, the case of plane stress may be assumed. Plane stress implies that  $\sigma_{zz}$ ,  $\sigma_{xz}$  and  $\sigma_{yz}$  are zero. From Equation (C2c) we note  $F_z$  must also be zero. The equations of motion then become

$$\partial_x \sigma_{xx} + \partial_y \sigma_{xy} = -\rho F_x \quad (C9a)$$

$$\partial_x \sigma_{xy} + \partial_y \sigma_{yy} = -\rho F_y \quad (C9b)$$



The body forces,  $F_x$  and  $F_y$ , will be neglected in the static equilibrium Equations (C9). For the plane stress case, the constitutive equations become

$$\sigma_{xx} = \frac{E}{1-\nu^2} [\epsilon_{xx} + \nu\epsilon_{yy} - (1+\nu)\alpha T] \quad (C10a)$$

$$\sigma_{yy} = \frac{E}{1-\nu^2} [\epsilon_{yy} + \nu\epsilon_{xx} - (1+\nu)\alpha T] \quad (C10b)$$

$$\sigma_{xy} = G \epsilon_{xy} \quad (C10c)$$

To obtain the equilibrium equations in terms of displacements we substitute Equations (C10) into Equations (C9) and make use of the following strain-displacement relation for small displacements:

$$\epsilon_{xx} = \partial_x u \quad (C11a)$$

$$\epsilon_{yy} = \partial_y v \quad (C11b)$$

$$\epsilon_{xy} = \partial_x v + \partial_y u \quad (C11c)$$

Equations (C9) then become:

$$\frac{E}{1-\nu^2} = \partial_x [\partial_x u + \nu \partial_y v] + \frac{E}{2(1+\nu)} \partial_y [\partial_y u + \partial_x v] = \frac{\alpha E}{1-\nu} \partial_x T \quad (C12a)$$

$$\frac{E}{1-\nu^2} = \partial_y [\partial_y v + \nu \partial_x u] + \frac{E}{2(1+\nu)} \partial_x [\partial_y u + \partial_x v] = \frac{\alpha E}{1-\nu} \partial_y T \quad (C12b)$$

In order to eliminate the need for the solution of two simultaneous partial differential equations we introduce a function  $\psi$  such that

$$\partial_x \psi = u \quad (C13a)$$

$$\partial_y \psi = v \quad (C13b)$$

This function,  $\psi$ , is known as the strain potential function.<sup>26</sup> Substituting Equations (C13) into Equations (C12) we have:

$$\begin{aligned} \partial_x [\partial_{xx} \psi + \nu \partial_{yy} \psi] + (1-\nu) \partial_y \partial_{xy} \psi &= \\ \partial_x (\partial_{xx} \psi + \partial_{yy} \psi) &= (1+\nu) \alpha \partial_x T \end{aligned} \quad (C14a)$$

$$\begin{aligned} \partial_y [\partial_{yy} \psi + \nu \partial_{xx} \psi] + (1-\nu) \partial_x \partial_{xy} \psi &= \\ \partial_y (\partial_{xx} \psi + \partial_{yy} \psi) &= (1+\nu) \alpha \partial_y T \end{aligned}$$

Collecting like terms, Equations (C14) become

$$\partial_x [\partial_{xx} \psi + \partial_{yy} \psi - (1+\nu) \alpha T] = 0 \quad (C15a)$$

$$\partial_y [\partial_{xx} \psi + \partial_{yy} \psi - (1+\nu) \alpha T] = 0 \quad (C15b)$$

Integrating Equations (C15), we have

$$\partial_{xx}\psi + \partial_{yy}\psi - (1+\nu)\alpha T = f_1(y) + C_1 \quad (C16a)$$

$$\partial_{xx}\psi + \partial_{yy}\psi - (1+\nu)\alpha T = f_2(x) + C_2 \quad (C16b)$$

From Equations (C16) we can see that  $f(x) = f(y) = 0$  and the basic equations become:

$$\partial_{xx}\psi + \partial_{yy}\psi = (1+\nu)\alpha T + C \quad (C17)$$

The constant  $C$  is evaluated from a boundary condition on  $\partial_{xx}\psi + \partial_{yy}\psi - (1+\nu)\alpha T$  or its derivatives. Thus the solution of the thermal stress problem rests with the solution of Equation (C17) for the one variable,  $\psi$ .

The solution of the dynamic problem can also be simplified so the complete solution to Equations (C2) through (C5) are not required. The left-hand sides of Equations (C2) are the components of acceleration with respect to the coordinate axes. It is assumed that the components of acceleration in the  $x$  and  $y$  directions can be neglected, and that lateral deflections are small compared with the thickness of the panel. In the present case, it is assumed that the stress in the  $z$  direction,  $\sigma_{zz}$ , may be neglected which implies that all loads in the  $z$  direction are applied to the midplane. Equations (C2) then become, for zero body forces,

$$0 = \partial_x \sigma_{xx} + \partial_y \sigma_{xy} + \partial_z \sigma_{xz} \quad (C18a)$$

$$0 = \partial_x \sigma_{xy} + \partial_y \sigma_{yy} + \partial_z \sigma_{yz} \quad (C18b)$$

$$\rho a_z = \partial_x \sigma_{xz} + \partial_y \sigma_{yz} \quad (C18c)$$

From Equations (C18) the equation of plate bending under normal dynamic loading is

$$\partial_{xxxx}(Dw) + 2\partial_{xxyy}(Dw) + \partial_{yyyy}(Dw) = \frac{\rho a_z}{g} \quad (C19)$$

The derivation of this equation is not presented here but may be found in several references<sup>27,28</sup>. In addition to the lateral loading, a plate subjected to thermal loading develops thermal stresses in the plane of the plate which must be taken into account. Thermal stresses result in traction forces at the boundary which produce moments about the deflected surface. The resulting modification to Equation (C19), again derived in the literature, for a constant plate stiffness,  $D$ , is:

$$D \left\{ \partial_{xxxx}w + 2\partial_{xxyy}w + \partial_{yyyy}w \right\} = \frac{\rho c}{g} \partial_{tt}w + N_{xx}\partial_{xx}w + 2N_{xy}\partial_{xy}w + N_{yy}\partial_{yy}w \quad (C20)$$

Assuming  $w = AW(x,y)\cos(\omega_n t + \theta)$  Equation (C20) becomes

$$D \left\{ \partial_{xxxx}W + 2\partial_{xxyy}W + \partial_{yyyy}W \right\} - \left\{ N_{xx}\partial_{xx}W + 2N_{xy}\partial_{xy}W + N_{yy}\partial_{yy}W \right\} - \frac{\rho c \omega_n^2}{g} W = 0 \quad (C21)$$

The determination of  $N_{xx}$ ,  $N_{xy}$ , and  $N_{yy}$  can be accomplished by noting that Equation (C11) and (C13) yield the following relations

$$\epsilon_{xx} = \partial_{xx}\psi, \quad \epsilon_{yy} = \partial_{yy}\psi, \quad \epsilon_{xy} = 2\partial_{xy}\psi \quad (C22)$$

The forces per unit length may be computed by integrating the stress over the thickness, thus

$$N_{xx} = \int_{-c/2}^{c/2} \sigma_{xx} dz \quad (C23a)$$

$$N_{yy} = \int_{-c/2}^{c/2} \sigma_{yy} dz \quad (C23b)$$

$$N_{xy} = \int_{-c/2}^{c/2} \sigma_{xy} dz \quad (C23c)$$

Substituting Equations (C22) into the generalized Hooke's law (Equation (C10)) and performing the integrations indicated in Equation (C23) the forces per unit length are expressed in terms of the strain potential function as:

$$N_{xx} = \frac{Ec}{1-\nu^2} [\partial_{xx}\psi + \nu\partial_{yy}\psi - (1+\nu)\alpha T] \quad (C24a)$$

$$N_{yy} = \frac{Ec}{1-\nu^2} [\partial_{yy}\psi + \nu\partial_{xx}\psi - (1+\nu)\alpha T] \quad (C24b)$$

$$N_{xy} = \frac{Ec}{1+\nu} \partial_{xy}\psi \quad (C24c)$$

Equation (C21) may now be solved for  $W$  in terms of the frequency and potential function  $\psi$  for given boundary conditions. It should be noted that  $W$  in Equation (C21) was normalized with respect to the coefficient  $A$  which must be included to obtain the actual mid-plane deflection. The assumption that lateral deflections are small compared to the thickness allows us to neglect, for this case, the stretching of the mid-plane. It is also assumed that all in-plane loads are applied to the mid-plane of the plate and there are no thermal gradients through the thickness of the plate (i.e., the plate is initially flat). The peak stress at the surface due to dynamic loading and inplane forces is:

$$\sigma_{xx} = -\frac{Ec}{2(1-\nu^2)} [\partial_{xx}w + \nu\partial_{yy}w] \quad (C25a)$$

$$\sigma_{yy} = -\frac{Ec}{2(1-\nu^2)} [\partial_{yy}w + \nu\partial_{xx}w] \quad (C25b)$$

$$\sigma_{xy} = 2Gc \partial_{xy}w \quad (C25c)$$

If the in-plane forces and deflections are very large, such that the mid-plane is stretched, second-order terms should be included in Equations (C25). These equations then become<sup>29</sup>

$$\sigma_{xx} = -\frac{Ec}{2(1-\nu^2)} [\partial_{xx}w + \frac{1}{2}(\partial_x w)^2 + \nu\partial_{yy}w + \frac{\nu}{2}(\partial_y w)^2] \quad (C26a)$$

$$\sigma_{yy} = -\frac{Ec}{2(1-\nu^2)} [\partial_{yy}w + \frac{1}{2}(\partial_y w)^2 + \nu\partial_{xx}w + \frac{\nu}{2}(\partial_x w)^2] \quad (C26b)$$

$$\sigma_{xy} = 2Gc [\partial_{xy}w + \partial_x w \partial_y w] \quad (C26c)$$

## APPENDIX D

### COMPUTER PROGRAMS FOR THERMAL STRESS CALCULATION

Print-outs of four computer programs used to calculate, subject to various restrictions, thermal stresses in panels are presented in this appendix. These programs are written in the FORTRAN language and in a manner compatible with the GE430 time sharing computer. The four programs presented here can be merged into one program when sufficient storage capacity is available. In the present case four separate programs, each within the capacity of the GE430, are used. The outputs from one program are read into a storage file and later recalled as inputs to subsequent programs. A block diagram showing the basic inputs and outputs of the four programs is presented in Figure 42. The potential program is presented on pages 122 through 125, the strain program on pages 126 through 128, the normal stress program on pages 129 through 130, and the shear stress program on pages 131 and 132. A list of the symbols used in these programs is presented on pages 120 through 121 of this appendix.

The first program in the series is used to calculate the strain potential.<sup>30</sup> In all subsequent statements it is assumed that a state of plane stress exists. The basic equation to be solved is

$$\partial_{xx}\psi + \partial_{yy}\psi = (1+\nu)\alpha T + C \quad (D1)$$

where  $\psi$  is the strain potential function and  $C$  is a constant of integration. Figure 43 shows the model used in computing the potential function by the finite difference technique.<sup>31</sup>

In the potential program, the user is requested to supply a boundary code of "1" for a free boundary and "0" for a fixed boundary. The user is then asked to supply five coefficients of the temperature distribution in the x direction. The form of this distribution is

$$T(x,y) = A_1 + A_2 |X| + A_3 |X^2| + A_4 |X^3| + A_5 |X^4| \quad (D2a)$$

$$-7.5 \leq X \leq 7.5, -|X| \leq Y \leq |X|$$

$$T(x,y) = A_1 + A_2 |Y| + A_3 |Y^2| + A_4 |Y^3| + A_5 |Y^4| \quad (D2b)$$

$$-7.5 \leq Y \leq 7.5, -|Y| \leq X \leq |Y|$$

In lines 390 through 520 of the potential program the two-dimensional temperature distribution is computed. This distribution has the desired centerline distribution and a constant boundary temperature. Lines 80 through 100, 300 through 320, and 400 through 520 may be modified for various other temperature distributions.

The user is next asked to supply the value of center temperature, Poisson's ratio, the coefficient of thermal expansion, the length of the increments used for finite difference calculations, and the number of increments in each direction. The dimension statements may be modified to  $NX+1$  by  $NY+1$  arrays. The user is then asked to supply a code which is "1" if the coefficients have been normalized to  $A_1$  and "0" if they have not. This corresponds to a temperature distribution which is normalized to the center temperature.

To evaluate the potential function it is necessary to determine the constant of integration in Equation (D1). This constant is evaluated from the boundary conditions. The value of the constants for free and fixed panels with a constant boundary temperature are

$$(1 - \nu)\alpha T_B \quad (D3a)$$

FIGURE 42  
THERMAL STRESS PROGRAMS

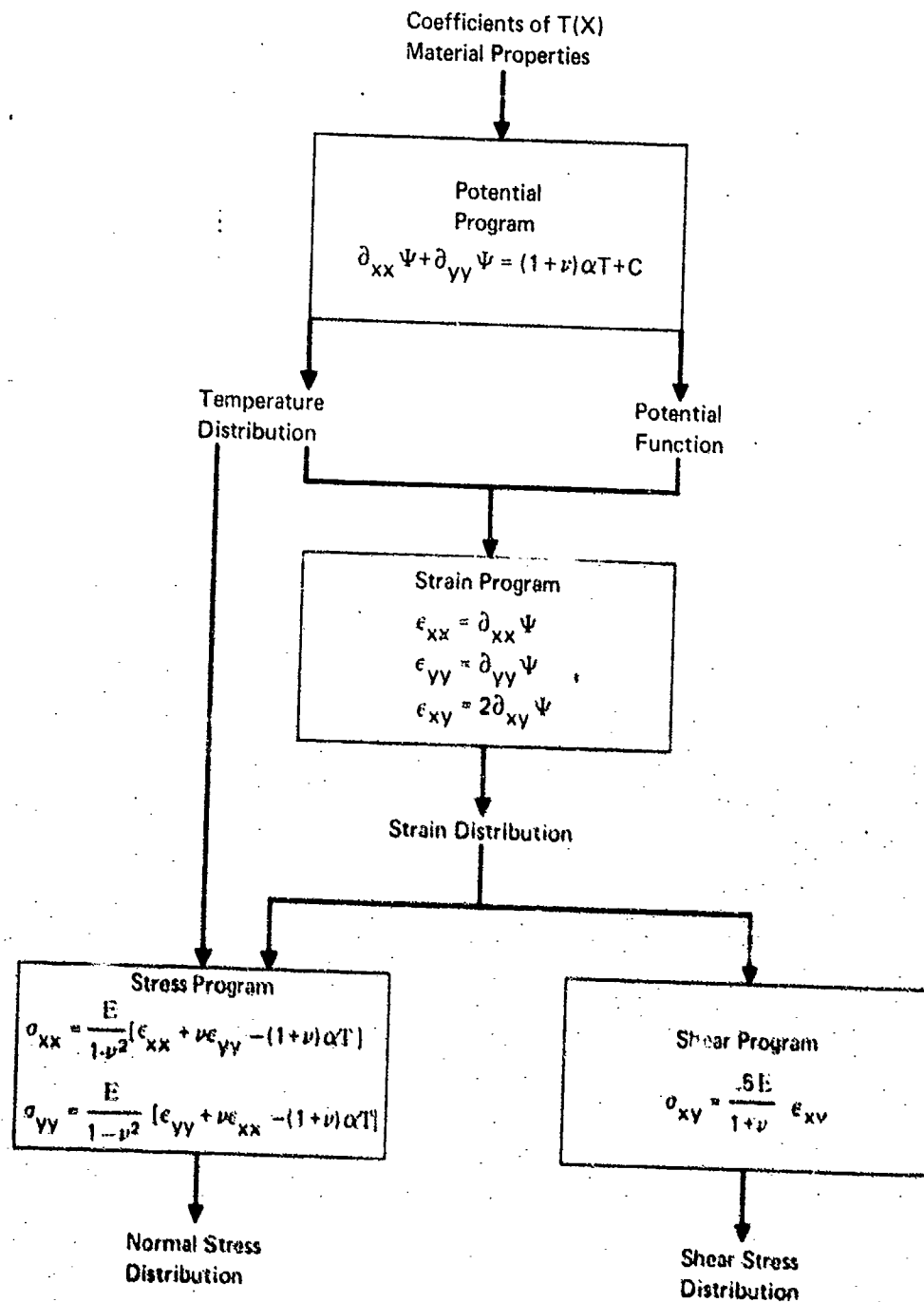
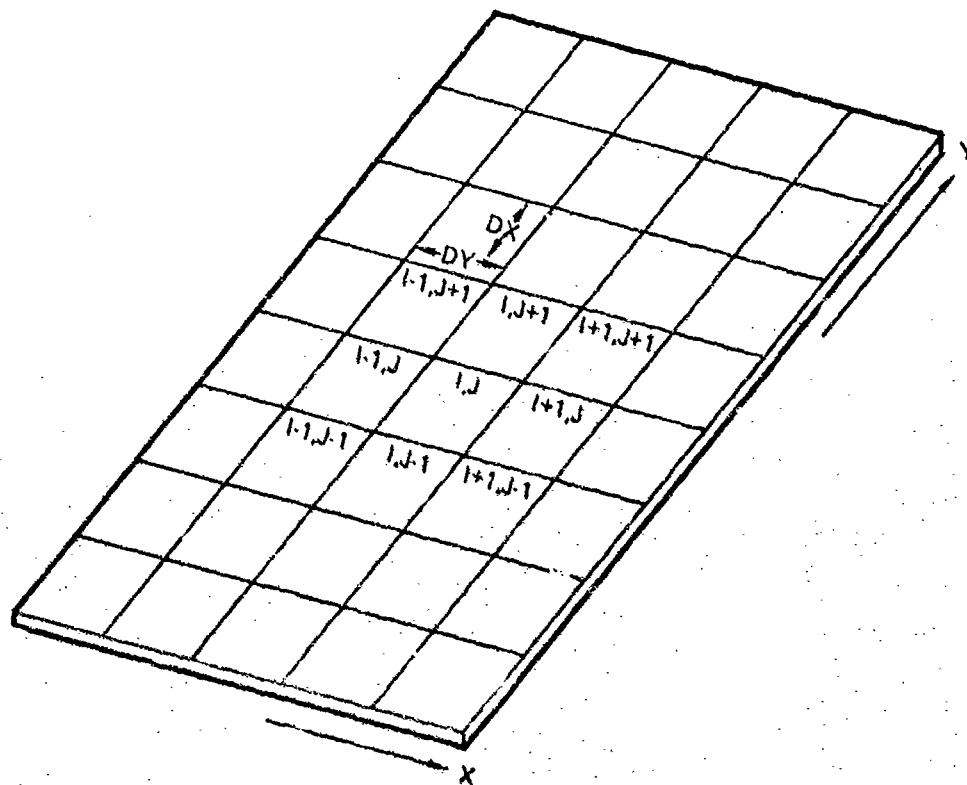


FIGURE 43  
FINITE DIFFERENCE MODEL OF PANEL



and

$$-(1 + \nu) \alpha T_B \quad (D3b)$$

respectively. If boundary conditions other than fixed or free are to be used the value of the constant  $C$  (TPC, lines 540 and 560) must be computed from Equation (D1) and the relationship between strain and potential. If the strain at a point is known then

$$C = \epsilon_{xx}|_{a,b} + \epsilon_{yy}|_{a,b} - (1 + \nu) \alpha T|_{a,b} \quad (D4)$$

If stress, forces, displacements, etc., are known then the other equations of elasticity must be applied to obtain  $\epsilon_{xx}|_{a,b}$  and  $\epsilon_{yy}|_{a,b}$

The solution of the differential equation will be restricted to a bounded plane region  $R$  with boundary  $S$ , and where  $\psi$  is defined and piecewise continuous on  $S$ . The problem is to find a function  $\psi(x, y)$  which is continuous on  $R + S$ , is twice differentiable in  $R$ , and satisfies in  $R$  the linear second order partial differential equation (Equation D1).

The finite difference representation of Equation (D1) is:

$$\frac{\psi(I, J+1) + \psi(I, J-1) - 2\psi(I, J)}{DY^2} + \frac{\psi(I+1, J) + \psi(I-1, J) - 2\psi(I, J)}{DX^2} \quad (D5)$$

$$= (1 + \nu) \alpha T(I, J) + C$$

Solving Equation (D5) for  $\psi(I, J)$  we obtain

$$\psi(I, J) = \frac{1}{2(DX^2 + DY^2)} \left\{ DY^2 [\psi(I-1, J) + \psi(I+1, J)] + \right. \quad (D6)$$

$$\left. DX^2 [\psi(I, J-1) + \psi(I, J+1)] - DX^2 DY^2 [(1 + \nu) \alpha T(I, J) + C] \right\}$$

This equation may be solved by using assumed values within the region  $R$  and the known values at the boundary  $S$  for the function  $\psi(I, J)$  on the right side of Equation (D6). This process is then repeated by replacing the old values within the region  $R$  by the new computed values of  $\psi(I, J)$ . The iterations are continued until the old and new values of  $\psi(I, J)$  are sufficiently close; that is, until  $\psi(I, J)$  solves Equation (D1) and the boundary conditions, with sufficient accuracy. The above method is the Jacobi method.<sup>32</sup> An extension of this method is the Gauss-Seidel method. This differs from the Jacobi method in that the new values of  $\psi(I, J)$  for adjacent points are used as soon as they are computed. This technique increases the convergence rate by a factor of two over the Jacobi method. The equation utilizing this method is given in lines 900 through 990.

In order to compute the potential function, the boundary conditions for Equation (D1) must be supplied. In the case of a free panel with constant boundary temperature the traction forces per unit area are zero at the boundary and the following condition for stress results:

$$\sigma_{xx} = \sigma_{yy} = \sigma_{xy} = 0 \quad (D7)$$

From the generalized Hooke's law and the strain displacement relations it can be shown that this condition reduces to

$$\partial_x u + \nu \partial_v = \partial_y v + \nu \partial_x u = (1 + \nu) \alpha T \quad (D8)$$

$$\partial_y u + \partial_x v = 0 \quad (D9)$$

The simultaneous solution of Equation (D8) and the application of the shear restriction (Equation D9) results in an expression for the displacements at the boundary.

$$u(x, y) = \alpha T_B x + a + by \quad (D10)$$

$$v(x, y) = \alpha T_B y + d - bx \quad (D11)$$

The coefficients a, b, and d represent rigid body translations and rotations. These coefficients were zero for the cases analyzed in this study.

When the expressions for the strain potential are substituted into Equations (D10) and (D11) and the results are integrated, the expressions for the strain potential at the boundary are as follows:

$$\psi \Big|_{|x|=a} = \alpha T_B y^2/2 + C_1 \quad (D12)$$

$$\psi \Big|_{|y|=b} = \alpha T_B x^2/2 + C_2 \quad (D13)$$

Since the potential can only be known within an arbitrary constant and this constant does not enter into the strain or stress calculation, we assume  $C_1 = C_2 = 0$ . Thus the boundary conditions for the free panel, used in the potential program, are

$$\psi \Big|_{|x|=a} = \alpha T_B y^2/2, \quad \psi \Big|_{|y|=b} = \alpha T_B x^2/2 \quad (D14)$$

These conditions are supplied in lines 720 and 760 through 790 of the potential program.

The boundary conditions for the fixed panel are  $u = v = 0$  at the boundary. This implies that

$$\partial_x \psi = \partial_y \psi = \partial_{xy} \psi = 0 \quad (D15)$$

$$\psi \Big|_{|x|=a} = f(y) + C_1 \quad (D16)$$

$$\psi \Big|_{|y|=b} = f(x) + C_2 \quad (D17)$$

which implies  $f(x) = f(y) = 0$ . As with the free panel we may choose  $C = 0$  thus  $\psi = 0$  at the boundary. The boundary conditions for the fixed panel are given in lines 740 and 760 through 790.

In addition to the use of the Gauss-Siedel method of successive displacements the convergence rate was increased by using a successive over-relaxation technique.<sup>33</sup> The coefficient for relaxation operations used in this program is 0.443, as suggested in reference 33. When different increment sizes are to be used the value of the relaxation factor should be changed. The over-relaxation technique is employed in line 1030 of the potential program.

Once the potential has been calculated with sufficient accuracy it is placed in a storage file for use in the strain program.

The strain program is used to compute both normal and shear strains from the potential function. The strains are related to the potential function by the following equations:

$$\epsilon_{xx} = \partial_{xx} \psi, \epsilon_{yy} = \partial_{yy} \psi, \epsilon_{xy} = 2\partial_{xy} \psi \quad (D18)$$

The finite difference approximations of the above equations are



$$\epsilon_{xx}(I,J) = \frac{\psi(I+1,J) + \psi(I-1,J) - 2\psi(I,J)}{DX^2} \quad (D19)$$

$$\epsilon_{yy}(I,J) = \frac{\psi(I,J+1) + \psi(I,J-1) - 2\psi(I,J)}{DY^2} \quad (D20)$$

$$\epsilon_{xy}(I,J) = \frac{2[\psi(I,J) + \psi(I+1,J+1) - \psi(I,J-1) - \psi(I-1,J)]}{DXDY} \quad (D21)$$

These equations are solved in lines 670 through 720 in the strain program.

The solution of Equations (D19) through (D21) can only be found within the region R. In the program for free panels the strain at the boundaries is known and thus may be supplied directly. For the fixed panel the normal and shear strains at the boundary are zero corresponding to zero deflection at the boundary. From Equations (D12) and (D13) it can be shown that for the free panel.

$$\epsilon_{xx} \big|_B = \epsilon_{yy} \big|_B = \alpha T_B \quad (D22)$$

$$\epsilon_{xy} \big|_B = 0 \quad (D23)$$

The boundary conditions for the fixed and free panel are supplied in lines 340 through 480 and 510 through 650, respectively. The values of normal and shear strain are then stored in a file for use in subsequent programs.

The normal stress program applies the generalized Hooke's law to obtain the stress distribution from the normal strains and the temperature. The relations for calculating normal stress are

$$\sigma_{xx} = \frac{E}{(1-\nu^2)} [\epsilon_{xx} + \nu\epsilon_{yy} - (1+\nu)\alpha T] \quad (D24)$$

$$\sigma_{yy} = \frac{E}{(1-\nu^2)} [\epsilon_{yy} + \nu\epsilon_{xx} - (1+\nu)\alpha T] \quad (D25)$$

These equations are solved in lines 410 through 470 in the program. A routine to compute the maximum normal stresses in the x and y directions is given in lines 630 through 810. If the value of maximum stress occurs at more than one point only the first point is retained.

The shear stress program uses the Hooke's law relation between shear stress and shear strain shown below:

$$\sigma_{xy} = G \epsilon_{xy} \quad (D26)$$

The equation is solved in line 220 of the program. A routine for calculating the maximum shear stress is given in lines 390 through 510. This routine is subject to the same restriction as the maximum normal stress routine.

The output of a typical computer run is presented on pages 148 through 156. Responses which the user types into the computer are underlined. The example analysis is for a 15 x 15 inch steel panel with free boundaries and a temperature distribution with  $T(X)$  of the form.

$$T(X) = 800 - 13.33X - 8.88X^2 \quad (D27)$$

This corresponds to a 880°F center temperature and 280°F boundary temperature, since the temperatures used in the program are referenced to ambient.

(The following symbols appear first in the potential program)

SYMBOL	MEANING
X(I)	coordinate in x direction
Y(I)	coordinate in y direction
A(I)	coefficients of temperature distribution
P(I,J)	old value of potential function
POT(I,J)	new value of potential function
DIF(I,J)	difference between new and old potential function
T(I,J)	temperature distribution
TP(I,J)	nonhomogeneous term in potential equation
NU	Poisson's ratio
MAX	maximum percentage value of DIF(I,J)
BOUND	code identifying boundary type
TC	center temperature
AL	coefficient of thermal expansion
XL	length in x direction
YL	length in y direction
NX	number of increments in x direction
NY	number of increments in y direction
DX	element length in x direction for finite difference calculations
DY	element length in y direction for finite difference calculations
NXI	number of points in the x direction
NYI	number of points in the y direction
NXC	x index value at the center
NYC	y index value at the center
DX2	square of DX
DY2	square of DY
REB	code to identify whether the A(i) are normalized to A(1) or not
CO	coefficient for relaxation operations
TPC	constant of integration in potential equation
IK	counter, determined number of integrations per series
TEST	sequence code to obtain another series of iterations
CHECK	printing code
TEST 2	sequence code to obtain another series of iterations
DIRECT	print code, used to file data or not
POTFIL	file containing final values of potential function
TEMPF	file containing values of temperature distribution

(The following symbols appear first in the strain program)

SYMBOLS	MEANING
P(I,J)	values of potential function from POTFIL
EPSXX(I,J)	strain in x direction
EPSYY(I,J)	strain in y direction
EPSXY(I,J)	shear strain
DELX	same as DX
DELY	same as DY
E	Young's modulus
DXY	one half product of DX and DY

## SYMBOLS

## MEANING

EPSXXF	file containing values of strain in x direction
EPSYYF	file containing values of strain in y direction
EPSXYF	file containing values of shear strain

(The following symbols appear first in the stress program)

## SYMBOLS

## MEANING

NXP	same as NX1 in potential program
NYP	same as NY1 in potential program
NX1	value of x coordinate of the maximum stress in the x direction
NY1	value of y coordinate of the maximum stress in the x direction
NX2CH	value of x coordinate of the maximum stress in the y direction
NY2CH	value of y coordinate of the maximum stress in the y direction
SIGXX(I,J)	stress in the x direction
SIGYY(I,J)	stress in the y direction
ALPHA	same as AL
NX1	dummy x coordinate to compute location of maximum stress in x direction
NY1	dummy y coordinate to compute location of maximum stress in x direction
NX2	dummy x coordinate to compute location of maximum stress in y direction
NY2	dummy y coordinate to compute location of maximum stress in y direction
CKVAL1	dummy variable to compute maximum stress in x direction
CKVAL2	dummy variable to compute maximum stress in y direction
TEMPT1	temperature at point of maximum stress in x direction
TEMPT2	temperature at point of maximum stress in y direction

(The following symbols appear first in the shear program)

## SYMBOLS

## MEANING

SIGXY(I,J)	shear stress
SX1	dummy x coordinate to compute maximum shear stress
SY1	dummy y coordinate to compute maximum shear stress
CKVAL	dummy variable used to compute maximum shear stress
SXF	value of x coordinate of maximum shear stress
SYF	value of y coordinate of maximum shear stress

# POTENTIAL

```

10 DIMENSION X(17),Y(17),A(5)
20 DIMENSION P(17,17),POT(17,17),DIF(17,17)
30 DIMENSION T(17,17)
40 DIMENSION TP(17,17)
50 PEAL NU,MAX
60 PRINT," FOR FREE TYPE 1, FOR FIXED TYPE 0"
70 READ,BOUND
80 PRINT, "SUPPLY THE 5 COEFFICIENTS FOR T(X)."

```

POTENTIAL CONTINUED

```

510 T(M,K)=T(I,J)
520 14 CONTINUE
530 IF(BOUND.EQ.0) GO TO 738
540 TPC=-(AL*T(I,1)*(1.-NU))*(DY2*DX2/(2.*(DX2+DY2)))
550 GO TO 739
560 738 TPC=(AL*T(I,1)*(1+NU))*(DY2*DX2/(2.*(DY2+DX2)))
570 739 CONTINUE
580 DO 2 I=1,NX1
590 DO 2 J=1,NY1
600 TP(I,J)=- (DX2*DY2*(1.+NU)*AL*T(I,J))/(2.*(DX2+DY2))
610 TP(I,J)=TP(I,J)+TPC
620 P(I,J)=TP(I,J)
630 2 CONTINUE
640 15 CONTINUE
650 IK=0
660 7 CONTINUE
670 MAX=0
680 675 CONTINUE
690 DO 88 I=1,NX1
700 DO 88 J=1,NY1
710 IF(BOUND.EQ.0) GO TO 741
720 POT(NX1,J)=AL*T(NX1,J)*Y(J)*Y(J)/2.
730 GO TO 742
740 741 POT(17,K)=0.
750 7.2 CONTINUE
760 POT(1,J)=POT(NX1,J)
770 POT(1,NY1)=POT(NX1,J)
780 POT(1,1)=POT(NX1,J)
790 88 CONTINUE
800 POT(NX1,J)=0.
810 DD=DX2/(2.*(DX2+DY2))
820 DDY=DY2/(2.*(DX2+DY2))
830 NX2=NX-1
840 NY2=NY-1
850 DO 20 I=2,NX2
860 DO 20 J=2,NY2
870 POT(I,J)=((DDY*(POT(I-1,J)+POT(I+1,J)))+(DD*(POT(I,J-1)+
880 &POT(I,J+1))))+TP(I,J)
890 20 CONTINUE
900 DO 24 J=2,NY2
910 POT(NX,J)=((DDY*(POT(NX2,J)+POT(NX1,J)))+(DD*(POT(NX,J-1)+
920 &POT(NX,J+1))))+TP(NX,J)
930 24 CONTINUE
940 DO 26 I=2,NX2
950 POT(I,NY)=((DDY*(POT(I,NY2)+POT(I,NY1)))+(DD*(POT(I-1,NY)+
960 &POT(I+1,NY))))+TP(I,NY)
970 26 CONTINUE
980 POT(NX,NY)=((DDY*(POT(NX2,NY)+POT(NX1,NY)))+(
990 &(DD*(POT(NX,NY2)+POT(NX,NY1))))+TP(NX,NY)
1000 DO 49 I=1,NX1

```

# POTENTIAL CONTINUED

```

1010 D0 49 J=1,NY1
1020 DIF(I,J)=POT(I,J)-P(I,J)
1030 P(I,J)=(1+C0)*POT(I,J)-C0*P(I,J)
1040 IF (ABS((DIF(I,J)/POT(I,J))*100.).LE.MAX) G0 T0 49
1050 IF (POT(I,J).EQ.0.)G0 T0 49
1060 MAX=ABS((DIF(I,J)/POT(I,J))*100)
1070 49 CONTINUE
1080 PRINT 2001,IK,MAX,DIF(NXC,NYC),POT(NXC,NYC),POT(NX1,NY1)
1090 2001 FORMAT (3X,16,4E11.3)
1100 PRINT,
1110 IK=IK+1
1120 IF(IK.LE.20) G0 T0 7
1130 PRINT 2000, MAX
1140 PRINT," SUPPLY STEP SIZE FOR PRINT STATEMENTS FOR I AND J"
1150 READ, INCRX, INCY
1160 2000 FORMAT("THE MAXIMUM PERCENTAGE DIFFERENCE IS ",E10.3)
1170 PRINT,"IF MORE ITERATIONS ARE DESIRED TYPE 1 ,IF NOT 0"
1180 READ, TEST
1190 IF (TEST.EQ.0)G0 T0 15
1200 38 CONTINUE
1210 PRINT," IF ONLY THE CENTERLINE VALUES ARE DESIRED TYPE 1,"
1220 PRINT," OTHERWISE TYPE 0"
1230 READ,CHECK
1240 PRINT,"          X          Y          POT"
1250 IF(CHECK.EQ.1) G0 T0 95
1260 D0 78 I=1,NX1,INCRX
1270 D0 78 J=1,NY1,INCRY
1280 PRINT 79, X(I),Y(J),P(I,J)
1290 79 FORMAT (5X,F4.1,5X,F4.1,5X,D12.5)
1300 78 CONTINUE
1310 95 CONTINUE
1320 D0 85 I=1,NX1,INCRX
1330 PRINT 79,X(I),Y(NYC),P(I,NYC)
1340 85 CONTINUE
1350 D0 90 J=1,NY1, INCY
1360 PRINT 79,X(NXC),Y(J),P(NXC,J)
1370 90 CONTINUE
1380 PRINT 79,X(NXC),Y(NYC),P(NXC,NYC)
1390 PRINT,
1400 PRINT,
1410 PRINT,
1420 PRINT,"IF ANOTHER ITERATION IS DESIRED TYPE 0; OTHERWISE 1"
1430 READ,TEST2
1440 IF(TEST2.EQ.0) G0 T0 15
1450 PRINT, "IF IT IS DESIRED TO WRITE INTO A FILE, TYPE 1; IF"
1460 PRINT, "NOT, TYPE 0. (THIS IS FOR BOTH POTFIL & TEMPF)"
1470 READ, DIRECT
1480 IF (DIRECT.EQ.0) G0 T0 71
1490 CALL SPENT (1,"POTFIL",7)
1500 D0 72 I=1,NX1

```

POTENTIAL CONTINUED

```
1510 D0 72 J=1,NY1
1520 WRITE (1;70) P(1,J)
1530 70 F0RMAT (E14.7)
1540 72 C0NTINUE
1550 CALL 0PENF (4,"TEMPF",7)
1560 D0 3 K=1,NX1
1570 D0 3 L=1,NY1
1580 WRITE (4;4) T(K,L)
1590 4 F0RMAT (F15.5)
1600 3 C0NTINUE
1610 71 C0NTINUE
1620 PRINT,
1630 PRINT, "      X      Y      TEMP"
1640 PRINT,
1650 D0 5 I=1,NX1,INCRX
1660 D0 5 J=1,NY1,INCRY
1670 PRINT 6, X(I),Y(J),T(I,J)
1680 6 F0RMAT(3X,F4.1,5X,F4.1,5X,E12.5)
1690 5 C0NTINUE
1700 END
```

# STRAIN

```

10 REAL NU
20 DIMENSION P(17,17)
30 DIMENSION EPSXX(17,17),EPSYY(17,17)
40 DIMENSION EPSXY(17,17),T(17,17)
50 DIMENSION X(17),Y(17)
60 PRINT,"SUPPLY YOUNG'S MODULUS, POISSON'S RATIO, COEF.OF"
70 PRINT,"THERMAL EXPANSION, LENGTH IN X AND Y DIRECTION,"
80 PRINT,"NUMBER OF INCREMENTS IN X AND Y DIRECTION."
90 READ,E,NU,AL,XL,YL,NX,NY
100 DELX=XL/NX
110 DELY=YL/NY
120 NX1=NX+1
130 NY1=NY+1
140 CALL OPENF (1,"POTFIL",7)
150 CALL E0FTST (1,M)
160 DO 2 I=1,NX1
170 DO 2 J=1,NY1
180 READ (1:3) P(I,J)
190 3 FORMAT (E14.7)
200 2 CONTINUE
210 CALL OPENF (4,"TEMPF",7)
220 CALL E0FTST (4,M)
230 DO 57 I=1,NX1
240 DO 57 J=1,NY1
250 READ (4:59) T(I,J)
260 59 FORMAT (F15.5)
270 57 CONTINUE
280 PRINT,"PRINT 1 FOR FREE BOUNDARY, 0 FOR FIXED BOUNDARY."
290 DX2=DELX*DELX
300 DY2=DELY*DELY
310 DXY=DELX*DELY*.5
320 READ, BOUND
330 IF (BOUND.EQ.1) GO TO 53
340 DO 4 K=1,NX1
350 DO 4 L=1,NY1
360 EPSXX(K,1)=0.
370 EPSXX(1,L)=0.
380 EPSXX(K,NY1)=0.
390 EPSXX(NX1,L)=0.
400 EPSYY(K,1)=0.
410 EPSYY(1,L)=0.
420 EPSYY(K,NY1)=0.
430 EPSYY(NX1,L)=0.
440 EPSXY(K,1)=0.
450 EPSXY(1,L)=0.
460 EPSXY(K,NY1)=0.
470 EPSXY(NX1,L)=0.
480 4 CONTINUE
490 GO TO 54
500 53 CONTINUE

```



# STRAIN CONTINUED

```

510 D0 61 K=1,NX1
520 D0 61 L=1,NY1
530 EPSXX(K,1)=AL*T(K,1)
540 EPSXX(1,L)=AL*T(1,L)
550 EPSXX(K,NX1)=AL*T(K,NX1)
560 EPSXX(NX1,L)=AL*T(NX1,L)
570 EPSYY(K,NX1)=AL*T(K,NX1)
580 EPSYY(1,L)=AL*T(1,L)
590 EPSYY(NX1,L)=AL*T(NX1,L)
600 EPSYY(17,K)=EPSXX(17,K)
610 EPSXY(1,L)=0.
620 EPSXY(NX1,L)=0.
630 EPSXY(K,1)=0.
640 EPSXY(K,NX1)=0.
650 61 CONTINUE
660 54 CONTINUE
670 D0 5 I=2,NX
680 D0 5 J=2,NY
690 EPSXX(1,J)=(P(I+1,J)-2*P(I,J)+P(I-1,J))/(DELX**2)
700 EPSYY(1,J)=(P(I,J+1)-2*P(I,J)+P(I,J-1))/(DELY**2)
710 EPSXY(1,J)=(P(I,J)+P(I+1,J+1)-P(I,J+1)-P(I+1,J))/DXY
720 5 CONTINUE
730 NXC=NX/2+1
740 NYC=NY/2+1
750 PRINT 8,
760 D0 13 K=1,NY1
770 X(K)=0.
780 Y(K)=((K-1)*DELY)-(YL/2)
790 PRINT 9,X(NXC),Y(K),EPSXX(NXC,K),EPSYY(NXC,K),EPSXY(NXC,K)
800 13 CONTINUE
810 D0 12 K=1,NX1
820 Y(K)=0.
830 X(K)=((K-1)*DELX)-(XL/2)
840 PRINT 9,X(K),Y(NYC),EPSXX(K,NYC),EPSYY(K,NYC),EPSXY(K,NYC)
850 12 CONTINUE
860 8 FORMAT(3X,"X",6X,"Y",6X,"EPSXX",6X,"EPSYY",6X,"EPSXY")
870 9 FORMAT(1X,F4.1,3X,F4.1,3X,E10.3,2X,E10.3,2X,E10.3)
880 CALL OPENF (2,"EPSXXF",7)
890 D0 14 I=1,NX1
900 D0 14 J=1,NY1
910 WRITE (2;3) EPSXX(1,J)
920 14 CONTINUE
930 CALL OPENF (3,"EPSYYF",7)
940 D0 15 I=1,NX1
950 D0 15 J=1,NY1
960 WRITE (3;3) EPSYY(1,J)
970 15 CONTINUE
980 CALL OPENF (5,"EPSXYF",7)
990 D0 710 I=1,NX1
1000 D0 710 J=1,NY1

```

STRAIN CONTINUED

```
1010 WRITE(5:3)EPSXY(1,J)
1020 710 CONTINUE
1030 PRINT,"EPSXX, EPSYY, AND EPSXY HAVE BEEN FILED"
1040 6 CONTINUE
1050 END
```

# STRESS

```

10 REAL NU,NX1CH,NX2CH,NY1CH,NY2CH
20 DIMENSION EPSXX(17,17),EPSYY(17,17),T(17,17)
30 DIMENSION SIGXX(17,17),SIGYY(17,17)
40 DIMENSION X(17),Y(17)
50 PRINT,
60 PRINT," SUPPLY YOUNG'S MODULUS, POISSON'S RATIO, COEF."
70 PRINT,"OF THERMAL EXPANSION, LENGTH IN X AND Y DIRECTION,"
80 PRINT,"NUMBER OF INCREMENTS IN X AND Y DIRECTION."
90 READ,E,NU,ALPHA,XL,YL,NX,NY
100 DELX=XL/NX
110 DELY=YL/NY
120 NXP=NX+1
130 NYP=NY+1
140 NXC=NX/2+1
150 NYC=NY/2+1
160 CALL OPENF (2,"EPSXXF",7)
170 CALL E0FTST (2,N)
180 DO 10 I=1,NXP
190 DO 10 J=1,NYP
200 READ(2;23)EPSXX(I,J)
210 23 FORMAT(E14.7)
220 10 CONTINUE
230 CALL OPENF (3,"EPSYYF",7)
240 CALL E0FTST (3,N)
250 DO 15 I=1,NXP
260 DO 15 J=1,NYP
270 READ(3;23)EPSYY(I,J)
280 15 CONTINUE
290 PRINT,
300 17 FORMAT (3X,"X",5X,"Y",6X,"TEMP",6X,"SIGXX",6X,"SIGYY")
310 PRINT,
320 CALL OPENF (4,"TEMPF",7)
330 CALL E0FTST(4,N)
340 DO 21 I=1,NXP
350 DO 21 J=1,NYP
360 READ (4;22) T(I,J)
370 22 FORMAT (F15.5)
380 21 CONTINUE
390 19FORMAT(1X,F4.1,3X,F4.1,6X,F7.1,3X,E10.3,3X,E10.3)
400 PRINT,
410 DO 16 I=1,NXP
420 DO 16 J=1,NYP
430 SIGXX(I,J)=E*(EPSXX(I,J)+NU*(EPSYY(I,J))-(1+NU)*ALPHA*T
440 &(I,J))/(1-NU**2)
450 SIGYY(I,J)=E*(EPSYY(I,J)+NU*(EPSXX(I,J))-(1+NU)*ALPHA*T
460 &(I,J))/(1-NU**2)
470 16 CONTINUE
480 PRINT,"SIGXX AND SIGYY HAVE BEEN COMPUTED."
490 PRINT,
500 PRINT 17,

```

STRESS CONTINUED

```

510 PRINT,
520 DO 57 I=1,NXP
530 DO 57 J=1,NYP
540 X(I)=(I-1)*DELX-(XL/2.)
550 Y(J)=(J-1)*DELY-(YL/2.)
560 57 CONTINUE
570 DO 18 K=1,NYP
580 PRINT 17,X(NXC),Y(K),T(NXC,K),SIGXX(NXC,K),SIGYY(NXC,K)
590 18 CONTINUE
600 DO 20 K=1,NXP
610 PRINT 19,X(K),Y(NYC),T(K,NYC),SIGXX(K,NYC),SIGYY(K,NYC)
620 20 CONTINUE
630 NX1=1
640 NY1=1
650 NX2=1
660 NY2=1
670 CKVAL1=0.
680 CKVAL2=0.
690 DO 29 I=1,NXP
700 DO 29 J=1,NYP
710 IF (ABS(SIGXX(I,J)).LE.CKVAL1) GO TO 30
720 CKVAL1=ABS(SIGXX(I,J))
730 NX1=I
740 NY1=J
750 30 CONTINUE
760 IF (ABS(SIGYY(I,J)).LE.CKVAL2) GO TO 31
770 CKVAL2=ABS(SIGYY(I,J))
780 NX2=I
790 NY2=J
800 31 CONTINUE
810 29 CONTINUE
820 PRINT,
830 PRINT, "MAXIMUM VALUES FOR STRESS ARE:"
840 PRINT,
850 PRINT, "      X      Y      SIGXX      SIGYY      TEMP"
860 PRINT,
870 TEMPT1=T(NX1,NY1)
880 TEMPT2=T(NX2,NY2)
890 NX1CH=((NX1-1)*DELX)-(XL/2.)
900 NY1CH=((NY1-1)*DELY)-(YL/2.)
910 NX2CH=((NX2-1)*DELX)-(XL/2.)
920 NY2CH=((NY2-1)*DELY)-(YL/2.)
930 PRINT 32, NX1CH,NY1CH,SIGXX(NX1,NY1),SIGYY(NX1,NY1),TEMPT1
940 PRINT 32, NX2CH,NY2CH,SIGXX(NX2,NY2),SIGYY(NX2,NY2),TEMPT2
950 32 FORMAT (1X,F4.1,3X,F4.1,2X,E10.3,2X,E10.3,2X,F6.1)
960 28 CONTINUE
970 END

```

# SHEAR

```

10 DIMENSION EPSXY(17,17),SIGXY(17,17),X(17),Y(17)
20 INTEGER SX1,SY1
30 REAL NU
40 PRINT,"SUPPLY E, NU, THE NUMBER OF INCREMENTS IN THE X AND Y"
50 PRINT,"DIRECTIONS, AND PANEL LENGTH ALONG X AND Y"
60 READ, E,NU,NX,NY,XL,YL
70 NX1=NX+1
80 NY1= NY+1
90 NXC=NX/2+1
100 NYC=NY/2+1
110 DX=XL/NX
120 DY=YL/NY
130 PRINT 201,
140 201 FORMAT(6X,"X",9X,"Y",8X,"STRAIN",8X,"SHEAR")
150 CALL OPENF(5,"EPSXYF",7)
160 CALL E0FTST(5,N)
170 G=E/(2.*(1.+NU)**
180 DO 19 I=1,NX1
190 DO 19 J=1,NY1
200 READ (5;23) EPSXY(I,J)
210 23 FORMAT(E14.7)
220 SIGXY(I,J)=G*EPSXY(I,J)
230 19 CONTINUE
240 DO 21 I=1,NX1
250 X(I)=((I-1)*DX)-(XL/2.)
260 21 CONTINUE
270 DO 22 J=1,NY1
280 Y(J)=((J-1)*DY)-(YL/2.)
290 22 CONTINUE
300 PRINT,"SUPPLY PRINT INCREMENT FOR X AND Y"
310 READ, INCRX,INCRY
320 DO 27 K=1,NY1,INCRY
330 PRINT 200,X(NXC),Y(K),EPSXY(NXC,K),SIGXY(NXC,K)
340 27 CONTINUE
350 DO 29 K=1,NX1,INCRX
360 PRINT 200,X(K),Y(NYC),EPSXY(K,NYC),SIGXY(K,NYC)
370 29 CONTINUE
380 200 FORMAT(3X,F7.2,3X,F7.2,3X,E10.3,3X,E10.3)
390 SX1=1.
400 SY1=1.
410 CKVAL=0.
420 DO 290 I=1,NX1
430 DO 290 J=1,NY1
440 IF(ABS(SIGXY(I,J)).LE.CKVAL) GO TO 30
450 CKVAL=ABS(SIGXY(I,J))
460 SX1=I
470 SY1=J
480 30 CONTINUE
490 290 CONTINUE
500 SXF=((SX1-1.)*DX)-(XL/2.)

```

SHEAR CONTINUED

```
510 SYF=((SYI-1.)*DY)-(YL/2.)
520 PRINT 270,
530 270 FORMAT(3X,"X",7X,"Y",2X," MAX SHEAR          MAX STRESS")
40 PRINT271,SXF,SYF,EPsXY(SX1,SY1),SIGXY(SX1,SY1)
550 271 FORMAT(3X,F4.1,3X,F4.1,3X,E10.3,3X,E10.3)
560 END
```

## REFERENCES

1. Kinsler, L. E. and Frey, A. R., *Fundamentals of Acoustics*, John Wiley and Sons, Inc., 1966, p. 108.
2. Beranek, L. L., *Acoustics*, McGraw-Hill Book Co., Inc., 1954, p. 23.
3. Kinsler and Frey, *Acoustics*, p. 441.
4. Morse, P. M., *Vibration and Sound*, McGraw-Hill Book Co., Inc., 1948, p. 393.
5. Barnoski, R.L. and Maurer, J.R., "Distributed System Response Characteristics in Random Pressure Fields," NASA, CR-1660, Sept. 1970.
6. Hurty, C. W. and Rabinstein, M. F. *Dynamics of Structures*, Prentice-Hall, Inc., 1964, p. 289.
7. Shapiro, F. H., *The Dynamics and Thermodynamics of Compressible Fluid Flow*, Volume I, Ronald Press, Co., 1953, p. 266.
8. Boresi, A. P., *Elasticity in Engineering Mechanics*, Prentice-Hall, Inc., 1965, pp. 229-238.
9. Chester, C. R., *Techniques in Partial Differential Equations*, McGraw-Hill Book Co., Inc., 1971, pp. 64-95.
10. Todd, J., *Survey of Numerical Analysis*, McGraw-Hill Book Co., Inc., 1962, pp. 380-435.
11. Hicks, C. R., *Fundamental Concepts in the Design of Experiments*, Holt, Rinehart, and Winston, 1964.
12. *ibid.*, pp. 66-72.
13. Wedekind, G.L., "Utilization of Latin Square Experimental Design Plans in Parametric Studies of Theoretical Problems," U.S. Army Tank Command, 1968.
14. Timoshenko, S. P. and Goodier, S. N., *Theory of Elasticity*, McGraw-Hill Book Co., Inc., 1951, pp. 399-404.
15. Harris, C. M. and Crede, C. E., *Shock and Vibration Handbook*, Volume I, McGraw-Hill Book Co., Inc., 1961, chapter 7.
16. Warburton, G.H., "The Vibration of Rectangular Plates," *Proc. of Inst. of Mechanical Engineering*, Volume 168, 1954.
17. McNeal, R.H. and McCormick, C.W., "The NASTRAN Computer Program for Structural Analysis," NASA, 1969.
18. Zienkiewicz, O. C. and Holister, G. S., *Stress Analysis*, John Wiley and Sons, 1965.
19. Unger, E. and Lee, K.S., "Considerations in the Design of Supports for Panels in Fatigue Tests," AFFDL TR-67-86, 1967.
20. Lee, Y. W., *Statistical Theory of Communication*, John Wiley and Sons, Inc., 1960, p. 6.
21. *ibid.*, p. 50.
22. Davenport, W. B. and Root, W. L., *Random Signals and Noise*, McGraw-Hill Book Co., Inc., 1958, p. 184.

#### REFERENCES (Continued)

23. Prager, W., *Introduction to Mechanics of Continua*, Ginn and Company, 1961, pp. 81-92.
24. Boley, B. A. and Weiner, J. H., *Theory of Thermal Stresses*, John Wiley and Sons, Inc., 1960.
25. Kreith, F., *Principles of Heat Transfer*, International Textbook Co., 1965, pp. 76-92.
26. Timoshenko and Goodier, *Theory of Elasticity*, pp. 433-437.
27. Timoshenko, S., *Theory of Plates and Shells*, McGraw-Hill Book Co., Inc., 1959, pp. 378-425.
28. Harris and Crede, *Shock and Vibration Handbook*, Volume I, pp. 7-24 through 7-36.
29. *ibid.*, pp. 7-26.
30. Timoshenko and Goodier, *Theory of Elasticity*, pp. 433-437.
31. *ibid.*, pp. 451-490.
32. Todd, *Survey of Numerical Analysis*, pp. 390-391.
33. *ibid.*, pp. 461-490.